PEOPLE'S DEMOCRATIC REPUBLIC OF ALGERIA

Ministry of Higher Education and Scientific Research

Echahid Hamma Lakhdar University of El-Oued

FACULTY OF TECHNOLOGIES

DEPARTMENT OF MECHANICAL ENGINEERING

FINAL STUDY DISSERTATION

In the aim obtaining of

2emeMASTER DEGREE

Domain: Sciences and Technology

Option: Electromechanical

Specialty: Electromechanical

THEME

Prediction of Power Transformer Lifetime and Performance Using Dissolved Gas Analysis (DGA) and Machine Learning Algorithms

Presented by:

- Salhi Ali
- Hoggui Youcef
- Ghribi Salman

Supervised by:

- Dr. Miloudi Khaled

Academic year :2025/2026

بسم الله الرحمن الرحيم

﴿ رَبَّنَا لاَ تُؤَاخِذْنَا إِن نَّسِينَا أَوْ أَخْطَأْنَا رَبَّنَا وَلاَ تَحْمِلْ عَلَيْنَا إِصْرًا كَمَا حَمَلْتَهُ عَلَى الَّذِينَ مِن قَبْلِنَا رَبَّنَا وَلاَ تُحَمِّلْنَا مَا لاَ طَاقَةَ لَنَا بِهِ وَاعْفُ عَنَّا وَاغْفِرْ لَنَا وَارْحَمْنَا أَنتَ مَوْلاَنَا فَانصُرْنَا عَلَى الْقَوْمِ الْكَافِرِينَ﴾ **سورة البقرة : الآية286 .**

" صدق الله العظيم"

ACKNOWLEDGEMENTS

By the grace and blessings of Almighty Allah, this work has been completed. All praise and gratitude are due to Him for granting us strength and determination throughout this academic journey.

We would like to express our deepest appreciation and sincere gratitude to Dr. Miloudi Khaled for his valuable guidance and continuous supervision, which greatly contributed to the completion of this research.

We also extend our sincere thanks to Mr. Hachifa Abdelmoumen, assistant supervisor, for his support, cooperation, and constructive remarks that helped enrich and improve this work.

We are equally grateful to the members of the examination committee for accepting to evaluate and discuss this work.

Furthermore, we would like to thank everyone who contributed, directly or indirectly, to the accomplishment of this dissertation and provided assistance throughout its preparation.

DEDICATION

In the name of Allah, the Most Gracious, the Most Merciful, all praise is due to Allah for His blessings and guidance.

We dedicate the fruit of this humble work to the dearest people in our lives, to our beloved parents and dear brothers, who have always been our support throughout our journey.

We also dedicate this effort to everyone who contributed to helping and encouraging us, and to all those who had a positive impact on the completion of this work.

To all those for whom we hold love and appreciation.

Abstract

الملخص

Abstract :

Fault diagnosis of oil-immersed power transformers plays a central role in ensuring system reliability and supporting predictive maintenance in power networks. This study proposes an intelligent diagnostic framework based on dissolved gas analysis (DGA) and machine learning for transformer fault classification. The methodology relies on the extraction of ratio-based and graphical features from DGA data, followed by Z-score normalization and dimensionality reduction using t-distributed stochastic neighbor embedding (t-SNE) to obtain a compact and informative feature representation. The reduced features are then evaluated using supervised classification algorithms. Model performance is assessed through multiple metrics, including accuracy, precision, recall, F1-score, and specificity. The findings indicate that integrating heterogeneous DGA-derived features within a unified framework improves the robustness and reliability of transformer fault diagnosis, highlighting the potential of intelligent data-driven approaches for condition monitoring and maintenance decision support in modern power systems .

Keywords— Oil-immersed power transformer; Dissolved gas analysis (DGA); Fault diagnosis; Machine learning; Feature extraction; Dimensionality reduction; t-SNE; Condition monitoring; Predictive maintenance; Intelligent classification.

الملخص (بالعربي) :

يُعد تشخيص أعطال محولات القدرة المغمورة بالزيت عنصرًا أساسيًا لضمان موثوقية الأنظمة الكهربائية ودعم الصيانة التنبؤية في شبكات الطاقة. تقترح هذه الدراسة إطارًا ذكيًا لتشخيص الأعطال يعتمد على تحليل الغازات المذابة (DGA) وتقنيات التعلم الآلي لتصنيف أعطال المحولات. تعتمد المنهجية على استخراج خصائص قائمة على النِّسب والخصائص البيانية من بيانات تحليل الغازات المذابة، يلي ذلك تطبيق تطبيع Z-score وتقليل الأبعاد باستخدام تقنية التضمين العشوائي الموزع t-SNE للحصول على تمثيل مدمج وغني بالمعلومات للخصائص المستخرجة. بعد ذلك، يتم تقييم الخصائص المختزلة باستخدام خوارزميات تصنيف خاضعة للإشراف. ويتم تقييم أداء النماذج اعتمادًا على عدة مؤشرات، تشمل الدقة (Accuracy)، والإحكام (Precision)، والاسترجاع (Recall)، ودرجة F1، والنوعية (Specificity). وتشير النتائج إلى أن دمج الخصائص غير المتجانسة المستخرجة من بيانات DGA ضمن إطار موحد يُحسن من متانة وموثوقية تشخيص أعطال المحولات، مما يبرز إمكانات الأساليب الذكية المعتمدة على البيانات في مراقبة الحالة ودعم قرارات الصيانة في أنظمة الطاقة الحديثة.

الكلمات المفتاحية: محول القدرة المغمور بالزيت؛ تحليل الغازات المذابة (DGA)؛ تشخيص الأعطال؛ التعلم الآلي؛ استخراج الخصائص؛ تقليل الأبعاد؛ t-SNE؛ مراقبة الحالة؛ الصيانة التنبؤية؛ التصنيف الذكي.

TABLE OF CONTENTS

TABLE OF CONTENTS

List of Figures

LIST OF FIGURES

List of Tables

LIST OF TABLES

Abbreviations

List of Abbreviations and Symbols

Symbol / Acronym	Full Term
H_2	Hydrogen
CH_4	Methane
C_2H_2	Acetylene
C_2H_4	Ethylene
C_2H_6	Ethane
CO	Carbon Monoxide
CO_2	Carbon Dioxide
DGA	Dissolved Gas Analysis
GC	Gas Chromatography
FRA	Frequency Response Analysis
BDV	Breakdown Voltage
PDC	Polarization and Depolarization Current
RVM	Recovery Voltage Measurement
IFT	Interfacial Tension
TRT	Three-Ratio Technique
t-SNE	t-Distributed Stochastic Neighbor Embedding
AI	Artificial Intelligence
ML	Machine Learning
SVM	Support Vector Machine

Symbol / Acronym	Full Term
k-NN	k-Nearest Neighbors
RF	Random Forest
AUC	Area Under the Curve
ROC	Receiver Operating Characteristic
F1	F1-Score (Harmonic Mean of Precision and Recall)
IEC	International Electrotechnical Commission
CIGRE	International Council on Large Electric Systems
CSUS	California State University, Sacramento
HV	High Voltage
EHV	Extra-High Voltage
AC	Alternating Current
EMF	Electromotive Force
CRGO	Cold-Rolled Grain-Oriented (Silicon Steel)

General Introduction

GENERAL INTRODUCTION

Electric power transformers represent one of the most vital and irreplaceable components of modern electrical power systems. As static electromagnetic devices responsible for stepping voltage levels up and down across transmission and distribution networks, they ensure the efficient and reliable delivery of electrical energy from generation sources to industrial facilities and domestic consumers alike. Among the various transformer technologies in service today, oil-immersed power transformers occupy a dominant position, particularly in high-voltage (HV) and extra-high-voltage (EHV) networks. This technical preference stems from the unique physical and chemical properties of mineral oil, which simultaneously acts as a superior electrical insulator and an effective heat transfer medium, enabling the design of high-capacity transformers with compact dimensions and exceptional thermal efficiency.

Despite their robustness, oil-immersed power transformers are subjected to continuous thermal, electrical, and mechanical stresses throughout their operational lifetime. These stresses gradually degrade the insulating oil and cellulose paper insulation, and can lead to the development of incipient internal faults such as partial discharges, low-temperature and high-temperature thermal faults, and electrical arcing. If left undetected, these faults can escalate into catastrophic failures, causing prolonged power outages, costly equipment replacement, and serious safety hazards. For this reason, the condition monitoring and early fault detection of power transformers have become priorities for power utilities worldwide, driving continuous research and development in the field of transformer diagnostics.

Among the various diagnostic techniques available for monitoring transformer health, Dissolved Gas Analysis (DGA) has established itself as the most widely recognized and reliable method for the early detection of incipient faults in oil-filled equipment. The principle of DGA is based on the observation that thermal and electrical stresses decompose the insulating oil and cellulosic paper, generating characteristic combustible and non-combustible gases that dissolve into the oil. The primary gases monitored in DGA include hydrogen (H_2), methane (CH_4), ethylene (C_2H_4), ethane (C_2H_6), acetylene (C_2H_2), carbon monoxide (CO), and carbon dioxide (CO_2). The type, concentration, and rate of generation of these gases serve as reliable chemical fingerprints that allow the identification of specific fault mechanisms operating inside the transformer.

Over the decades, numerous conventional DGA interpretation methods have been developed and standardized by international organizations, including key gas methods, ratio-based techniques such as the Rogers method, the IEC 60599 method, the Dornenburg method, the CIGRE ratio method, and the ETRA method, as well as graphical approaches such as the Duval Triangle, the Duval Pentagon, the Mansour Pentagon, and the Gouda Heptagon. While these methods have demonstrated practical value in the field, they suffer from several inherent limitations. Most rely on fixed threshold rules and expert-defined boundaries that struggle to capture the overlapping and nonlinear nature of fault signatures in real-world DGA data. Furthermore, conventional ratio features, when used alone, often fail to provide sufficient discriminative power for accurate multi-class fault classification, particularly in the presence of mixed or complex fault conditions.

To overcome these limitations, the growing field of Artificial Intelligence (AI) and Machine Learning (ML) has offered promising new perspectives for DGA-based transformer fault diagnosis. Data-driven classification algorithms, including Support Vector Machines (SVM), k-Nearest Neighbors (k-NN), Random Forest (RF), and ensemble methods such as AdaBoost , are capable of learning complex decision boundaries from historical DGA datasets without relying on manually crafted rules. These approaches have shown significant potential for improving the accuracy, robustness, and scalability of transformer fault classification systems.

In this context, the present dissertation proposes an intelligent DGA-based diagnostic framework for the fault classification of oil-immersed power transformers. The proposed methodology combines two complementary feature extraction strategies ratio based features and graphical features and integrates them through a feature fusion approach to produce a richer and more discriminative representation of DGA data. The extracted features are preprocessed using Z-score normalization and projected into a reduced two-dimensional space using t-distributed Stochastic Neighbor Embedding (t-SNE), before being evaluated using four supervised classification algorithms. The work addresses six transformer fault classes and assesses model performance through a comprehensive set of evaluation metrics, including accuracy, AUC, recall, F1-score, G-Mean, and confusion matrix analysis.

This dissertation is structured into four chapters. The first chapter provides a general overview of oil-immersed power transformers, covering their structure, operating principles, types of faults, and applications. The second chapter presents a thorough literature review of DGA interpretation methods, encompassing key gas, ratio-based, and graphical techniques. The third chapter introduces the theoretical foundations of machine learning, with particular attention to the classification algorithms and performance evaluation metrics selected for this study. Finally, the fourth chapter describes the experimental setup, the proposed methodology, and a detailed analysis of the obtained results, demonstrating the effectiveness of the feature fusion approach in improving transformer fault diagnosis accuracy

Chapter I

Chapter I : Oil-Immersed Power Transformers

I.1• General Overview

Electrical transformers constitute the fundamental pillar and backbone of modern power systems; without them, the transmission of electrical energy over long distances would be practically impossible. Their core function lies in interconnecting different voltage levels within the electrical grid, enabling voltage to be stepped up at generation stations to reduce losses caused by electrical resistance, and then stepped down at consumption centers to ensure safe and efficient power transmission.

Oil-immersed transformers emerge as the most widespread and commonly used type in high-voltage (HV) and extra-high-voltage (EHV) networks [figure 01] . This technical preference is attributed to the unique physical and chemical properties of mineral oil; it not only serves as an excellent electrical insulating medium that prevents electrical breakdowns between windings, but also acts as an efficient heat transfer medium (coolant), significantly outperforming dry-type transformers that rely on air. Oil has a higher capacity for heat absorption and dissipation, which allows the design of high-capacity transformers with relatively smaller sizes compared to dry-type transformers, which remain limited to medium- and low-voltage ranges [1].

Moreover, insulating sensitive components (the core and windings) within a sealed tank filled with oil protects them from external environmental factors such as moisture, dust, and corrosion, thereby significantly extending the service life of the equipment.

Accordingly, this study aims to provide a precise and comprehensive analysis of these devices, particularly oil-immersed transformers, from several complementary perspectives:

1. The historical aspect: tracing the development of this technology from its initial invention to contemporary intelligent technologies.
2. The structural aspect: detailing the components from the magnetic core to mechanical and electrical protection devices.
3. The operational aspect: examining transformer behavior under different loading conditions and its modes of operation.

Special emphasis is placed on the role of oil, not only as an insulating medium, but also as a diagnostic tool and a critical factor in transformer durability and overall electrical grid stability, as oil is considered the “blood” that reflects the internal health condition of the transformer [2].

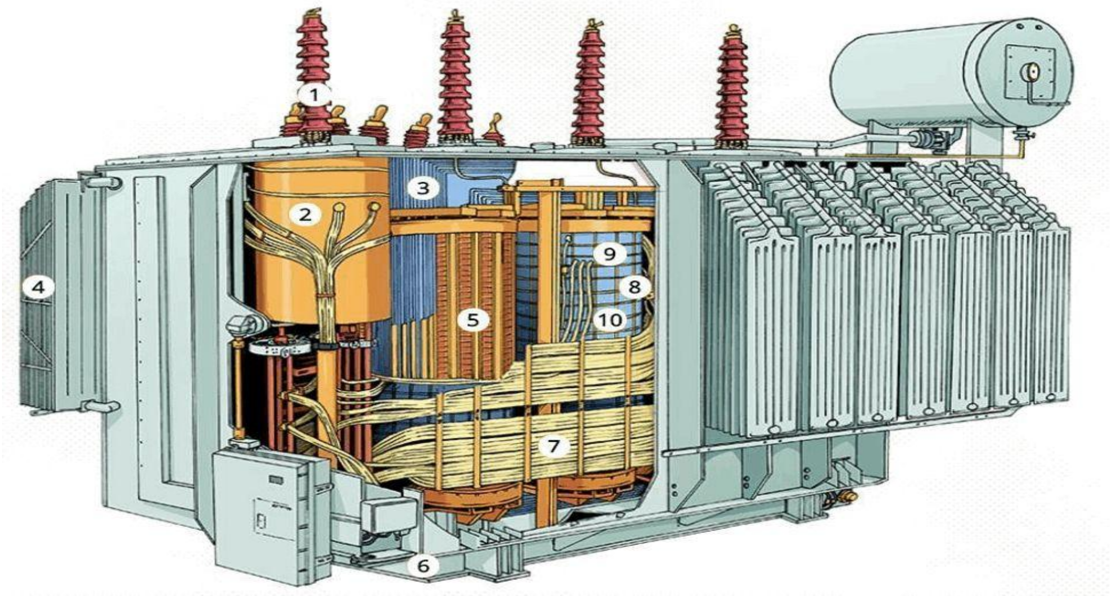

Figure I.1 Structural Overview of a Power Transformer

1. High Voltage (HV) Bushings
2. Tap Changer
3. Low Voltage (LV) Bushings
4. Cooling Radiators
5. Magnetic Core
6. Main Tank
7. Windings
8. Internal Leads
9. Insulating Cylinders
10. Winding Taps / Lead Supports

I.2• Introduction

Electrical transformers constitute one of the most essential components of modern electrical power systems, due to the pivotal role they play in the efficient and safe transmission and distribution of electrical energy. These devices have undergone significant development over time in terms of design, materials used, as well as operating and protection methods, which has made them indispensable elements in electrical networks across various voltage levels. Building on this vital role, this introduction aims to provide a general overview of electrical transformers, including their definition, historical development, basic structure, and the types of faults that may affect them, while also addressing operational aspects and various fields of application. Particular emphasis will be placed on oil-immersed transformers, as they are the most widely used in high-voltage and extra-high-voltage networks, owing to their technical characteristics that make them more efficient and reliable compared to other types.

I.2.1 • Definition of Power Transformers :

A power transformer is a static electromagnetic device specifically designed to transfer electrical energy from one alternating current (AC) system with given voltage and current values to another system with different voltage and current levels, while maintaining a constant frequency and power (except for minor losses). The transformer contains no moving mechanical parts, which makes it highly efficient and requires relatively low maintenance compared to rotating electrical machines [3].

From a physical perspective, the operation of a transformer is based on Faraday's law of electromagnetic induction and Lenz's law. The process begins when the primary winding is supplied with an alternating current, generating a time-varying magnetic flux. This flux is guided through the magnetic core, which acts as a low-reluctance path, and links the turns of the secondary winding, thereby inducing an electromotive force (EMF) and producing a current in the load circuit. In oil-immersed transformers, this system is further enhanced by a liquid medium that serves as a primary electrical insulator and an effective cooling agent, enabling the transformer to handle very high power densities without insulation breakdown [4].

I.2.2 • Historical Evolution of Transformers

The development of electrical transformers went through key milestones that transformed electricity from laboratory experiments into an industrial energy source powering the modern world. These stages can be summarized as follows:

I.2.2.1 Discovery Stage (1831):

The British scientist Michael Faraday laid the foundation when he discovered the principle of electromagnetic induction using his famous device known as Faraday's Ring. Although this discovery demonstrated the possibility of transferring energy between two coils through magnetic flux, the device remained primitive and unsuitable for practical long-distance power transmission due to low efficiency and the absence of a technically designed magnetic core [5].

I.2.2.2 The Hungarian Revolution and Practical Transformers (1885):

This year marked the birth of the modern transformer through the work of the Hungarian trio Zipernowsky, Bláthy, and Déri (ZBD) at the Ganz company. Their major innovation was the closed-core transformer. This design made commercial alternating current (AC) power transmission possible by enabling highly efficient voltage step-up and step-down. This structural model is still regarded in engineering literature as the foundation of all contemporary transformers [6].

I.2.2.3 The Era of Oil-Immersed Transformers (1891):

With the expansion of power networks, engineers faced a major challenge, as conventional insulation materials (air and dry paper) failed and burned when voltage levels were increased. At this point, the technical ingenuity of Charles Brown [figure 02] emerged with the introduction of the first oil-immersed transformer. Oil proved to be an effective solution, offering insulation far superior to air and providing efficient heat dissipation. This allowed voltage levels to rise to unprecedented values at the time (exceeding 25 kV). This innovation was a key factor in reducing electrical losses and enabling power transmission over continental distances [2].

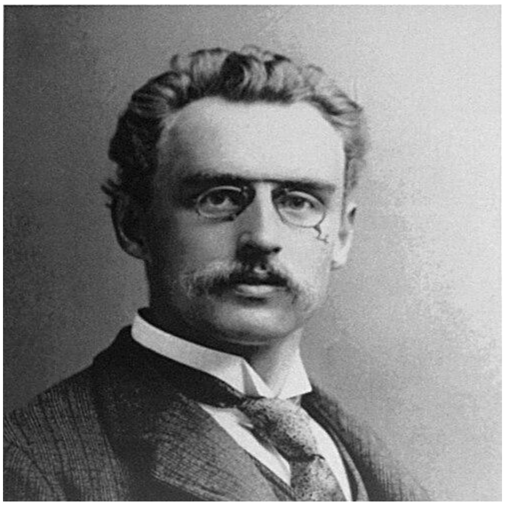

Figure I.2 Charles Brown – Pioneer of Oil-Immersed Transformers

I.3 • Structure and Components of Power Transformers

Regardless of the type of cooling or insulation system, all power transformers share the presence of two active parts that constitute the core of the transformer, namely the magnetic core and the windings. However, in the case of oil-immersed transformers, an additional complex set of mechanical components is incorporated to contain and protect the oil [1], [3].

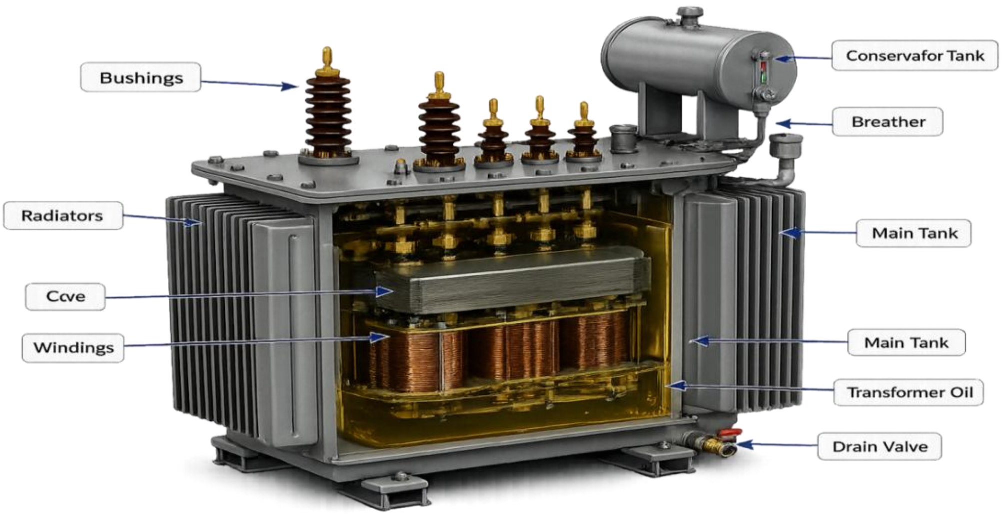

Figure I.3 illustrating the components of an oil-immersed electrical transformer

I.3.1 • General Active Components (General Active Parts): These components are common to both dry-type and oil-immersed transformers:

I.3.1.1 Magnetic Core: It represents the path through which the magnetic flux flows. The core is not manufactured as a solid iron piece; instead, it is constructed by stacking thousands of very thin laminations of cold-rolled grain-oriented silicon steel (CRGO). Each lamination is insulated from the others by a thin varnish layer. [figure 03]

This precise design aims to minimize eddy current losses as much as possible, thereby improving transformer efficiency [4].

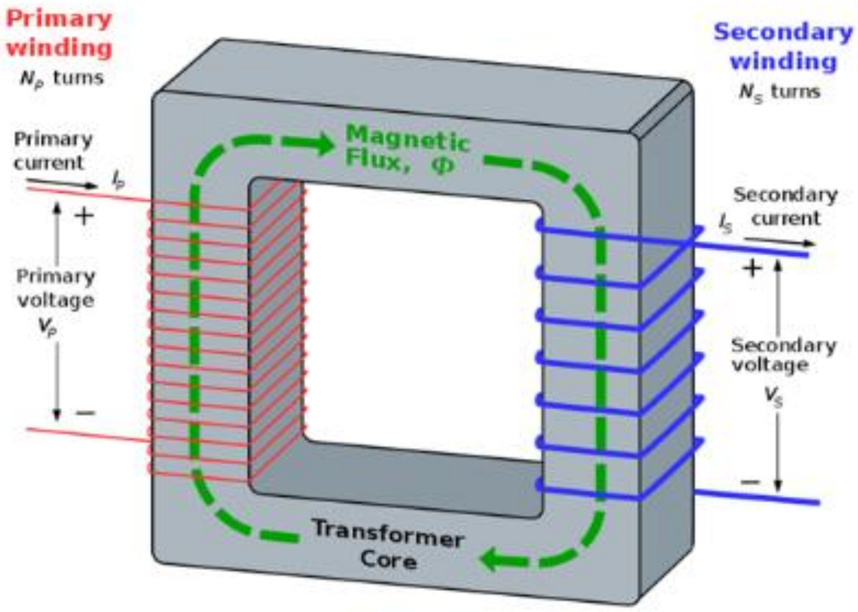

Figure I.4 Magnetic Core and Flux Path in the Electrical Transformer

I.3.1.2 Windings: These are the electrical conductors that carry current. They are usually made of pure copper (or aluminum) and insulated with layers of pressboard paper or enamel. The windings (primary and secondary) are arranged around the core

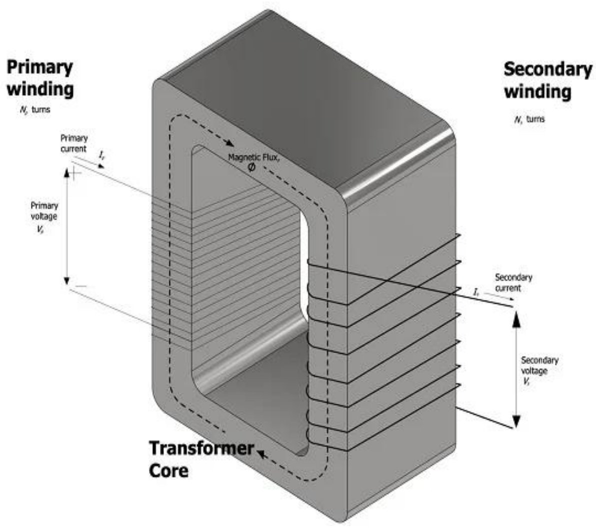

using specific geometrical configurations (such as cylindrical or disc windings) to ensure optimal magnetic coupling and to withstand mechanical stresses [3]. [figure04]

Figure I.5 Simple transformer showing primary winding, secondary winding and magnetic core

I.3.2 • Components Specific to Oil-Immersed Transformers (Oil-Immersed Specific Components):

Oil-immersed transformers are distinguished by additional components that ensure the efficient operation of the cooling medium (oil) [1], [7]:

• I.3.2.1 Main Tank:

A robust, tightly sealed steel vessel that houses the core and windings completely immersed in oil [figure 05]. The tank serves as a heat dissipation surface and provides mechanical protection for the internal components.

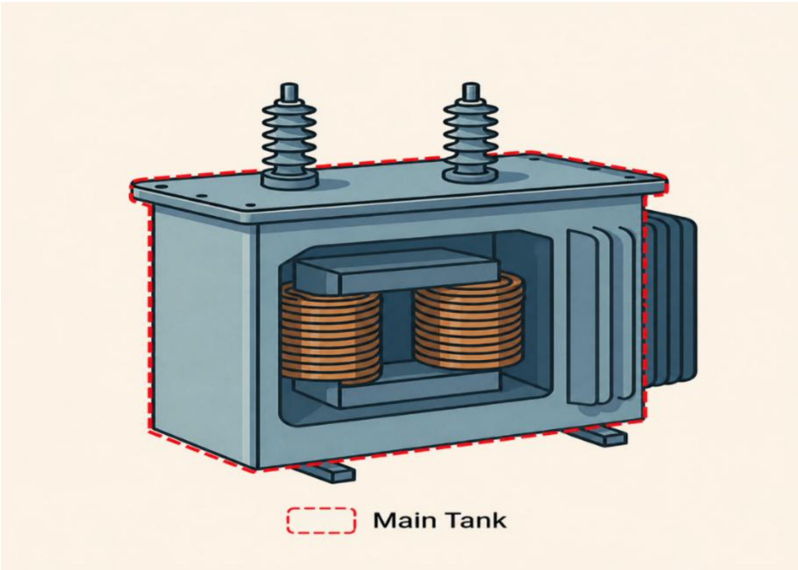

Figure I.6 High Frequency Power Electric Oil Immersed Transformer Storage Tank

I.3.2.2 Bushings: These are porcelain or composite insulating terminals mounted on the top of the tank [figure 06]. Their function is to conduct high current from outside the transformer to the internal windings (or vice versa) while ensuring complete insulation between the live conductor and the grounded metallic tank.

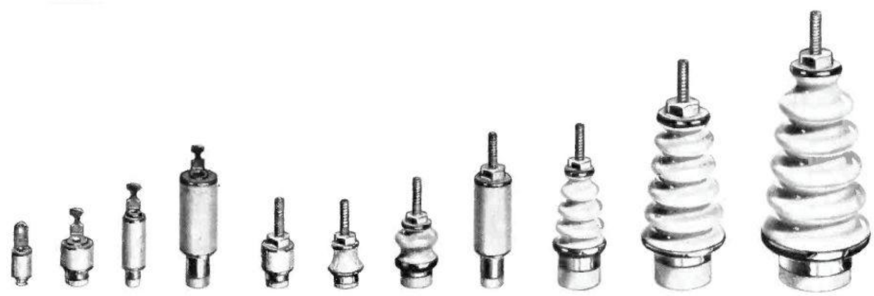

Figure I.7 Electrical Insulators of Different Sizes According to Voltage Level

I.3.2.3 Conservator Tank: A cylindrical metal tank installed above the transformer and connected to the main tank. Its function is to accommodate the expansion of oil when heated and its contraction when cooled, ensuring that the main tank remains fully filled and preventing the formation of air bubbles inside. [figure 07]

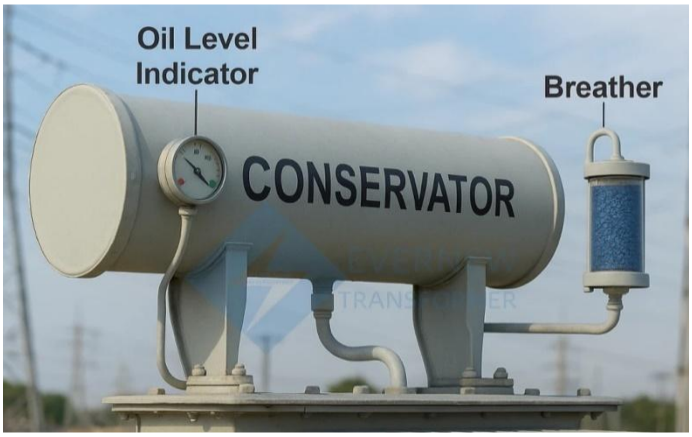

Figure I.8 Transformer Oil Protection and Monitoring SystemTr

I.3.2.4 Breather: Considered the “lungs” of the transformer, it is a glass container filled with silica gel [figure 08] . This material absorbs moisture from the air drawn into the transformer during oil contraction, as moisture is the primary enemy of insulating oil.

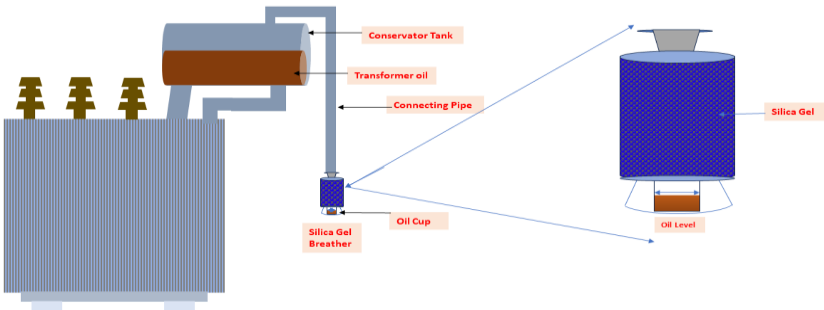

Figure I.9 Breathing system of an oil-immersed transformer.

I.3.2.5 Radiators/Fins:

Hollow metallic tubes mounted on the sides of the tank. Hot oil flows through them, cools by contact with the surrounding air, and then returns to the transformer, creating a continuous cooling cycle. [figure 09]

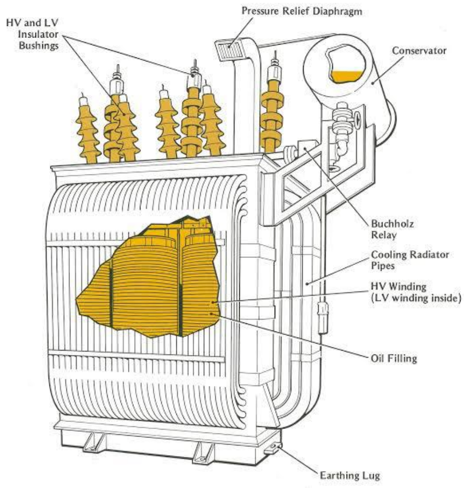

Figure I.10 Working Principle of Cooling Fins in an Oil-Immersed Electrical Transformer

I.4 • Types of Faults

Power transformers are subjected to various stresses during operation. The resulting faults can be classified into two levels: general faults that affect the active parts (windings and core) in all types of transformers, and special faults that are related to the type of insulation and cooling used (oil) [8].

I.4.1 • General Faults (Common in All Transformers):

These faults occur in the core and windings regardless of whether the transformer is oil-immersed or dry-type (air-cooled):

I.4.1.1 Winding Electrical Faults:

These are considered the most common and most dangerous faults, arising from the breakdown of insulation between conductors. They include [figure 10]

- Inter-turn Fault: Breakdown of insulation between two adjacent turns within the same winding.
- Earth Fault: Breakdown of insulation between the winding and the grounded core or tank.

Such faults are often caused by lightning surges or by the natural aging of solid insulation [1].

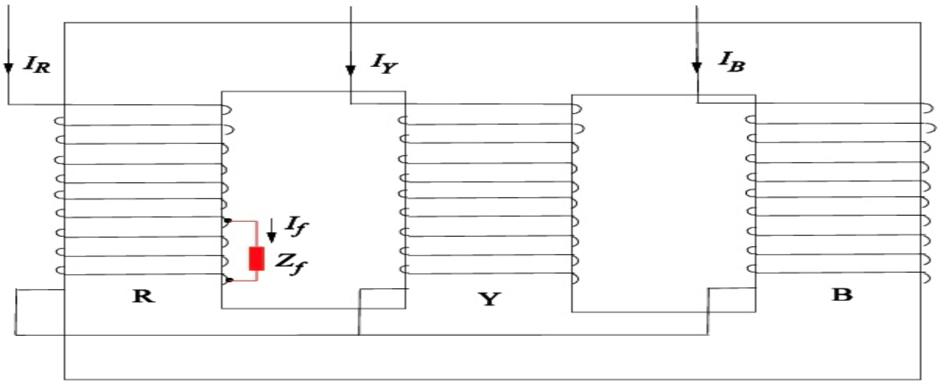

Figure I.11 Schematic representation of an inter-turn short-circuit fault in a three-phase power transformer

I.4.1.2 Mechanical Faults: These occur when the transformer is subjected to a severe external short circuit. The resulting current generates enormous electromagnetic forces that attempt to tear apart or compress the windings, leading to winding deformation or displacement. This phenomenon can physically occur in any transformer carrying high current [8].

I.4.2 • Oil-Specific Faults in Oil-Immersed Transformers:

Here lies the uniqueness of oil-filled transformers, where the liquid medium plays a central role in the occurrence and detection of faults. These faults do not exist in dry-type transformers [9], [10]:

I.4.2.1 Oil Degradation and Contamination:

- Moisture: Water ingress into the oil sharply reduces its dielectric strength.
- Oxidation: The reaction of oil with oxygen and heat produces acids that attack paper insulation, and forms sludge deposits that accumulate in cooling ducts and hinder heat dissipation.

I.4.2.2 Gas Generation (Dissolved Gas Analysis – DGA):

In oil-immersed transformers, any internal fault (such as overheating or electrical arcing) immediately causes chemical decomposition of the oil molecules, producing specific gases that dissolve in the oil.

- For example, electrical arcing produces acetylene (C_2H_2).
- Overheating produces methane (CH_4).

This phenomenon makes the oil act as a “black box” that records the history of faults [10].

I.4.2.3 Oil Leakage:

Cracks in the tank or damage to gaskets lead to a reduction in oil level, which may expose the windings to air and cause immediate insulation failure, or result in the malfunction of the Buchholz relay, which is responsible for gas-based protection [7].

I.5 • Study of Insulating Oil: Its Properties and Importance

Oil in transformers is not merely a filling liquid; rather, it is an active structural material that performs a dual role (insulation and cooling). The vast majority of transformers use mineral oils, derived from crude oil distillation, which must achieve a precise balance among the following properties in accordance with international standards [9]:

I.5.1 Physical Properties

These properties relate to the behavior of oil as a heat-transfer fluid:

I.5.1.1 Viscosity:

It is the most important factor in cooling efficiency. The viscosity of the oil should be as low as possible, because light oil flows quickly and smoothly

through the narrow channels between windings and through the cooling radiators by natural convection currents, ensuring rapid heat dissipation.

I.5.1.2 Flash Point:

It is the lowest temperature at which the oil releases flammable vapors. For safety and fire protection reasons, the flash point must be very high (usually

above 140 °C) to avoid ignition risks during emergency overload conditions [1].

I.5.1.3 Pour Point:

It is the lowest temperature at which the oil remains fluid. It must be very low to ensure that the transformer can operate in cold and freezing environments without the oil solidifying and stopping circulation.

I.5.2 •Electrical Properties

These properties relate to the oil’s ability to prevent electrical arcing:

I.5.2.1 Dielectric Strength:

Also known as breakdown voltage, it measures the voltage that the oil can withstand before electrical breakdown and sparking occur. Clean and dry oil has a very high dielectric strength; however, the presence of microscopic water droplets or solid contaminants causes this value to drop sharply [8].

I.5.2.2 Dissipation Factor (Tan Delta):

It is a measure of the electrical energy losses within the oil itself, which are converted into heat. A low value indicates excellent insulating properties, whereas a high value indicates the presence of dissolved contaminants [9].

I.5.3 • Chemical Properties

These properties determine the transformer's service life:

I.5.3.1 -Oxidation Stability:

The oil is exposed to high temperatures in the presence of oxygen and metallic catalysts (such as copper and iron). The oil must resist chemical reactions to prevent the formation of sludge, which adheres to windings and blocks cooling, or acids, which corrode paper insulation [1].

I.5.3.2 Water Content:

The oil must be completely dry (with moisture measured in parts per million, ppm), because water is attracted to cellulose fibers (paper insulation) and severely degrades their mechanical and electrical strength.

I.6 Applications of Transformers

Electrical transformers are widespread in every part of the power system However, the selection of the transformer type (dry-type or oil-immersed) mainly depends on the installation location, the required power rating, and the surrounding environmental conditions [1].

I.6.1 • General Applications of Electrical Transformers

Transformers are used in any system that requires a change in voltage levels. Examples include:

I.6.1.1 Electronic and household devices:

Very small transformers (mostly dry-type) are used to operate chargers and computers at low voltages (e.g., 12 V or 19 V).

I.6.1.2 Industrial control panels:

Transformers are used to provide a safe voltage level (24 V) for machine control circuits.

I.6.1.3 Residential buildings and hospitals:

Dry-type transformers are used inside enclosed rooms because they are safer against fire hazards in densely populated areas [3]

I.6.2 • Applications of Oil-Immersed Transformers

Due to the high efficiency of oil in cooling and insulation, this type of transformer is mainly used in applications that require high power ratings and harsh outdoor conditions [1], [2]:

I.6.2.1 Power generating stations:

Oil-immersed transformers are used as step-up transformers. They increase the voltage generated by generators (e.g., from 15 kV) to extra-high voltage levels (such as 400 kV or 765 kV) to transmit power over long distances with minimal losses. Oil is essential for insulating such high voltages and cooling the heat produced by large currents [2].

I.6.2.2 Transmission and main substations:

These substations act as interconnection nodes between cities and major power networks. They contain large oil-immersed transformers that step down

voltage from extra-high levels to medium transmission levels (such as 132 kV or 66 kV).

I.6.2.3 Urban and rural distribution networks:

These are the transformers mounted on poles or installed in distribution rooms within residential areas. Oil-immersed transformers are preferred here due to their high ability to withstand environmental variations (rain, dust, and high temperatures), as sensitive components are fully protected inside a sealed oil tank [3].

I.6.2.4 Large factories and heavy industries:

Such as steel smelting plants and petrochemical industries. These facilities require huge and continuous power (high duty cycle), making dry-type transformers uneconomical. Therefore, oil-immersed transformers are used due to their ability to operate continuously under heavy loads [8].

I.7 Conclusion

Power transformers, in general, are considered the backbone upon which the modern power system is built. Without their exceptional capability to efficiently step up and step down voltage levels, it would not be possible to transmit electrical energy over long distances, nor would electricity reach our homes and industries with the level of reliability we experience today. Throughout their history, these static devices have proven to be the most stable means of interconnecting generation sources with consumption areas, while maintaining economic efficiency that ensures technical losses are reduced to the lowest possible levels [3], [8].

With regard to oil-immersed transformers in particular, they continue to represent the "technological pinnacle" in high-power and extra-high-voltage applications. To date, no other insulating medium has been able to match the dual properties of oil as both a superior electrical insulator and an ideal heat transfer medium at the same time. Despite the challenges associated with oil maintenance and leakage risks, digital advancements in Dissolved Gas Analysis (DGA) techniques have transformed this type of transformer into an intelligent device capable of predicting faults before they occur [10]. The future direction of this field is now focused on achieving a balance between "high performance" and "environmental sustainability." It is expected that the coming years will witness a widespread replacement of mineral oils with natural ester oils, providing oil-immersed transformers with a longer operational lifespan and enhanced fire safety, while ensuring full compliance with stringent environmental standards [1], [11]. Consequently, oil-filled transformers remain an indispensable technology for securing the future of global energy systems.

Chapter II

Chapter II. Literature review on internal faults diagnosis in power transformers

II.1 Comprehensive review of condition monitoring methods

The maintenance and monitoring of power transformers are vital to energy and system management. A transformer's condition is a cornerstone of efficient electricity transmission, as any failure can jeopardize the stability of the entire grid [9]. Among the various diagnostic techniques, Frequency Response Analysis (FRA) also known as the transfer function method—stands out as an effective tool for identifying mechanical faults, such as winding deformation [10-12].

Partial Discharge (PD) Analysis is another critical method for monitoring insulation health. PD refers to localized electrical discharges within liquid or solid insulation; early detection is essential to mitigate aging and extend the transformer's operational life [13-15]. Complementing these techniques is Vibration Analysis. While vibration is typically a byproduct of mechanical movement useful for detecting looseness, imbalance, and misalignment [16, 17] its application has expanded in recent years to include the monitoring of power transformer health [18].

Several chemical and electrical tests provide deeper insights:

Interfacial Tension (IFT): A chemical test used to detect acidic contaminants in oil resulting from the oxidative degradation of paper [19, 20].

Insulation Resistance (IR): Evaluates the deterioration of winding insulation, often utilizing the Polarization Index to interpret resistance data more accurately [21].

Thermography Analysis: Employs infrared cameras to detect Hot Spot Temperatures (HST). In these thermal profiles, red and white indicate high-heat areas, while blue and black represent cooler regions [22-24].

Degree of Polymerization (DP): A key indicator of the mechanical strength of paper insulation, which relies on the integrity and bonding of cellulose molecules [25, 26].

Advanced time-domain and dielectric tests include Polarization and Depolarization Current (PDC), which evaluates high-voltage insulation by determining moisture levels in the oil-paper system [27, 28]. Furthermore, Breakdown Voltage (BDV) testing, conducted at room temperature per the IEC 60156 standard, determines the dielectric strength of the oil [29, 30]. Although an older technique, Recovery Voltage Measurement (RVM) remains an effective indicator of oil insulation degradation [31-33]. Additionally, Voltage and Current Measurements analyze the correlation and differences between incoming and outgoing currents; identifying the severity of faults through this method requires a combination of simulation, experimentation, and online detection [34-36].

Finally, Dissolved Gas Analysis (DGA) is widely regarded as the premier technique for tracking a transformer's condition over time. Its significance in diagnosing faults in oil-filled transformers has led to continuous evolution in interpretation methods [37], ranging from traditional ratios to modern Artificial Intelligence (AI) applications. Figure II.1 illustrates the various power transformer evaluation methods, with a specific focus on DGA interpretation.

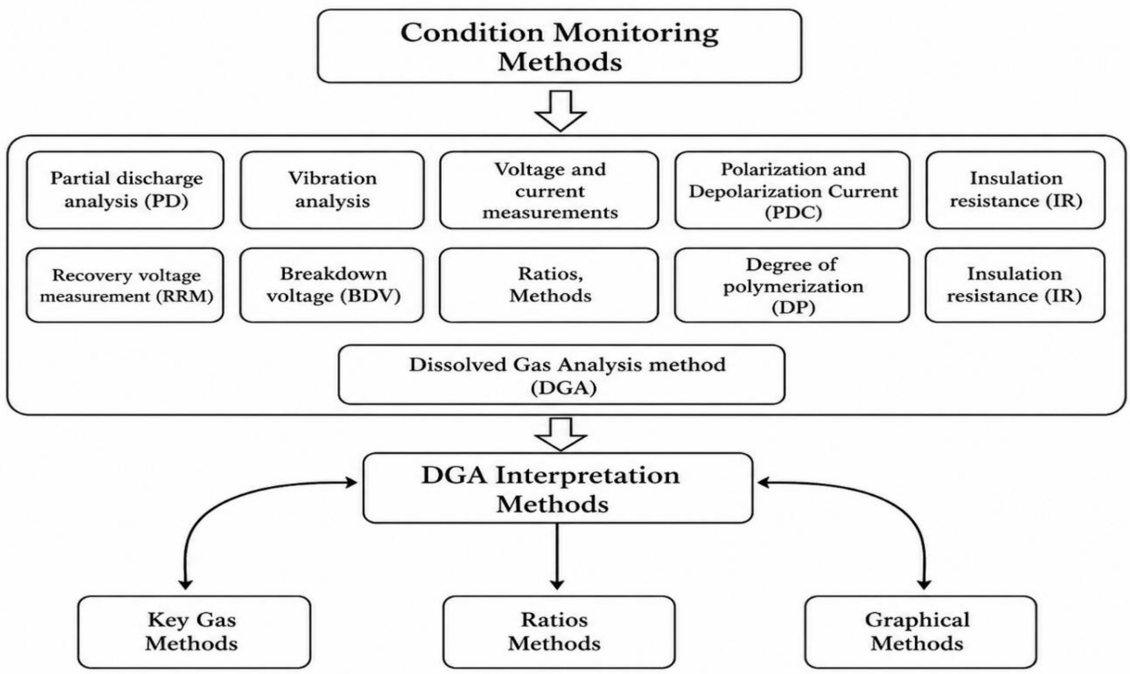

Figure II.1 Power transformer condition assessment and DGA interpretation methods

II.2 Dissolved Gas Analysis Methods

Dissolved Gas Analysis (DGA) serves as a fundamental diagnostic tool for the early detection of incipient faults in oil-immersed power transformers [38]. This technique is primarily utilized to examine gases dissolved within the insulating oil, which are generated by thermal and electrical stresses that threaten the transformer's operational integrity [39, 40]. The primary gases monitored during DGA include hydrogen (H_2), methane (CH_4), ethane (C_2H_6), ethylene (C_2H_4), and acetylene (C_2H_2). Additionally, carbon monoxide (CO) and carbon dioxide (CO_2) serve as significant indicators of cellulose (paper) insulation degradation [41, 42].Historically, the Buchholz relay, introduced in 1928 [43], represented an early innovation in equipment protection by responding to gas formation caused by internal faults. As illustrated in Figure II. 2, the relay operates by detecting gas accumulation in the pipe connecting the transformer main tank to the expansion (conservator) tank. The resulting gas flow triggers the relay, which either activates an alarm or disconnects the transformer entirely to prevent catastrophic damage. By the late 1950s, advancements in analytical methodologies enabled more precise sampling and analysis of gases and liquids. This progress led to the development of a field chromatography analyzer by H.H. Wagner in 1959 [44]. Today, Gas Chromatography (GC) is the most widely adopted method for identifying and quantifying dissolved gases in transformer oil, particularly those generated by electrical faults [45]

The chromatographic analysis of dissolved gases in oil involves several systematic stages. It begins with sampling, typically performed using syringes or flexible aluminum bottles; notably, gases can also be temporarily stored in the Buchholz relay [46]. Subsequently, the gases are extracted and processed via Gas Chromatography (GC), which facilitates the separation of various gas components for precise identification and quantification [47]. Figure II.3 illustrates this systematic workflow—encompassing sample collection, gas extraction, and analytical separation. This rigorous approach ensures diagnostic accuracy, enabling proactive maintenance and the prevention of critical transformer failures

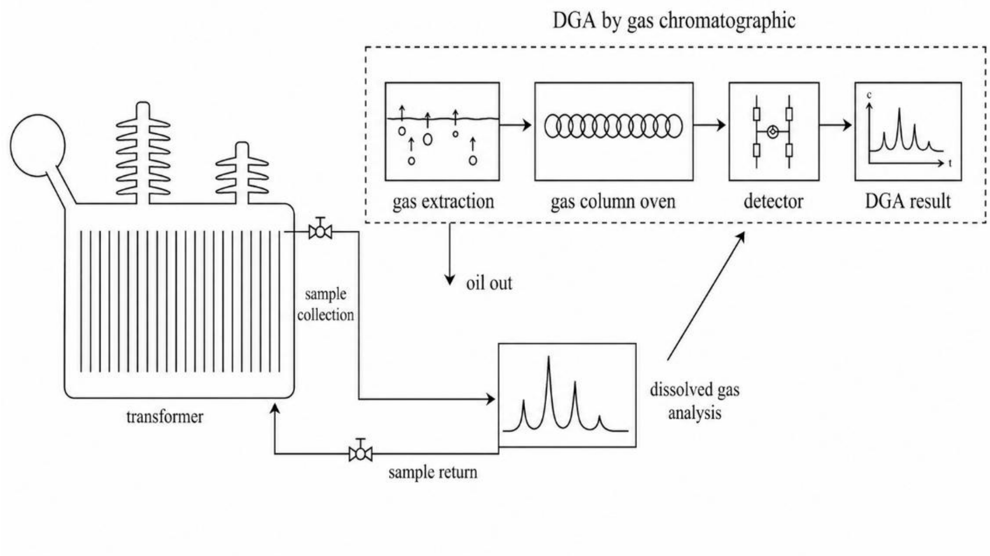

Figure II.2 Steps for gas chromatography analysis [1]

II.3 The principal DGA interpretation methods

This section provides a comprehensive overview of various Dissolved Gas Analysis (DGA) techniques, emphasizing those that have emerged as industry standards due to their high reliability and diagnostic precision. By analyzing these widely adopted frameworks, we aim to highlight contemporary trends and established best practices in power transformer diagnostics.

II.3.1 Key Gas Methods

II.3.1.1 IEEE Key Gas Method:

The IEEE Key Gas method, pioneered by the Doble Engineering Company in 1973, serves as a foundational framework for evaluating transformer health by analyzing gas compositions triggered by thermal and electrical stresses. Initially introduced by David

Pugh in 1974 [49], the method was subsequently refined and integrated into the IEEE C57.104 Standard.

This diagnostic approach relies on the concentrations of specific gases—namely hydrogen, various hydrocarbons, and carbon monoxide—which are released during the thermal decomposition of insulating oil and cellulosic paper. Table II.1 summarizes the primary gases and their associated faults, while Table II.2 presents the specific gas ratios corresponding to the four major fault categories identified by this technique. These percentage values and thresholds are derived from extensive empirical data and expert observations within the field [50].

Despite its widespread use, the IEEE Key Gas method has notable limitations. It is prone to delivering ambiguous or occasionally inaccurate diagnoses. Furthermore, instances occur where the dominant gas is not accounted for within the method's primary criteria, or where the presence of carbon monoxide is misinterpreted, leading to false conclusions regarding the involvement of paper insulation in a malfunction [51].

Table II.1 Key gas generated according to a fault type

Key gas	Fault type	Typical proportions
C_2H_4	Overheating, oil	Mainly C_2H_4; Smaller proportions of C_2H_6, CH_4, and H_2; Traces of C_2H_2 at very high fault temperature
CO	Overheating, paper and oil	Mainly CO; Much smaller quantities of hydrocarbon gases (Predominantly C_2H_4 with smaller proportions of C_2H_6, CH_4, and H_2)
H_2	Partial discharge	Mainly H_2; Small quantities of CH_4; Traces of C_2H_4 and C_2H_6
H_2& C_2H_2	Arcing	Mainly H_2 and C_2H_2; Minor traces of CH_4, C_2H_4, and C_2H_6; Also, CO if cellulose is involved

Table II.2 Key gas proportions of fault types of IEEE key gas method

	Key gas percentages (%)					
Fault type	H_2	CH_4	C_2H_6	C_2H_4	C_2H_2	CO
Partial discharges	85	13	1	1	-	-
Arcing	60	5	2	3	30	-
Overheating, oil	2	16	19	63	-	-
Overheating, paper	-	-	-	-	-	92

II.3.1.2 CSUS Key gas:

The CSUS Key Gas method, commonly known as the Key Gas Quantity method, was established through a joint collaboration between California State University, Sacramento, and the Pacific Gas and Electric Company [52]. This diagnostic approach is based on the direct and individual comparison of hydrocarbon and carbonaceous gas concentrations against their specific threshold limits. As detailed in Table II.3, the method provides both standard and non-standard limit values for each gas to facilitate precise condition monitoring.

The transformer is considered to be in healthy operating condition if all monitored gas concentrations remain below the defined normal thresholds. Identifying specific fault types relies on a direct, one-to-one comparison of individual gas levels against these established limits. However, while the CSUS Key Gas method is characterized by its procedural simplicity, it is hindered by relatively low diagnostic precision. A significant drawback of this approach is its tendency to produce overlapping diagnoses of multiple faults simultaneously, which complicates the interpretation of the transformer's actual condition.

Table II.3 Determination of the type of fault according to the CSUS method

	Limit concentrations		
Key gas	Normal	Anormal	Fault type
H_2	150	1000	Corona discharges, arcing
CH_4	25	80	Corona discharges
C_2H_6	10	35	Local overheating
C_2H_4	20	150	Severe overheating
C_2H_2	15	70	arcing
CO	500	1000	Overload, paper decomposition
CO_2	10 000	15 000	Overload, paper decomposition

II.3.1.3 CIGRE Key gas:

The CIGRE Key Gas method facilitates condition assessment through a direct comparison between measured gas concentrations and their permissible limits. Proposed by the CIGRE Task Force 15.01.01 [53], this approach enhances diagnostic capabilities by detecting paper insulation degradation in addition to the three standard fault categories. Typical concentration thresholds and their corresponding malfunctions are detailed in Table II.4. While this method offers significant diagnostic utility, it is seldom employed as a standalone tool for transformer assessment. Instead, the CIGRE TF 15.01.01 guidelines advocate for the integration of gas ratios into the interpretation process to refine accuracy. Similar to the CSUS approach, its primary disadvantage is the tendency to indicate multiple simultaneous faults, which can obscure a precise diagnostic conclusion.

. **Fallou Key gas:**

Introduced in a 1975 CIGRE publication [54], the Fallou method represents a significant diagnostic approach derived from experimental data on gas evolution in mineral oils under fault conditions. Developed through Fallou's research, this technique prioritizes the percentage concentration of each gas generated during thermal or electrical stress. Specifically, it identifies carbon dioxide (CO_2) and three-carbon hydrocarbons as the primary indicators for fault detection, as detailed in Table II.5.

Table II.4 Determination of the type of fault according to the CIGRE method

Key gas	Limit	Fault
C_2H_2	> 20	Arcing
H_2	> 100	Partial discharges
$\sum C_xH_y$	> 1 000	Thermal fault
$\sum CO_x$	> 10 000	Cellulosic degradation

Table II.5 Key gas method proposed by Fallou

	Key gas percentage (%)							
Fault type	H_2	CH_4	C_2H_6	C_2H_4	C_2H_2	C_3H_x	CO	CO_2
Low-energy discharge (PD1)	88	7	2	-	-	1	1	1
High-energy discharge (PD2)	55	7	5	6	15	6	1	6
Arcing	39	10	-	6	35	3	4	2
Overheating, oil 300°C	-	37	13	19	-	31	-	-
Overheating, oil 500°C	17	25	8	25	-	23	-	-
Overheating, oil 800°C	16	16	6	41	-	21	-	-
Overheating, paper 300°C	26	1	-	-	-	-	-	73
Overheating, paper 500°C	6	1	-	-	-	-	33	59
Overheating, paper 800°C	9	8	1	4	-	1	50	25

II.3.1.1 Characteristic gas ensemble:

The Characteristic Gas Ensemble (CGE) method, introduced in 2018 by Davidenko and Ovchinnikov [55], represents the latest progression in key gas analysis. This technique evaluates the relative weight of primary gases using the following relationship:

$$c_r^i = C^i / C_{lim}^i \qquad \text{(II.1)}$$

Where c_r^i , C^i and C_{lim}^i denote relative, observed, and permissible concentration of the ith key gas.

The CGE method is executed via a systematic three-stage workflow. In the primary stage, the relative concentrations of the identified key gases are calculated. Subsequently, these values are utilized to establish a letter-code system, which ranks the diagnostic significance of each gas within the ensemble (the definitions of these alphanumeric indicators are detailed in Table II.6). The final stage involves fault classification, where the specific malfunction is identified by cross-referencing the generated codes with the fault-type parameters defined in Table II.7

Table II.6 Alphanumeric coding of major gases

Letter	Fault type
A	Primary gas with the highest relative concentration
B	Gas with the second-highest relative concentration $c_r^i \geq 1$
C	Gas at the second or third level with $c_r^i < 1$
D	Corresponds to all other gases not categorized under the previous letters

Table II.7 Determine the fault of the method of gas ensembles characteristic

	Key gas				
Fault type	H_2	CH_4	C_2H_6	C_2H_4	C_2H_2
Overheating, T < 300°C	C, D	B	A	C, D	D
Overheating, 300°C < T < 700°C	D	A	C	B	D
Overheating, T > 700°C	D	B	C	A	D
Partial discharges	A	C	D	D	D
Discharges of low energy	A	C	D	D	B
Discharges of high energy	B	C	D	D	A
A set of faults with electrical fault propagation	D	B	D	C	A

A set of faults with thermal fault propagation	C, D	A	B	D	C, D

II.3.2 Ratios Methods DGA:

II.3.2.1 Dornenburg ratios method:

Established in 1974, the Dornenburg ratios method represents one of the pioneering frameworks for interpreting dissolved gas data [56]. This approach is designed to categorize transformer anomalies into three primary fault types: thermal decomposition, corona discharge, and arcing (as detailed in Table II.8).The validity of this diagnostic tool depends on a specific prerequisite: the concentration of at least one key gas hydrogen (H_2), methane (CH_4), ethylene (C_2H_4), or acetylene (C_2H_2) must exceed twice its defined standard limit (Table II.9). Furthermore, this method accounts for instances where ethane (C_2H_3) or carbon monoxide (CO) levels surpass their respective threshold values [57].

Table II.8 Fault classification by Dornenburg Ratio Method

Fault	$R_1 = \frac{CH_4}{H_2}$	$R_2 = \frac{C_2H_2}{C_2H_4}$	$R_3 = \frac{C_2H_4}{C_2H_6}$	$R_4 = \frac{C_2H_2}{CH_4}$
Thermal decomposition	>1.0	<0.75	<0.3	>0.4
Corona	<0.1	/	<0.3	>0.4
Arcing	0.1–1.0	> 0.75	>0.3	<0.4

Table II.9 Permitted limit for Dornenburg Ratio Method

Gas	H_2	CH_4	C_2H_6	C_2H_2	C_2H_4	CO
Limit (ppm)	100	120	65	50	1	350

II.3.2.2 The four ratios method of Rogers:

The Rogers' Four Ratio Method (RFRM) [58], as its name implies, identifies transformer faults by analyzing four specific gas ratios: methane-hydrogen (CH_4/H_2), ethane-methane (C_2H_6/CH_4), ethylene-ethane (C_2H_4/C_2H_3) , and acetylene-ethylene (C_2H_2/C_2H_4). These diagnostic parameters are determined by classifying them into defined ranges and assigning numerical rules ranging from zero to five, as detailed in Table II.10. This approach facilitates the identification of 12 possible faults, which are displayed in Table II.11 [59]

Table II.10 Rogers Ratio Code

Gas Ratio	Ranges	Code
$R_1 = \frac{CH_4}{H_2}$	< 0.1	5
	0.1- 1	0
	1--3	1
	> 3	2
$R_2 = \frac{C_2H_2}{C_2H_4}$	< 1	0
	> 1	1
$R_3 = \frac{C_2H_4}{C_2H_6}$	< 1	0
	1-3	1
	> 3	2
$R_4 = \frac{C_2H_6}{CH_4}$	< 0.5	0
	0.5-3	1
	> 3	2

Table II.11 Fault Types as stated in Rogers Ratio Method

No	CH_4/H_2	C_2H_6/CH_4	C_2H_4/C_2H_6	C_2H_2/C_2H_4	Fault type
1	0	0	0	0	No fault
2	1-2	0	0	0	<150 ºC thermal fault
3	1-2	1	0	0	150–200 ºC thermal fault
4	0	1	0	0	200–300 ºC thermal fault
5	0	0	1	0	General conductor overheating
6	1	0	1	0	Winding circulating currents
7	1	0	2	0	Core and tank circulating currents overheated joints
8	5	0	0	0	Partial discharge
9	5	0	0	1-2	Partial discharge with tracking
10	0	0	0	1	Flashover without power follow through

11	0	0	1-2	1-2	Arc with power follow- through
12	0	0	2	2	Continuous sparking to floating potential

II.3.2.3 IEC Ratio Method:

The IEC Ratio Method stands as a key technique for the interpretation of DGA results [60]. While it shares similarities with the Rogers' four-ratio method, it notably excludes the ethane-to-methane (C_2H_3/CH_4) ratio. Instead, the diagnostic process utilizes established gas concentration limits and their respective codes for three fundamental gaseous parameters: acetylene to ethylene (C_2H_2/C_2H_4), methane to hydrogen (CH_4/H_2), and ethylene to ethane (C_2H_4/C_2H_2), as specified in Table II.12. Furthermore, Table II.13 provides an extensive description of each fault type categorized according to these ratio-based codes

Table II.12 IEC code

Ratio Codes	Range	Code
R1 = CH_4/H_2	$R1<0.1$	1
	$0.1\leq R1\leq 1$	0
	$R1>1$	2
R2 = C_2H_2/C_2H_4	$R2<0.1$	0
	$0.1\leq R2\leq 3$	1
	$R2>3$	2
R3 = C_2H_4/C_2H_6`	$R3<1$	0
	$1\leq R3\leq 3$	1
	$R3>3$	2

Table II.13 Fault diagnosis using IEC code

N	Fault type	code		
1	No Fault	0	0	0
2	Partial discharge with low energy density	0	1	0
3	Partial discharge with high energy density	1	1	0
4	discharge of low energy	1.2	0	1.2
5	discharge of high energy	1	0	2
6	Overheating T<150 °C	0	1	0

7	Overheating 150<*T*<300 °C	2	1	0
8	Overheating 300≤ *T*≤ 700 °C	2	1	0
9	Overheating ≥ 700 °C	2	2	2

II.3.2.4 CIGRE Ratio Method:

The CIGRE ratio method [48] proposed by CIGRE Working Group 15.01.01 uses five specific gas ratios acetylene-ethane (C_2H_2/C_2H_3), hydrogen-methane (H_2/CH_4), ethylene-ethane (C_2H_4/C_2H_6), acetylene- hydrogen (C_2H_2/H_2), and carbon dioxide to carbon monoxide (CO_2/CO) to detect transformer failures, including electrical faults, thermal problems, and solid insulation problems. These ratios are outlined in detail in Table II.14.

Table II.14 Determination of the type of fault according to the CIGRE ratio method

Ratio	limit	Fault type
C_2H_2/C_2H_6	≥ 1.0	Arcing
H_2/CH_4	≥ 10.0	Partial discharges
C_2H_4/C_2H_6	≥ 1.0	Thermal fault
C_2H_2/H_2	≥ 2.0	Discharges in OLTC
CO_2/CO	≥ 10.0	Overheating, paper
	< 3.0	Cellulose decomposition due to electrical fault

When all the gas ratios fall within the specified limits provided in Table II.14 [3], the transformer is deemed to be in normal condition. CIGRE ratio method is often used in conjunction with the CIGRE Key Gas Method, with their combined identification framework described in Table II.15 [56]. The CIGRE methods employ a letter-coding system to classify gas concentrations and ratios. "K1" indicates that all key gases are below the concentration limits in Table II.4, while "K2" shows that at least one gas exceeds these limits. For gas ratios, "R1" means all values are within the limits in Table II.14, and "R2" signals that at least one ratio surpasses these limits.

Table II.15 identification procedures using CIGRE ratios and major gas methods

Ratios	Key gases	Explanation
R1	K1	No action, transformer most probably healthy
R2	K2	Transformer most probably faulty, additional analyses needed
R2	K1	Possible incipient failure, additional analyses needed

R1	K2	Possibility of more than one failure, further investigations needed

II.3.2.5 SOU-N EE 46.501: 2006 method:

The SOU-N EE 46.501:2006 method, established as a standard in 2007, serves as a guideline for conducting DGA within the Ukrainian power engineering sector. This method allows for the identification of various fault conditions through the analysis of gas ratio ranges, as detailed in Table II.16 [57].

In addition to detecting 6 fundamental faults defined by the IEC, the method also identifies the normal operating condition and creeping discharges (D3), which are discharges occurring on the surface and within the solid insulation. Thise ratios used in this method are based on those initially proposed in the Russian Standard RD 153-34.0-46.302-00, introduced in 1989 and later revised in the 2001 standard. The diagnostic criteria employed in the SOU-N EE 46.501:2006 method align with the ratio-based approach of the RRM/IEC methods, offering nine diagnostic outcomes. However, the specific ratio ranges for these diagnoses differ from those used in the RRM/IEC approach.

Table II.16 Identification scheme according to SOU-N EE 46.501:2006

Fault type	C_2H_2/C_2H_4	CH_4/H_2	C_2H_4/C_2H_6
No fault	no significant	0.1 – 1.0	< 0.2
PD	no significant	< 0.1	< 0.2
D1	> 1.0	0.1 – 0.5	> 1.0
D2	> 1.0	0.1 – 1.0	> 2.0
D3	< 1.0	0.3 – 0.5	> 5.0
T12	Not significant	> 1.0	< 1.0
T2	Not significant	> 1.0	1.0 – 4.0
T3	< 0.2	> 1.0	> 4.0

II.3.2.6 ETRA ratios method:

The ETRA Ratios Method utilizes three distinct gas ratios derived from the concentrations of ethane (C_2H_6) , ethylene (C_2H_4), and acetylene (C_2H_2) to diagnose the six fundamental faults established by the IEC. As referenced in [63], the specific coding system and corresponding diagnostic interpretations are systematically presented in Tables II.17 and II.18. This methodology offers a highly efficient and streamlined framework for the interpretation of DGA data within transformer maintenance and fault diagnostic protocols.

Table II.17 Gas ratio coding using ETRA ratio method

Ratio	Range	Code
$R_1 = C_2H_2/C_2H_4$	$R_1 \leq 0.01$	0
	$0.01 < R_1 < 0.2$	1
	$R_1 \geq 0.2$	2
$R_2 = C_2H_2/C_2H_6$	$R_2 \leq 0.01$	0
	$0.01 < R_2 < 1.0$	1
	$1.0 \leq R_2 < 10.0$	2
	$R_2 \geq 10.0$	3
$R_3 = C_2H_4/C_2H_6$	$R_3 < 1.0$	0
	$1.0 \leq R_3 < 4.0$	1
	$4.0 \leq R_3 < 10.0$	2
	$R_3 \geq 10.0$	3

Table II.18 Reference explanation using ETRA ratio method

Fault type	R_1	R_2	R_3
Thermal fault, T> 700°C	0	0/1	2/3
Thermal fault, T< 300°C	0	0	0
Thermal fault, 300°C <T< 700°C	0	0/1	1
Partial discharge	2	1	0/1/2
Low-energy discharge	2	2	0/1/2
High-energy discharge	2	2	3
High-energy discharge	2	3	/

II.3.2.7 Hyosun cooperation ratio:

The Hyosung Corporation Ratios Method [64], introduced in 2013 by a group of South Korean researchers from HYOSUNG Company in collaboration with the scientist Michel Duval, represents a significant advancement in transformer fault diagnostics. This method utilizes 6 specific gas ratios, as outlined in Table II.19, to identify the six fundamental IEC faults.

Table II.19 Gas ratios used in the HYOSUN Corporation gas ratio method

Ratio	R1	R2	R3	R4	R5	R6
Expression	$\frac{CH_4}{H_2}$	$\frac{C_2H_2}{C_2H_4}$	$\frac{C_2H_2}{CH_4}$	$\frac{C_2H_6}{C_2H_2}$	$\frac{C_2H_4}{C_2H_6}$	$\frac{C_2H_4}{CH_4}$

The core concept of this technique involves using these gas ratios to distinguish between various types of transformer faults. The diagnostic process begins with the use of two gas ratios (R1 and R2) to differentiate between thermal faults and electrical faults. Once this distinction is made, each fault group can be analyzed independently. For thermal faults, T1 faults are separated from other thermal categories using gas ratios R5 and R6. When T1 faults are detected, the method employs gas ratio pairs (R2, R5) to differentiate between T2 and T3 faults. In the case of electrical (power) faults, the same two ratios (R2, R5) are used to distinguish among partial discharge (PD), D1, and D2 faults. The overall diagnostic process is visually illustrated in the flow chart shown in Figure II.4 [64].

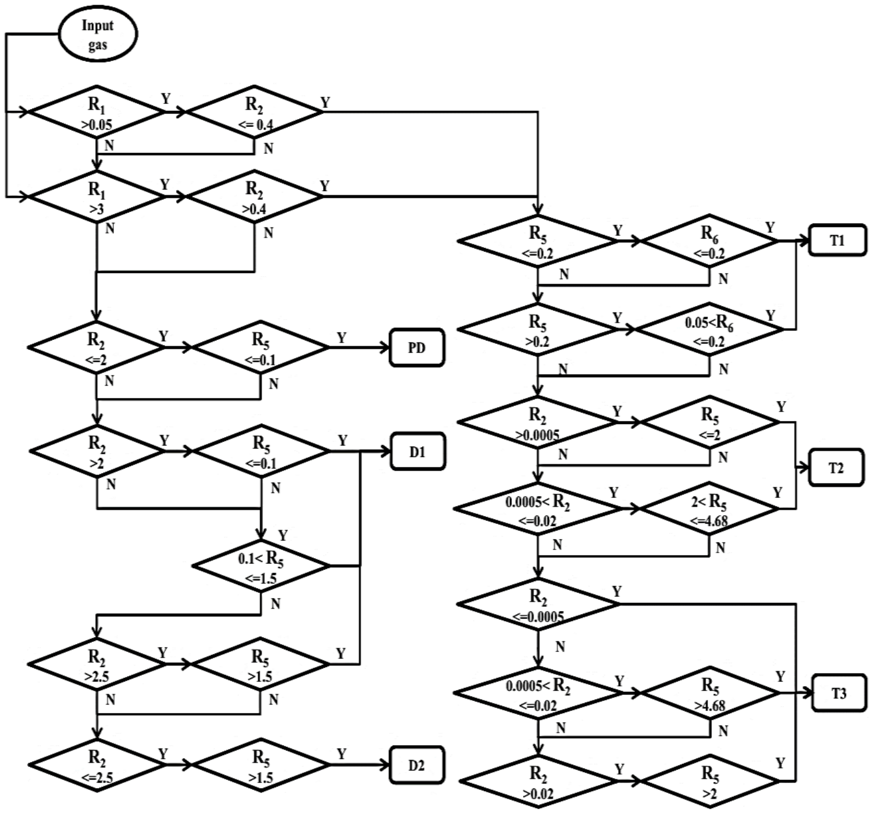

Figure II.3 Flowchart of gas ratio method of HYOSUN Corporation

II.3.2.8 Three Ratios Techniques:

Building upon existing gas analysis interpretation strategies, Gouda et al. introduced an advanced diagnostic approach known as the Three-Ratio Technique (TRT) [65]. This method incorporates three novel gas parameters specifically engineered to refine fault detection and magnitude assessment, as detailed in Table II.20 [66].

Table II.20 TRT codes

Ratio Codes	Range	Code
$R_1 = \frac{C_2H_2}{C_2H_4}$	R1 < 0.05	0
	0.05 ≤ R1 ≤ 0.9	1
	R1 > 0.9	2
$R_2 = \frac{(C_2H_6 + C_2H_4)}{(H_2 + C_2H_2)}$	R2 < 1	0
	1 ≤ R2 ≤ 3.5	1
	R1 > 3.5	2
$R_3 = \frac{(CH_4 + C_2H_2)}{C_2H_4}$	R3 < 0.05	0
	0.05 ≤ R3 ≤ 0.5	1
	R3 > 0.5	2

A primary fault detection framework, governed by various rules for identifying fault types and their severity, is presented in Table II.21 [66]. The TRT method operates on the fundamental principle that a gas concentration significantly higher than others may still reside within acceptable thresholds [66]. These standardized limits and normal operating conditions are cataloged in Table II.22 [66]. Ultimately, this analytical framework delivers a substantial improvement in both the reliability and diagnostic precision for power transformer monitoring.

Table II.21 Identify fault with TRT

Fault	type	R1	R1	R3
T > 700◦C	T3	1 or 2	0	0 or 1
300◦C < T < 700◦C	T2	1 or 2	1	0 or 1
150◦C < T < 300◦C	T1	1 or 2	2	0 or 1
Low temperature thermal T < 150◦C	T0	1	/	1
Low partial discharge	PD1	0	1 or 2	0 or 1
High partial discharge	PD1	0	1 or 2	2
High arcingdischarge	D2	0 or 1	0 or 1	2

Low arcingdischarge	D1	1 or 2	2	2
Mix of electrical and thermal fault	DT	2	0 or 1	2

Table II.22 Limit of dissolved gases concentrations for the TRT method application

Gas	H_2	CH_4	C_2H_6	C_2H_4	C_2H_2	CO	CO_2
Limt ppm	100	120	65	50	1	350	2500

II.3.3 graphical methods:

II.3.3.1 Duval triangle method:

The Duval Triangle Method (DTM) stands as the primary graphical alternative to traditional ratio-based techniques for interpreting dissolved gas analysis. Introduced by Canadian scientist Michel Duval in 1974 [67], this methodology utilizes three specific ratios (R1, R2, and R3) to plot a coordinate within a triangular graph, as illustrated in Figure II.5.

The triangle's geometry is partitioned into seven distinct diagnostic zones, each corresponding to specific faults: PD, D1, D2, DT, T1, T2, and T3. A fault is diagnosed based on the specific region where the plotted point resides [68]. Furthermore, Duval enhanced the original framework (Triangle 1) by introducing six additional triangles [69]. Notable among these are Triangle 4, optimized for low-temperature faults, and Triangle 5, designed for high-temperature thermal analysis [70], as shown in Figure II.6.

$$R1 = 100 * C4/CH4 + C2H4 + C2H2 \quad \text{(II.2)}$$

$$R2 = 100 * C2H2/\ CH4 + C2H4 + C2H2 \quad \text{(II.3)}$$

$$R3 = 100 * C2H4/\ CH4 + C2H4 + C2H2 \quad \text{(II.4)}$$

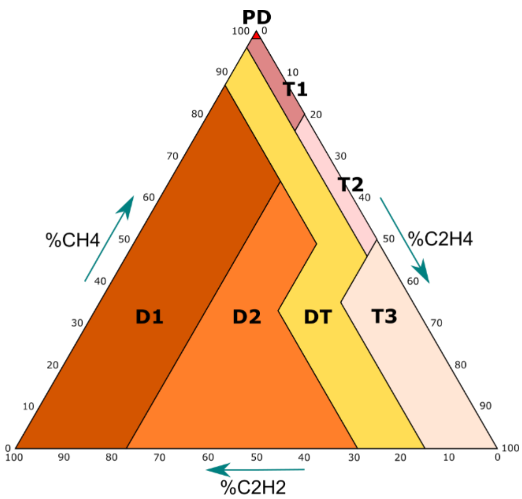

Figure II.4 Duval Triangle 1

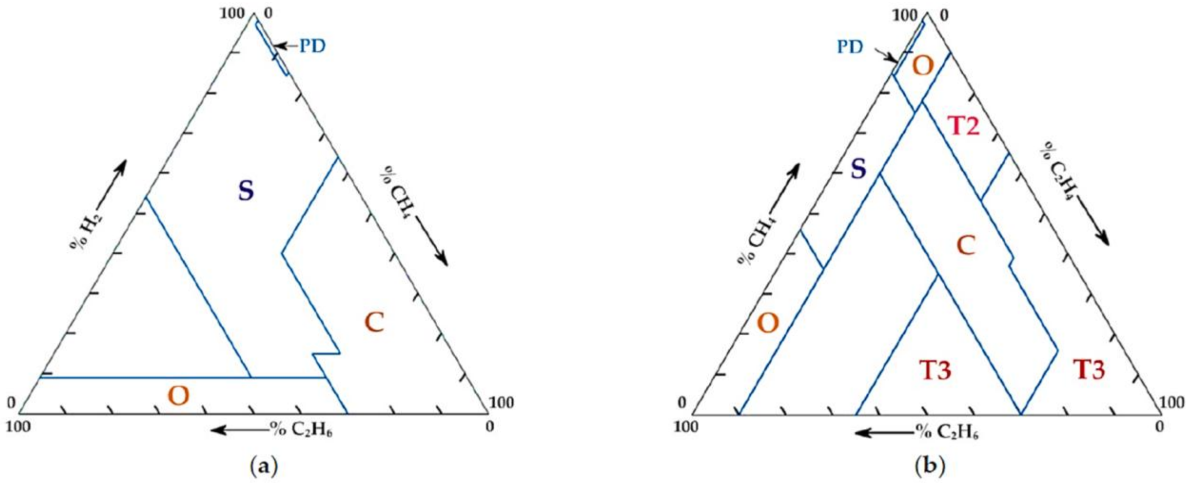

Figure II.5 (a) Duval 4 for a low-temperature fault (b) Duval 5 for a high-temperature fault

II.3.3.2 Duval Pentagon Method:

Developed by Duval and Lamarre [71], the Duval Pentagon Method serves as an advanced graphical framework for interpreting DGA results, as illustrated in Figure II.7. This technique utilizes a pentagonal chart featuring five axes, each representing the relative percentage (from 0% to 100%) of the five primary combustion gases: hydrogen (H_2), methane (CH_4), ethane (C_2H_3), ethylene (C_2H_4), and acetylene (C_2H_4).The Duval Pentagon is partitioned into six specialized diagnostic zones corresponding to thermal and electrical faults, with an additional distinct area for stray gases. The methodology is supported by a series of analytical equations used to calculate the specific coordinates within the pentagon, thereby enhancing the precision and reliability of DGA data interpretation.

$$\begin{cases} x_0 = \%H_2 \cos\left(\frac{\pi}{2}\right) \\ x_1 = \%C_2H_6 \cos\left(\frac{\pi}{2} + \frac{2\pi}{5}\right) \\ x_2 = \%CH_4 \cos\left(\frac{\pi}{2} + \frac{4\pi}{5}\right) \\ x_3 = \%C_2H_4 \cos\left(\frac{\pi}{2} + \frac{6\pi}{5}\right) \\ x_4 = \%C_2H_2 \cos\left(\frac{\pi}{2} + \frac{8\pi}{5}\right) \end{cases} \qquad \begin{cases} y_0 = \%H_2 \sin\left(\frac{\pi}{2}\right) \\ y_1 = \%C_2H_6 \sin\left(\frac{\pi}{2} + \frac{2\pi}{5}\right) \\ y_2 = \%CH_4 \sin\left(\frac{\pi}{2} + \frac{4\pi}{5}\right) \\ y_3 = \%C_2H_4 \sin\left(\frac{\pi}{2} + \frac{6\pi}{5}\right) \\ y_4 = \%C_2H_2 \sin\left(\frac{\pi}{2} + \frac{8\pi}{5}\right) \end{cases} \tag{II.5}$$

$$A = \frac{1}{2}\sum_{i=0}^{4}(x_i y_{i+1} - x_{i+1} y_i) \tag{II.6}$$

$$\begin{cases} X_C = \frac{\sum_{i=0}^{4}(x_i + x_{i+1})(x_i y_{i+1} - x_{i+1} y_i)}{6A} \\ Y_C = \frac{\sum_{i=0}^{4}(y_i + y_{i+1})(x_i y_{i+1} - x_{i+1} y_i)}{6A} \end{cases} \tag{II.7}$$

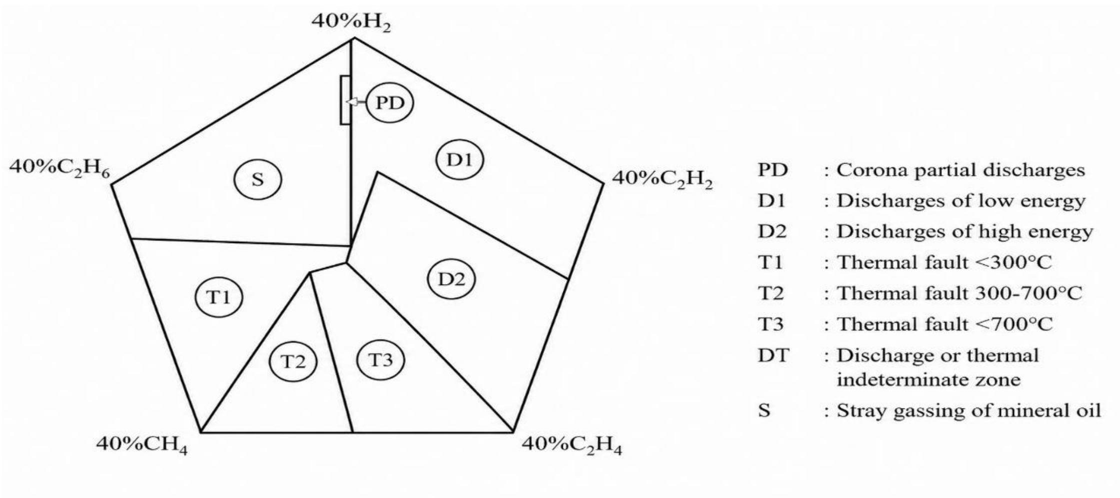

Figure II.6 Duval Pentagon Method

II.3.3.3 Mansour Pentagon Method:

In 2012, Mansour introduced the first graphical diagnostic framework in a pentagonal format [72], a methodology that was further refined in subsequent research [73]. This approach involves the construction of a pentagon where each vertex represents the percentage concentration of a specific gas relative to the total gas content.

Much like the Duval Pentagon, the Mansour Pentagon identifies six distinct diagnostic zones corresponding to various electrical and thermal malfunctions. However, the primary distinction lies in the specific coding system utilized for fault classification, as illustrated in Figure II.8. The method is governed by a series of analytical equations that define the relationship between gas concentrations and their respective geometric positions on the pentagon, thereby facilitating a precise and reliable fault diagnosis.

$$s = \sum_{i=5}^{5} P_i \quad \text{(II.8)}$$

$$P_{\%i} = \frac{P_i}{s} * 100 \quad \text{(II.9)}$$

$$\begin{cases} x_m = \dfrac{\sum_{i=1}^{n} P_{\%i} x_i}{P_{\%i}} \\ y_m = \dfrac{\sum_{i=1}^{n} P_{\%i} y_i}{P_{\%i}} \end{cases} \quad \text{(II.10)}$$

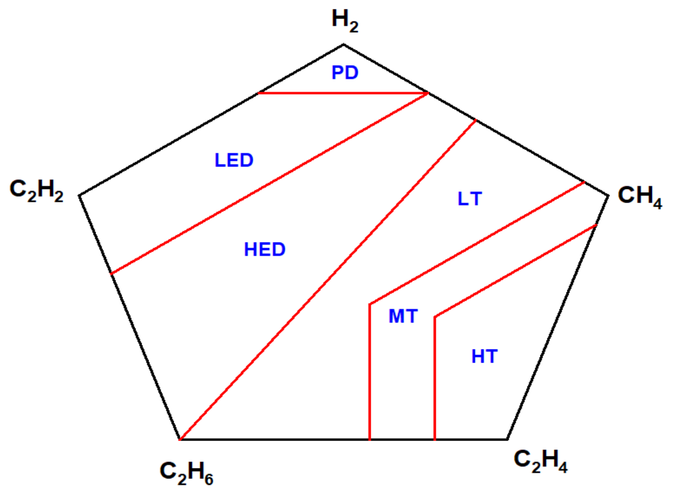

Figure II.7 Mansour Pentagon Method

II.3.3.4 Gouda Triangle Method:

The Gouda Triangle Method (GTM) is a sophisticated graphical diagnostic technique introduced by Gouda and a specialized research team [74]. This framework was specifically developed to refine the Duval Triangle Method by addressing its primary limitation: the reliance on only three diagnostic gases. The Gouda approach enhances fault identification by integrating two additional gases, hydrogen (H_2) and ethane (C_2H_6), into the analytical process.In the GTM framework, three ratios (R1, R2, and R3) are calculated and subsequently converted into percentage values (P1, P2, and P3). Each percentage corresponds to a vertex within a triangular coordinate system, forming a parallelogram-like structure. While it mirrors the Duval method in its triangular graphical representation and the definition of fault zones (as depicted in Figure II.9), the inclusion of a broader gas profile facilitates a more comprehensive and precise identification of transformer malfunctions.

$$\begin{cases} R_1 = \dfrac{CH_4}{CH_4 + C_2H_4 + C_2H_6 + C_2H_2} \\ R_2 = \dfrac{C_2H_2}{H_2 + C_2H_6 + CH_4 + C_2H_2} \\ R_3 = \dfrac{C_2H_4}{H_2 + C_2H_6 + CH_4 + C_2H_2} \end{cases} \tag{II.11}$$

$$\begin{cases} P_1 = \dfrac{R_1 \times 100}{R_3 + R_2 + R_1} \\ P_2 = \dfrac{R_2 \times 100}{R_3 + R_2 + R_1} \\ P_3 = \dfrac{R_1 \times 100}{R_3 + R_2 + R_1} \end{cases} \tag{II.12}$$

With

$$\begin{cases} x = 100 - P2 - P3\cos\left(\frac{\pi}{6}\right)\cot\left(\frac{\pi}{3}\right) \\ y = P3\cos\left(\frac{\pi}{6}\right) \end{cases} \quad \text{(II.13)}$$

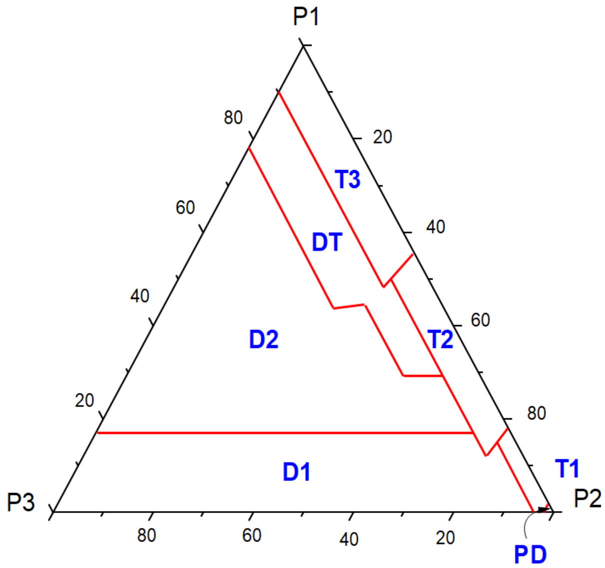

Figure II.8 Gouda Triangle method

II.3.3.5 Gouda heptagon method:

Introduced by Gouda et al. in 2018 [75], the Gouda Heptagon Method serves as a specialized graphical framework for diagnosing faults in oil-immersed power transformers. This methodology employs a heptagonal geometry where each segment represents the proportional concentration of seven key gases: hydrogen (H_2), methane (CH_4), ethylene (C_2H_4), ethane (C_2H_6), acetylene (C_2H_2), carbon monoxide (CO), and carbon dioxide (CO_2). These percentages are calculated using specific weighting factors provided in Table II.23 [75].The Gouda Heptagon is uniquely capable of identifying three distinct stages of cellulose degradation: High Concentration (HCCD), Medium Concentration (MCCD), and Low Concentration (LCCD). Furthermore, it encompasses the diagnosis of the six standard IEC faults and combined thermo-electrical malfunctions. As depicted in Figure II.10, this method provides a highly comprehensive diagnostic tool for detailed transformer fault investigation.

Table II.23 Main gas weighting factors in Gouda Heptagon Method

Key gas	H_2	C_2H_4	C_2H_6	CH_4	CO_2	CO	C_2H_2
Weighting factor	3.5	7	5.3846	2.9167	0.14	1	116.6667

$$H_2 = \frac{H_2 \times 3.5 \times 100}{(3.5 \times H_2) + (2.9167 \times CH_4) + (5.3846 \times C_2H_6) + (7 \times C_2H_4) + (116.6667 \times C_2H_2) + CO + (0.14 \times CO_2)} \quad \text{(II.14)}$$

$$\mathrm{CH_4} = \frac{\mathrm{CH_4} \times 2.9167 \times 100}{(3.5 \times \mathrm{H_2}) + (2.9167 \times \mathrm{CH_4}) + (5.3846 \times \mathrm{C_2H_6}) + (7 \times \mathrm{C_2H_4}) + (116.6667 \times \mathrm{C_2H_2}) + \mathrm{CO} + (0.14 \times \mathrm{CO_2})} \quad \text{(II.15)}$$

$$\mathrm{C_2H_6} = \frac{\mathrm{C_2H_6} \times 5.3846 \times 100}{(3.5 \times \mathrm{H_2}) + (2.9167 \times \mathrm{CH_4}) + (5.3846 \times \mathrm{C_2H_6}) + (7 \times \mathrm{C_2H_4}) + (116.6667 \times \mathrm{C_2H_2}) + \mathrm{CO} + (0.14 \times \mathrm{CO_2})} \quad \text{(II.16)}$$

$$\mathrm{C_2H_4} = \frac{\mathrm{C_2H_4} \times 7 \times 100}{(3.5 \times \mathrm{H_2}) + (2.9167 \times \mathrm{CH_4}) + (5.3846 \times \mathrm{C_2H_6}) + (7 \times \mathrm{C_2H_4}) + (116.6667 \times \mathrm{C_2H_2}) + \mathrm{CO} + (0.14 \times \mathrm{CO_2})} \quad \text{(II.17)}$$

$$\mathrm{C_2H_2} = \frac{\mathrm{C_2H_2} \times 116.6667 \times 100}{(3.5 \times \mathrm{H_2}) + (2.9167 \times \mathrm{CH_4}) + (5.3846 \times \mathrm{C_2H_6}) + (7 \times \mathrm{C_2H_4}) + (116.6667 \times \mathrm{C_2H_2}) + \mathrm{CO} + (0.14 \times \mathrm{CO_2})} \quad \text{(II.18)}$$

$$\mathrm{CO_2} = \frac{\mathrm{CO_2} \times 0.14 \times 100}{(3.5 \times \mathrm{H_2}) + (2.9167 \times \mathrm{CH_4}) + (5.3846 \times \mathrm{C_2H_6}) + (7 \times \mathrm{C_2H_4}) + (116.6667 \times \mathrm{C_2H_2}) + \mathrm{CO} + (0.14 \times \mathrm{CO_2})} \quad \text{(II.19)}$$

$$\mathrm{CO} = \frac{\mathrm{CO} \times 100}{(3.5 \times \mathrm{H_2}) + (2.9167 \times \mathrm{CH_4}) + (5.3846 \times \mathrm{C_2H_6}) + (7 \times \mathrm{C_2H_4}) + (116.6667 \times \mathrm{C_2H_2}) + \mathrm{CO} + (0.14 \times \mathrm{CO_2})} \quad \text{(II.20)}$$

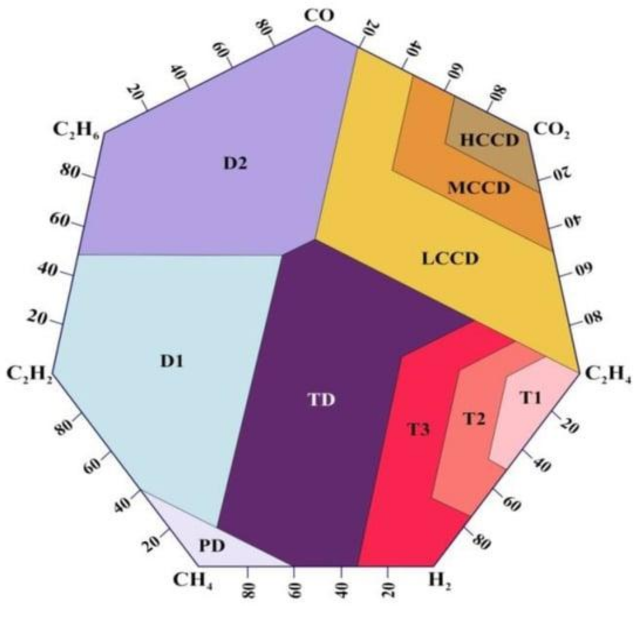

Figure II.9 Gouda's heptagon Method

II.3.3.6 Cartesian graphical method:

Proposed by Fathallah et al., the Cartesian Graphical Method [76] represents the most contemporary advancement in Dissolved Gas Analysis (DGA) and is esteemed as a state-of-the-art technique for transformer fault diagnosis. This methodology utilizes the concentration levels of four pivotal gases: hydrogen (H_2), methane (CH_4), ethylene (C_2H_4), and acetylene (C_2H_2). The framework involves the computation of three specific diagnostic ratios. These ratios are uniquely engineered to incorporate hydrogen (H_2) concentrations while simultaneously accounting for the influence of ethane (C_2H_6). The ratios are formulated as follows:

$$P_1 = \frac{\mathrm{CH_4} + \mathrm{H_2}}{2 \times \mathrm{H_2} + 2 \times \mathrm{CH_4} + \mathrm{C_2H_2} + \mathrm{C_2H_4}} \quad \text{(II.21)}$$

$$P_2 = \frac{\mathrm{C_2H_2} + \mathrm{H_2}}{2 \times \mathrm{H_2} + 2 \times \mathrm{CH_4} + \mathrm{C_2H_2} + \mathrm{C_2H_4}} \quad \text{(II.22)}$$

$$P_3 = \frac{C_2H_4 + CH_4}{2 \times H_2 + 2 \times CH_4 + C_2H_2 + C_2H_4} \qquad \text{(II.23)}$$

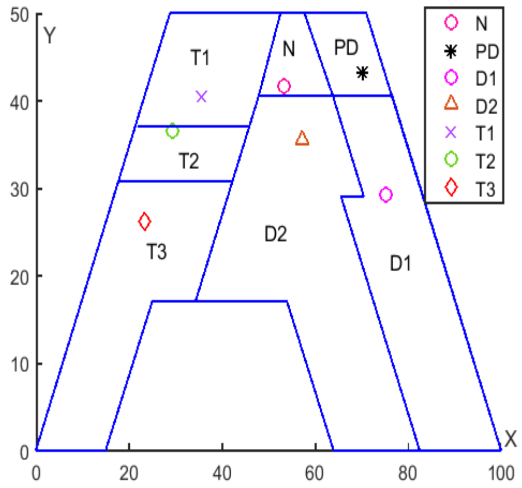

Figure II.10 Cartesian graphical Method

These ratios are subsequently used to determine the Cartesian coordinates $(x,y)$for graphical representation. The coordinates are computed as follows:

$$x_{\text{point}} = (P_2 + P_1 \times \sin{(30°)}) \times L \qquad \text{(II.24)}$$

$$y_{\text{point}} = (P_1 \times \sin{(60°)}) \times L \qquad \text{(II.25)}$$

Where L is a scaling factor.

The resulting coordinates allow for the visualization of fault types within a Cartesian graph, as shown in Figure II.11. This graph is splited into several zones wich represents different fault categories, including partial discharge (PD), low-energy discharge (D1), high-energy discharge (D2), and thermal faults (T1, T2, T3), along with a normal condition (N) zone. This method provides a refined and precise means of diagnosing faults through a straightforward graphical approach.

II.3.3.7 Circle Methods

The methods proposed by Hechifa et al. [78] are based on the use of advanced graphical techniques to analyze Dissolved Gas Analysis (DGA) data in order to achieve more accurate fault diagnosis in power transformers. These methods represent fault samples in a two- or three-dimensional space, where each sample corresponds to a transformer operating condition defined by gas concentrations. To enhance the discrimination between different types of faults, the coordinate axes of this space are dynamically rotated to obtain the best possible separation among fault clusters. This process is carried out using metaheuristic optimization algorithms such as the Gray Wolf Optimization (GWO) and the Whale Optimization Algorithm (WOA), which search for the optimal rotation angles that minimize the overlap between fault samples and maximize the distances between cluster centers. As a result, thermal faults and electrical faults can be more clearly distinguished. The mathematical formulation of this approach is provided in equations (25) and (26) of reference [5], giving the method a strong theoretical foundation and higher diagnostic reliability.

$$x_i = x_1 + x_2 - x_3 - x_4 + x_5 \quad (25)$$

. x_1=$\%H_2\cos(\theta 1)$. x_2=$\%CH_4\cos(\theta 2)$

. x_3=$\%C_2H_6\cos(\theta 3)$. x_4=$\%C_2H_4\cos(\theta 4)$

. x_5=$\%C_2H_2\cos(\theta 5)$

$$x_i = \%H_2\cos(\theta 1) + \%CH_4\cos(\theta 2) - \%C_2H_6\cos(\theta 3) - \%C_2H_4\cos(\theta 4) + \%C_2H_2\cos(\theta 5) \quad (25)$$

$$y_i = y_1 + y_2 + y_3 - y_4 - y_5 \quad (26)$$

. $y_1 = \%H_2\sin(\theta 1)$. $y_2 = \%CH_4\sin(\theta 2)$

. $y_3 = \%C_2H_6\sin(\theta 3)$. $y_4 = \%C_2H_4\sin(\theta 4)$

. $y_5 = \%C_2H_2\sin(\theta 5)$

$$y_i = \%H_2\sin(\theta 1) + \%CH_4\sin(\theta 2) + \%C_2H_6\sin(\theta 3) - \%C_2H_4\sin(\theta 4) - \%C_2H_2\sin(\theta 5) \quad (26)$$

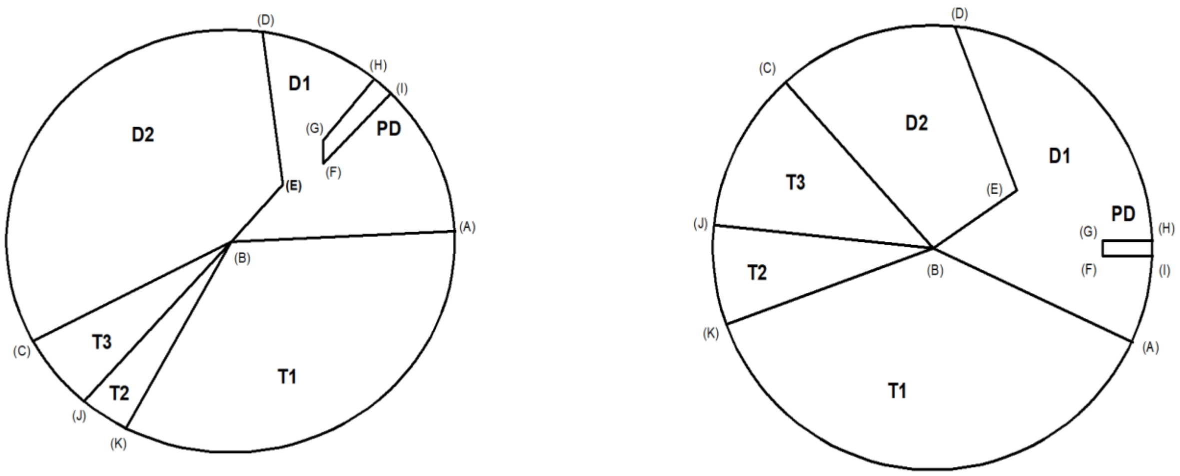

(a) (b)

Figure II.11 final Circle 1(a) and Circle 2(b)

II.4 Conclusion

The precise identification of primary faults in power transformers is paramount for establishing proactive maintenance strategies that align accurately with the actual operational health of the equipment, ensuring the continuity of the electrical grid. While maintenance practitioners rely heavily on conventional methodologies, the deep analytical review conducted in this chapter reveals a clear disparity in the efficiency of these tools. Consequently, the diagnostic frameworks were categorized into four core techniques: Key Gas methods, Gas Ratios, Graphical methods, and Combined hybrid systems.

The study demonstrates that while ratio-based methods (such as RRM and IEC) offer mathematical precision, they often face limitations when results fall outside standardized coding ranges—a challenge effectively addressed by graphical methods (such as Duval's triangles/pentagons and Gouda's heptagon) through their ability to provide a comprehensive visual diagnosis covering all fault probabilities, including cellulose degradation. Furthermore, modern combined techniques (such as the Ward and Fathallah methodologies) have emerged as a leading trend, aiming to minimize the margin of error by integrating multiple criteria into a single diagnostic framework, thereby providing the necessary reliability for critical maintenance decision-making. This critical examination of the merits and constraints of each technique not only provides a holistic view of their effectiveness but also establishes the foundation for selecting an optimal model that synthesizes ratio precision with graphical comprehensiveness, which will be tested and applied in the subsequent phases of this study.

Chapter III

Chapter III: Artificial Intelligence (AI)

III.1 Introduction

The theoretical foundations of machine learning are deeply rooted in a robust mathematical structure that includes statistics, probability theory, linear algebra, and optimization theory. These are essential pillars for understanding the dynamics of classification and regression algorithms, particularly when dealing with high-dimensional or nonlinear data that traditional analytical models fail to capture [3]. In this context, machine learning algorithms have demonstrated a superior ability to enhance diagnostic accuracy by exploring latent patterns and interrelated relationships that cannot be detected through conventional rule-based methods. The reliance on these data-driven models has created high flexibility in adapting to varying operating conditions, allowing for a transition from manual and graphical diagnostic methods to automated frameworks that enhance decision reliability and reduce dependence on human expertise alone, especially in complex engineering systems [5].

In its essence, Artificial Intelligence is considered the natural extension of this development, as it is classified as one of the most prominent branches of modern computer science aimed at simulating human cognitive abilities such as learning, reasoning, and problem-solving. According to the Encyclopaedia Britannica, artificial intelligence transcends mere traditional programming to focus on the systems' ability to adapt to new inputs and analyze complex information based on experience. The credit for formulating this concept dates back to the Dartmouth Conference in 1956, where John McCarthy established the scientific vision to transform computers from mere computational tools into systems capable of cognitive processing. Since then, the field has undergone several developmental stages, beginning with symbolic models and progressing toward advanced statistical models and neural networks, enabling it to permeate vital sectors such as healthcare, industrial automation, and smart transportation, becoming a fundamental pillar of contemporary digital transformation.

With this widespread proliferation, an urgent need has emerged to address the ethical and legal challenges resulting from the use of these technologies, particularly regarding data privacy, algorithmic bias, and accountability for automated decisions. This technological momentum necessitates the formulation of legal and ethical frameworks that ensure the responsible and safe use of artificial intelligence, ensuring the alignment of technical progress with human and societal standards, and achieving a balance between innovation and the legal protection of users.

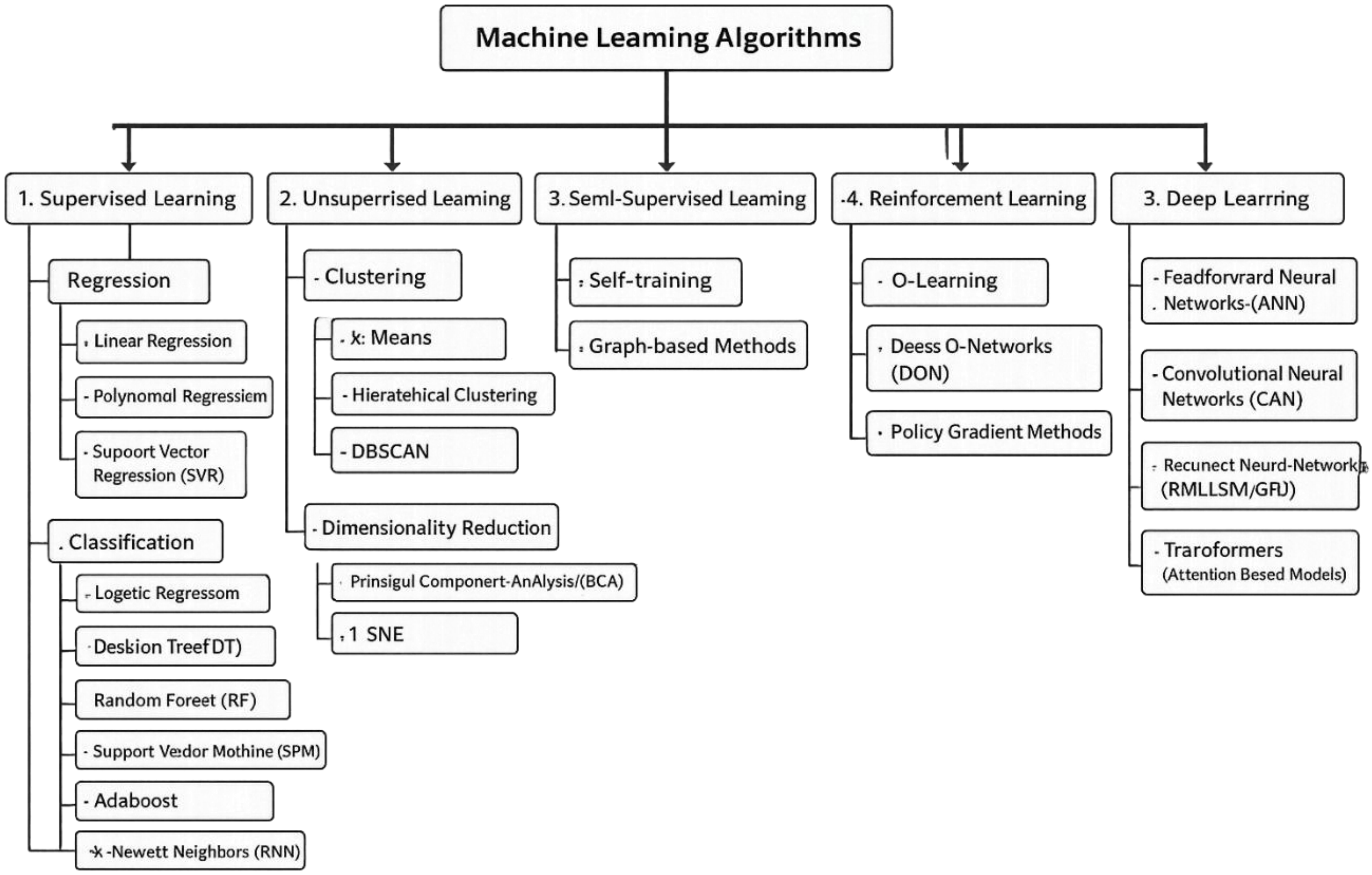

Figure III.1 General Classification of Machine Learning Algorithms and Their Core Models

Through this diagram, we will address the concepts of Machine Learning and Neural Networks. We will also focus on explaining the following algorithms: SVM, AdaBoost, Random Forest, and ANN.

III.2. Theoretical Foundations of Machine Learning (ML)

Machine Learning (ML) is considered a fundamental pillar of Artificial Intelligence, as it focuses on the development of computational models capable of improving their performance autonomously through learning from data, rather than relying on explicit programming. Unlike traditional approaches that depend on predefined rules, ML relies on analyzing data to extract hidden patterns and relationships, enabling it to perform tasks such as prediction, classification, and decision-making with high efficiency [1][2].

This field is inherently interdisciplinary, integrating applied mathematics, statistics, optimization theory, and computer science to design models with strong generalization capabilities, i.e., the ability to effectively handle unseen data that were not encountered during the training phase. This characteristic is a key factor distinguishing effective machine learning models [1][3].

From a mathematical perspective, most machine learning problems are formulated as optimization tasks aimed at minimizing a loss function, which quantifies the discrepancy between predicted and actual values. These problems are solved using various optimization algorithms. In addition, regularization techniques are employed to mitigate overfitting by balancing model accuracy and complexity, particularly in scenarios involving limited or noisy data [2][3].

Owing to this solid theoretical foundation, machine learning demonstrates a strong ability to handle complex, nonlinear, and high-dimensional systems. Consequently, it has become a powerful tool in advanced engineering applications, particularly in intelligent diagnostic systems and decision-support systems that require high levels of accuracy and reliability [3][4].5

III.2.1 Types of Machine Learning

III.2.2.1 Supervised Learning Concept

Supervised learning is considered one of the most widely used paradigms in machine learning, as it relies on training models using pre-labeled data to infer the relationship between input variables and corresponding outputs. During the training process, algorithms benefit from feedback obtained by comparing predicted values with actual outcomes, which helps progressively improve model performance and enhances its ability to generalize to new, unseen data .

This approach provides an effective framework for developing highly accurate intelligent systems, particularly in applications that require precise classification and clear interpretability of results. Therefore, supervised learning is widely employed in decision-support systems and engineering diagnostics, including fault analysis in complex systems, due to its ability to achieve a balance between accuracy and reliability [1][2][3].

III.2.2.2 Unsupervised Learning

Unsupervised learning is considered one of the fundamental paradigms in machine learning, where algorithms rely on unlabelled data without requiring known output labels. Rather than being guided by correct answers, these algorithms aim to explore the latent patterns and structures within the input data, including identifying relationships, clusters, and underlying distributions.

In contrast to supervised learning, unsupervised learning focuses on uncovering hidden structures and internal representations in the data, rather than predicting specific outputs. These methods serve as effective tools in a wide range of practical applications, such as customer behavior analysis, image and text processing, fraud detection, and the organization of large datasets. They are particularly valuable when labeled data are limited or difficult to obtain, making them a powerful approach for exploratory data analysis and for understanding the internal structure of complex systems [1][2][3].

III.2.2.3 Reinforcement Learning

Reinforcement Learning (RL) constitutes one of the fundamental pillars of machine learning, as it focuses on studying sequential decision-making processes through the interaction of an intelligent agent with a dynamic and evolving environment [1]. Unlike supervised learning approaches that rely on labeled datasets, the agent in this paradigm is not provided with predefined correct outputs for each state. Instead, it adopts a trial-and-error learning strategy, evaluating its actions based on feedback signals in the form of rewards or penalties [1][2].

The primary objective of this framework is to enable the agent to derive an optimal policy that maximizes the cumulative long-term reward

Moreover, this framework reflects the agent's ability to achieve an effective balance between exploration of the environment and exploitation of acquired knowledge [1]. This trade-off is a critical factor in designing models capable of making efficient sequential decisions in uncertain and complex environments [2][3].

Thanks to this conceptual foundation, reinforcement learning provides a powerful framework for developing intelligent systems with adaptive capabilities and dynamic decision-making skills. Consequently, it has become highly suitable for advanced applications, including automatic control systems, adaptive systems, and fault diagnosis in complex engineering systems [2][3].

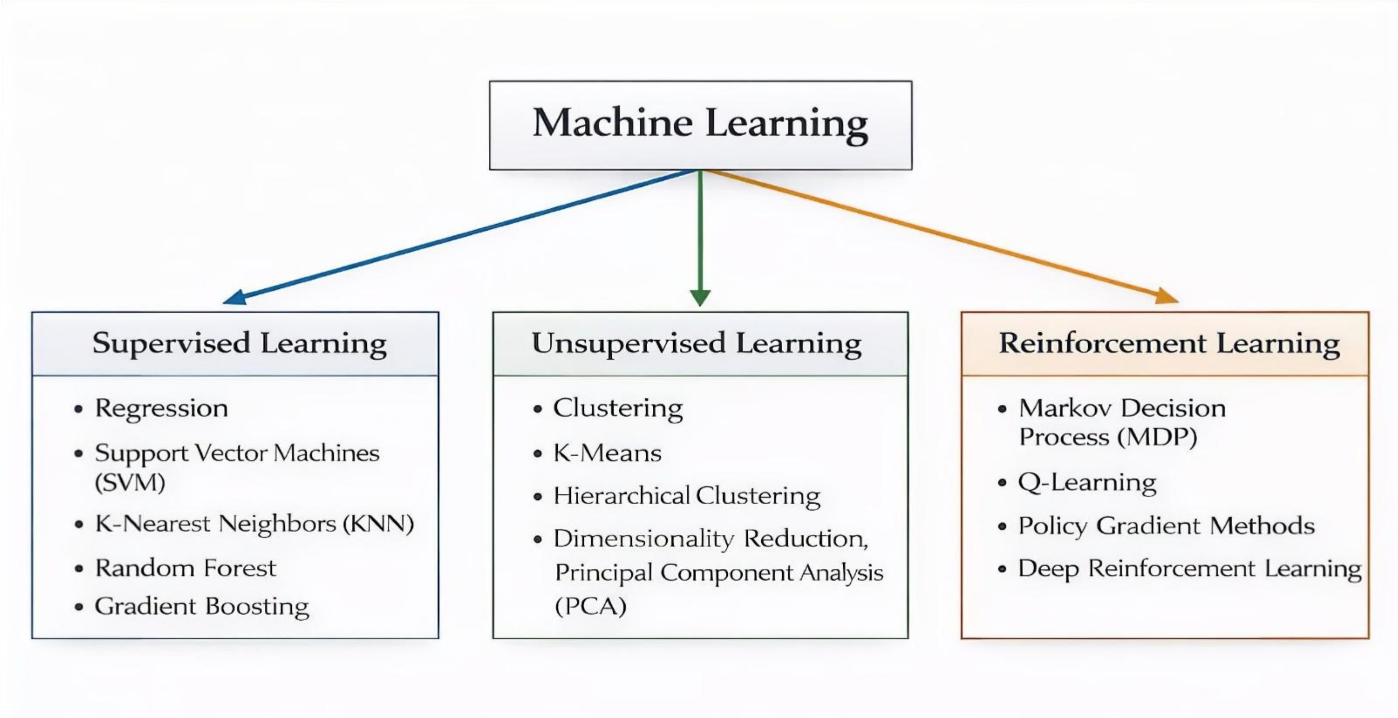

Figure III.2 : Taxonomy and Paradigms of Machine Learning Methods

III.3 Deep Learning

Deep Learning (DL) is a subfield of machine learning that leverages multi-layered Artificial Neural Networks (ANNs) to learn data representations hierarchically and autonomously. This approach enables models to extract complex features directly from raw data without the need for manual feature engineering, making it highly effective in processing high-dimensional data such as images, audio, and natural language. Compared to traditional machine learning models, deep learning is distinguished by its ability to automatically detect hierarchical and intricate patterns, facilitating the efficient handling of massive and diverse datasets. Source (Ian Goodfellow, Yoshua Bengio, Aaron Courville, MIT Press, 2016)

III.4 Ensemble Learning

Ensemble learning represents a paradigm shift in the philosophy of machine learning, transcending the logic of a single model to adopt a collaborative vision based on the idea of "wisdom of the crowd" [1]. This approach relies on aggregating multiple base learners within a unified integrative framework, aiming to develop a final model that outperforms any of its individual components in terms of accuracy and stability [2]. This proposition is grounded in well-established theoretical foundations, whereby the sophisticated combination of models contributes to addressing the classical bias-variance trade-off, thereby enhancing generalization capability and mitigating overfitting to training data [3].

This theoretical construct is built upon three fundamental and integrated pillars

III.4.1 Base Learners

These constitute the first building block of this construct, which can take two forms: either homogeneous, such as relying on a collection of decision trees, or heterogeneous, such as combining different models like Support Vector Machines, Artificial Neural Networks, and decision trees, thereby enriching the learning process through diversity.[4]

III.4.2 Diversity Mechanism

This represents the mechanism responsible for creating cognitive differentiation among the constituent models. It is achieved through various techniques, such as bootstrap sampling, introducing subtle variations to hyperparameters, or employing algorithms with different theoretical foundations.[5]

III.4.3 Aggregation Strategy

This forms the final integration vessel for the outputs of the various learners. Its mechanisms vary according to the task nature: for classification, majority voting is adopted; for regression, averaging is used; while in stacking, a meta-learner is employed to learn the optimal combination of predictions ,6] .[7

Ensemble learning techniques are classified in the specialized literature into three main approaches:

·Bagging: Exemplified by the "Random Forest" algorithm, which involves training parallel models on bootstrap samples drawn from the original data, aiming to tame high variance.[8]

· Boosting: Represented by the "AdaBoost" algorithm, which adopts the philosophy of sequential corrective learning, where each subsequent learner focuses on addressing the shortcomings left by its predecessor [9].

III.5 Study of Proposed Classification Algorithms

III 5.1 Support Vector Machine (SVM)

Support Vector Machines (SVM) represent an advanced paradigm within supervised learning algorithms, with mathematical origins tracing back to the theoretical frameworks established by Vapnik. The competitive advantage of this algorithm lies in its ability to derive an optimal hyperplane that ensures maximum class separation by maximizing the margin between the nearest training points, known as support vectors. The robustness and superior generalization capability of this model have established it as a pivotal tool in knowledge discovery and data mining, particularly due to its adaptability to both linear and complex non-linear patterns through kernel techniques [135]. Figure (IV.2) illustrates the functional architecture of the algorithm in identifying the optimal separating hyperplane, which is mathematically formulated by the following equation:

$$f(x)=w^{T}x+b \quad \text{for all } i \qquad \text{(III.1)}$$

Where w is the weight vector, x is the input feature vector, and b is the bias. The objective is to maximize the margin 2‖w‖ between the classes, subject to the constraints w is the weight vector, x is the input feature vector, and b is the bias. The objective is to maximize the margin $\frac{2}{\|w\|}$ between the classes, subject to the constraints:

$$\boldsymbol{w}^{\mathrm{T}}\boldsymbol{x}_i+\boldsymbol{b})\geq \mathbf{1} \qquad \text{(III.2)}$$

y_i the effectiveness of Support Vector Machines (SVM) largely depends on the selection of the Kernel Function, which enables the transformation of the input space into a higher-dimensional feature space. This transformation allows the model to perform linear discrimination efficiently, even when dealing with complex or nonlinear data [136].

Kernel Trick can be represented as

$$K(xi,xj)=\phi(xi)^{\mathrm{T}}\,\phi(xj) \qquad \text{(III.3)}$$

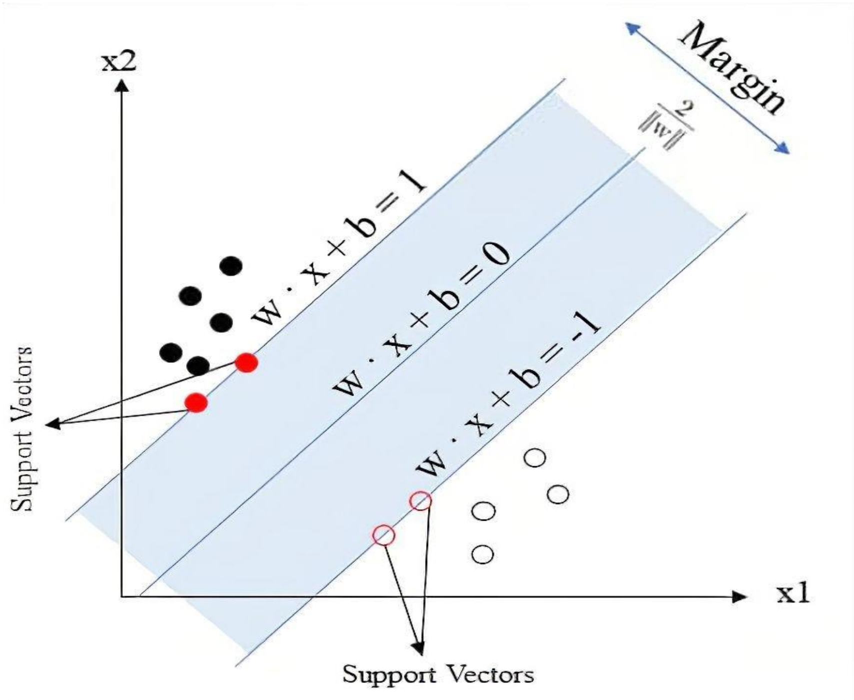

Figure III.3 Enhanced Hyperplane Optimization in SVM for High-Dimensional Data Classification.

III 5.2 k-Nearest Neighbors (k-NN)

The K-Nearest Neighbor (KNN) algorithm is considered one of the simplest learning algorithms, as it does not rely on a traditional training phase. Instead, it stores the training data and uses it directly during the classification process. Its mechanism is based on calculating the distance between a query point and the data points in the dataset, then selecting the closest k points. The class label assigned to the new point is determined by the class that appears most frequently among these nearest neighbors.

This can be mathematically expressed as:

$$\mathrm{y}^\wedge = \mathrm{argmaxc}\sum_{j=1}^{K} l(yj = c) \qquad \text{(III.4)}$$

where I is an indicator function that equals 1 if the class label y_j matches c and 0 otherwise. The distance between points is often measured using Euclidean distance:

$$\sqrt{(\text{ixi-y})^2 \sum_{i=1}^{n} = d(x,y)} \qquad \text{(III.5)}$$

This method enhances the classification process by extending the nearest neighbor concept, allowing the algorithm to leverage more information from multiple nearby points during the d

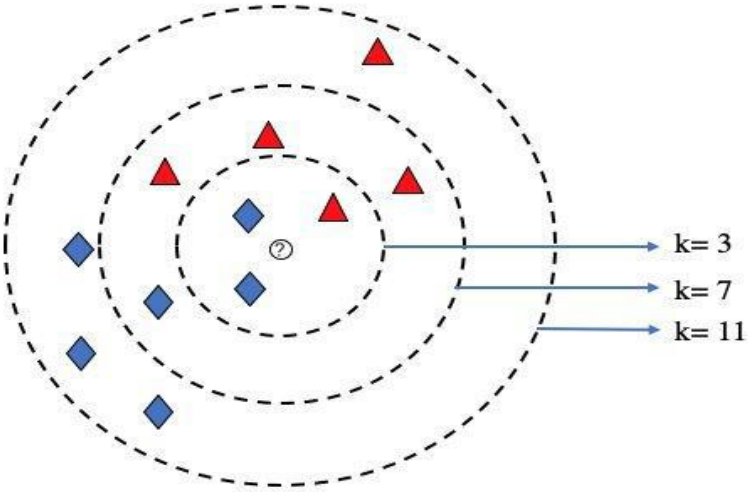

Figure III .4 Principle of KNN algorithm with different k value

III 5.3 Random Forest Algorithm

The Random Forest (RF) algorithm, introduced by Breiman in 2001 [99], is classified as one of the most prominent ensemble learning models based on the bagging methodology. This algorithm has gained a prestigious standing in research circles due to its statistical robustness and high operational efficiency, as well as its flexibility in processing complex data [100, 101].

The structural architecture of this model relies on generating a collection of independent decision trees, where each tree is constructed using a random vector derived from the original training data, ensuring a consistent statistical distribution across all components of the forest. The model's predictive accuracy is achieved through the bootstrap aggregation mechanism, coupled with the random selection of features to reduce correlation between trees and mitigate the issue of overfitting [102]. In the context of classification tasks, the final decision is derived via a voting mechanism or arithmetic averaging, which can be mathematically formulated as follows:

$$\hat{y} = \frac{1}{T}\sum_{t=1}^{T} ht(x)$$

Where:

T is the total number of trees.

$h_t(x)$ is the prediction of the $t\text{-}th$ tree for input x.

The final prediction $\hat{y}$ is obtained by averaging the predictions of all trees (for regression) or by majority voting (for classification).

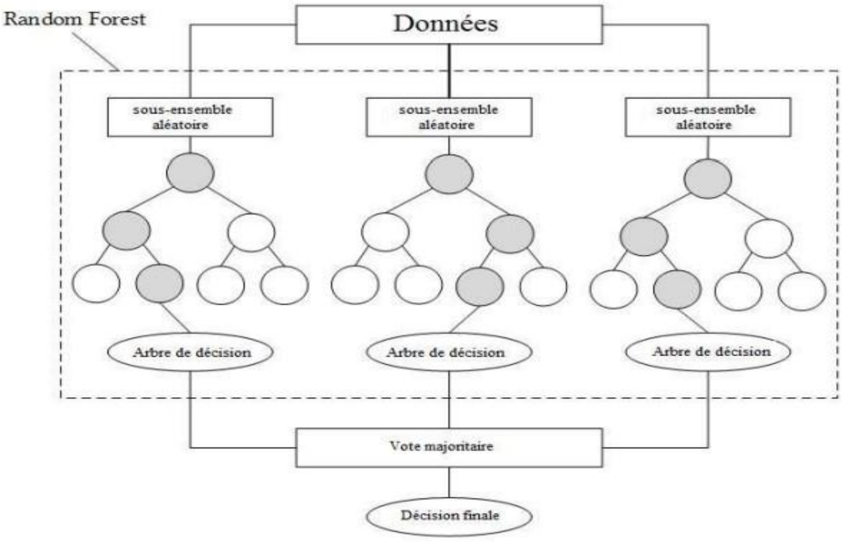

Figure III.5 Exemple de Random Forest

III 5.4 AdaBoost Ensemble

AdaBoost (Adaptive Boosting) is a sequential ensemble learning algorithm introduced by Yoav Freund and Robert Schapire. It is designed to improve the performance of weak learners by combining them into a strong classifier. The algorithm iteratively adjusts the weights of training samples, emphasizing those that are misclassified in previous iterations. As a result, subsequent models focus more on difficult cases, leading to improved overall accuracy and generalization capability

Unlike traditional learning methods, AdaBoost assigns a weight to each training instance and updates these weights dynamically after each iteration. Weak learners are trained sequentially, and each learner contributes to the final model with a weight proportional to its accuracy

The final strong classifier in AdaBoost can be expressed as .

. AdaBoost Model (Weighted Sum of Classifiers)

In AdaBoost, the final model is expressed as a weighted linear combination of the weak learners. Each individual classifier is assigned a specific weight (α_t) that reflects its accuracy and the model's overall confidence in its prediction:

$$H(x) = sign(\sum_{t=1}^{T} \propto (t)h(t)(x)) \quad \text{(III.10)}$$

Where:

- H(x): is the final prediction of the strong ensemble classifier for sample x.
- T: is the total number of weak learners (iterations).

- $h_t(x)$: represents the output of the t-th weak learner (typically $\pm$ 1).
- α_t :is the weight assigned to classifier t, calculated based on its training error rate.

. Classification Decision for Binary Classes

Unlike XGBoost, which relies on probability estimation via the Sigmoid function, traditional AdaBoost utilizes a "weighted voting" mechanism. The final class assignment is determined by the sign of the weighted sum:

$$y = sign(H(x)) \tag{III.11}$$

Where:

- If the weighted sum is positive, the sample is assigned to the positive class (+1).
- If the weighted sum is negative, the sample is assigned to the negative class (-1).
- The data weights D_t are updated at each step to ensure the model focuses on the most challenging samples.

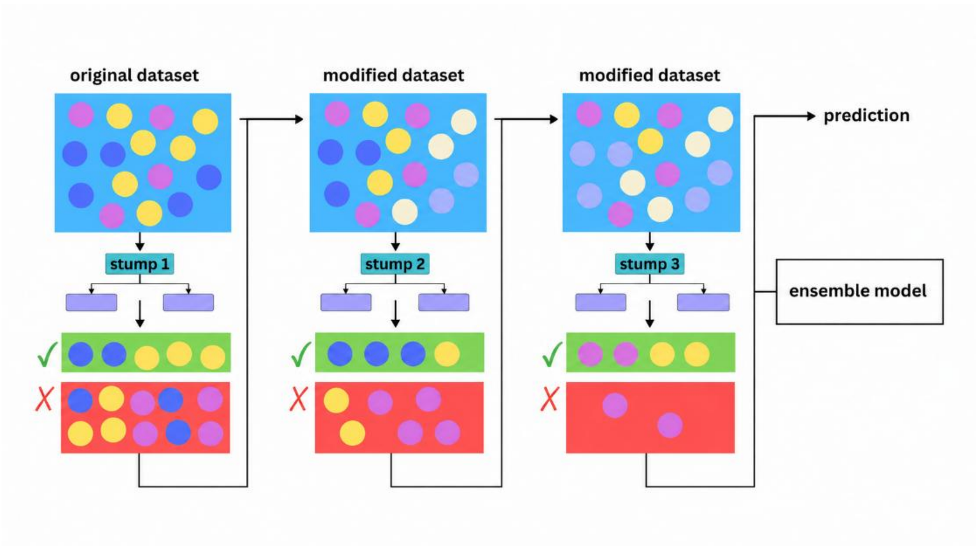

Figure III.6 The Structural Framework of the AdaBoost Algorithm

III.6 Statistical Indicators for Performance Evaluation in Classification

Performance evaluation constitutes a fundamental step in the development of machine learning models, as it aims to assess the model's effectiveness in accurately classifying data into their respective target categories. These evaluation metrics enable researchers to systematically compare different algorithms, identify the strengths and weaknesses of each model, and make informed decisions to enhance performance prior to the model's final deployment..

III. 6.1. Confusion Matrix

The confusion matrix is considered the primary structural tool for summarizing prediction outcomes in classification tasks. In the context of binary classification, the matrix consists of four fundamental components that represent the intersection between actual class labels and predicted class labels:

	Predicted Positive	Predicted Negative
Actual Positive	True Positive (TP)	False Negative (FN)
Actual Negative	False Positive (FP)	True Negative (TN)

- True Positive (TP): Instances that the model predicted as positive and are actually positive.
- True Negative (TN): Instances that the model predicted as negative and are actually negative.

- False Positive (FP): Instances that the model predicted as positive but are actually negative (Type I error).
- False Negative (FN): Instances that the model predicted as negative but are actually positive (Type II error).

III .6.2 Accuracy

is defined as the percentage of total correct predictions (both positive and negative) out of the total number of samples, and it is calculated using the following equation:

Accuracy=$\frac{TP}{TP+TN+FP+FN}$

Interpretation:

- High accuracy → The majority of predictions (both positive and negative) are correct.
- Low accuracy → A significant portion of predictions are incorrect.
- Methodological Note: Although this metric is widely used, it can be misleading in the case of imbalanced datasets, where the model tends to be biased toward the majority class.

III.6.3. Precision and Recall

- Precision: It measures the model's confidence when predicting the positive class, that is, the proportion of samples that are actually positive among all instances classified as positive by the model :

High precision indicates that the majority of samples classified as positive by the model are indeed correct, whereas low precision reflects a substantial proportion of incorrect positive predictions, commonly referred to as false alarms.

Precision = $\frac{TP}{TP+FP}$

. Recall (Sensitivity): Also referred to as Sensitivity, it measures the model's ability to identify all actual positive samples.

High recall reflects the model's ability to identify the vast majority of actual positive samples, whereas low recall indicates the model's failure to detect a substantial portion of positive instances.

Recall = $\frac{TP}{TP+FN}$

III.6.4 F1-Score

The F1-Score represents the harmonic mean of Precision and Recall and provides a balanced assessment of a model's performance, particularly in cases of imbalanced classes, where using Precision or Recall alone may not fully capture the model's effectiveness. It is mathematically defined as follows:

$F1 = 2 \cdot \frac{P \cdot R}{P+R}$. P = Precision . R = Recall

III.6. 5 ROC Curve and Area Under the Curve (AUC)

The Receiver Operating Characteristic (ROC) curve provides a visual tool for evaluating a classifier's performance across all possible decision thresholds by plotting the relationship between:

- True Positive Rate (TPR): equivalent to Recall.
- False Positive Rate (FPR): calculated as

$$FPR = \frac{FP}{FP + TN}$$

The Area Under the Curve (AUC) represents a numerical value ranging from 0 to 1, where values closer to 1 indicate the model's superior ability to discriminate between different classes.

Criteria for Selecting the Appropriate Metric

The choice of the most suitable evaluation metric depends on the nature of the data and the objective of the study:

- Balanced datasets: Accuracy is generally sufficient.
- Medical diagnosis: Priority is given to Recall to minimize the likelihood of missing positive cases (False Negatives, FN).
- Fraud detection or spam filtering: Focus is placed on Precision to avoid inconveniencing users with incorrect positive classifications (False Positives, FP).

III. 7 CONCLUSION

This chapter presented the theoretical and mathematical foundations of the classification algorithms adopted in this study, namely Artificial Neural Networks, Support Vector Machines, AdaBoost, and Random Forests, with particular emphasis on their role in constructing accurate and generalizable classification models within complex data environments. These algorithms were analyzed within the framework of statistical learning theory and empirical risk minimization, where the decision function is learned by optimizing an appropriate loss function under regularization constraints to ensure a balance between training accuracy and generalization capability [137].

Artificial Neural Networks (ANNs) represent nonlinear approximation models capable of modeling complex decision boundaries through a layered architecture of interconnected weighted neurons. They rely on the backpropagation algorithm to update weights, enabling the learning of nonlinear patterns in high-dimensional data [137][138].

Support Vector Machines (SVMs) constitute margin-based classifiers that aim to maximize the separating margin between classes. The optimal separating hyperplane is obtained by solving a convex optimization problem, with the possibility of employing kernel functions to handle nonlinear separability [137].

The AdaBoost algorithm is based on combining multiple weak classifiers into a strong predictive model through iterative reweighting of training samples, thereby focusing on difficult instances. This strategy reduces bias and enhances classification accuracy [138].

Random Forests, introduced by Leo Breiman, are ensemble models that construct a large number of decision trees using bootstrap sampling and random feature selection, and aggregate their outputs through majority voting. This approach effectively reduces variance and improves model stability [138].

The comparative analysis demonstrates that these four algorithms represent distinct methodological paradigms for addressing classification problems: ANNs provide flexible nonlinear representation learning; SVMs rely on margin maximization principles; whereas AdaBoost and Random Forests leverage ensemble strategies to enhance overall predictive performance and mitigate generalization errors. This chapter therefore establishes the theoretical foundation for conducting an objective experimental evaluation using standardized statistical performance metrics to accurately compare model effectiveness in practical applications.

Chapter IV

CHAPTER IV: Application and Evaluation of AI Technique for Diagnosis

IV.1 Introduction

The reliable operation of oil-immersed power transformers is essential for maintaining the stability and continuity of electrical power systems. Since internal faults may gradually develop before leading to severe failures, early and accurate diagnosis is considered a critical task in transformer condition monitoring. Dissolved Gas Analysis (DGA) is one of the most widely used diagnostic techniques for this purpose, as the decomposition of insulating oil and solid insulation under electrical or thermal stresses generates characteristic gases that can be linked to specific fault types.

This chapter presents the experimental implementation and evaluation of the proposed intelligent fault diagnosis framework. The main objective is to improve the classification of transformer faults by combining conventional DGA ratio-based features with graphical-method-based features and evaluating their effectiveness using machine learning techniques. The proposed approach investigates three feature configurations: ratio features, graphical features, and concatenated features obtained by fusing both representations into a 24 dimensional feature vector.

The chapter begins by describing the experimental setup, including the dataset, fault classes, feature extraction process, normalization, and dimensionality reduction using t-distributed Stochastic Neighbor Embedding ($t\text{-}SNE$). Then, several machine learning classifiers, namely K-Nearest Neighbors (KNN), Support Vector Machine (SVM), Random Forest (RF), and adaBoost, are employed to classify the transformer fault types. The performance of the proposed framework is assessed using multiple evaluation metrics, including accuracy, AUC, recall, F1-score, and G-Mean, in order to provide a comprehensive analysis of the diagnostic capability of each feature representation and classifier combination.

Finally, the obtained results are discussed through numerical tables and graphical analyses, including accuracy comparison, radar charts, confusion matrices, and per-class performance evaluation. This chapter therefore aims to demonstrate the effectiveness of feature fusion and machine learning in improving the reliability and accuracy of DGA-based transformer fault diagnosis.

IV.2 Experimental Setup

Figure IV.1 illustrates the proposed methodology for intelligent fault diagnosis of oil-immersed power transformers based on Dissolved Gas Analysis (DGA) and machine learning techniques. The proposed framework consists of four sequential stages: data collection, feature extraction, data processing, and model evaluation. Each stage is designed to transform raw DGA measurements into a compact and discriminative representation that can be effectively used for automatic fault classification.

The process begins with the collection of DGA samples from oil-immersed power transformers operating under different fault conditions. When electrical or thermal faults occur inside a transformer, the insulating oil and solid insulation materials decompose and generate characteristic gases. The concentrations of these gases provide valuable diagnostic information regarding the internal condition of the transformer. In this study, five key dissolved gases are considered, namely hydrogen (H_2), methane (CH_4), ethane (C_2H_6), ethylene (C_2H_4), and acetylene (C_2H_2). The collected samples are associated with six fault categories: partial discharge (PD), low-energy discharge $(D1)$, high-energy discharge $(D2)$, and three thermal fault levels $(T1, T2, T3)$.

After data acquisition, the feature extraction stage is performed using two complementary diagnostic approaches: ratio methods and graphical methods. First, twelve ratio-based features are computed from the dissolved gas concentrations. These ratios describe the relative relationships between gases and provide meaningful indicators of different fault mechanisms. Second, twelve graphical-method-based features are extracted to represent the position and distribution of each DGA sample in graphical diagnostic spaces. Unlike ratio features, graphical features provide a geometric interpretation of the gas composition and may capture additional fault-related patterns. The two feature groups are then concatenated to construct a final feature vector containing 24 features. This fused representation combines the chemical information provided by gas ratios with the geometric information provided by graphical methods, thereby improving the descriptive capability of the input data.

In the data processing stage, Z-score normalization is applied to the extracted features in order to standardize their numerical ranges. This step is essential because the extracted features may have different scales and magnitudes, which can negatively influence the learning process if left untreated. By transforming each feature to have approximately zero mean and unit variance, normalization ensures that all features contribute more equally to the subsequent analysis. After normalization, t-distributed Stochastic Neighbor Embedding $(t\text{-}SNE)$is employed to reduce the dimensionality of each feature set into a two-dimensional representation. Specifically, the ratio-based feature set, graphical feature set, and concatenated feature set are each projected into a 2D space. This dimensionality reduction step aims to preserve the local neighborhood structure of the data while producing a compact representation suitable for visualization and classification.

Finally, the processed feature representations are evaluated using several machine learning classifiers, including K-Nearest Neighbors (KNN), Support Vector Machine (SVM), Random Forest (RF), and a boosting-based ensemble classifier. In the implemented MATLAB code, the boosting model corresponds to RUSBoost, which is particularly suitable for imbalanced datasets because it combines boosting with random undersampling. For each feature configuration, the dataset is divided into training and testing subsets using a hold-out validation strategy, where 70% of the samples are used for training and 30% are reserved for testing. The classifiers are then trained on the reduced feature representations and evaluated on the test set.

To provide a comprehensive assessment of the proposed diagnostic framework, several performance metrics are computed from the confusion matrix, including accuracy, precision, recall, F1-score, specificity, geometric mean ($G\text{-}Mean$), Matthews correlation coefficient (MCC), and Cohen's kappa. These metrics allow a detailed evaluation of both the overall classification performance and the class-wise behavior of the models. This is particularly important in transformer fault diagnosis, where the distribution of samples among fault classes may be imbalanced and accuracy alone may not provide a complete indication of diagnostic reliability.

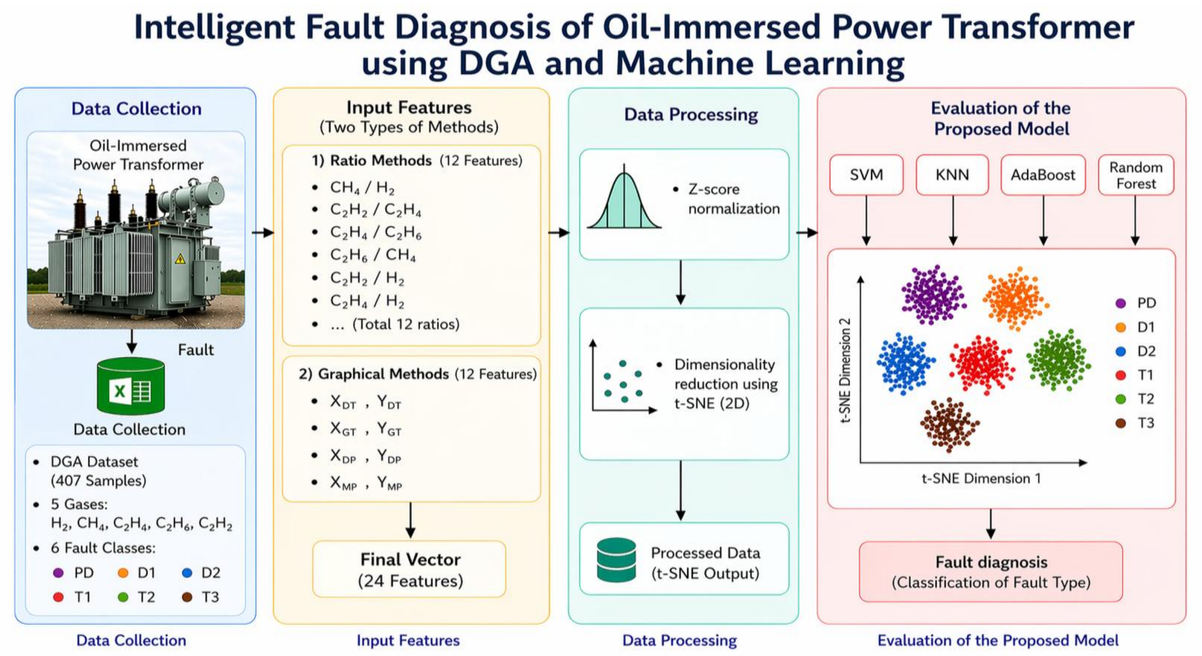

Figure IV.1 Proposed methodology

IV.2.1 Data Collection

The first stage of the proposed framework is the collection of dissolved gas analysis data corresponding to different transformer fault conditions. DGA is widely recognized as an effective diagnostic technique for oil-immersed power transformers because the degradation of insulating oil and cellulose insulation under abnormal electrical or thermal stresses leads to the generation of specific gases. The type and concentration of these gases reflect the nature of the fault occurring inside the transformer.

In this study, the dataset consists of 407 DGA samples distributed over six fault classes: partial discharge (PD), low-energy discharge ($D1$), high-energy discharge ($D2$), and thermal faults ($T1$, $T2$, $T3$). The diagnostic input data are represented by the concentrations of five dissolved gases: H_2, CH_4, C_2H_6, C_2H_4, and C_2H_2. These gases are selected because they are strongly associated with the main electrical and thermal fault mechanisms in oil-immersed transformers.

The distribution of the samples among the six fault classes is presented in Table IV.1. The dataset is not perfectly balanced, since the number of samples differs from one fault class to another. Therefore, the use of complementary evaluation metrics such as F1-score, G-Mean, and MCC is necessary to provide a more reliable assessment of the diagnostic models.

Table IV.1. Distribution of DGA samples by fault type

	PD	D1	D2	T1	T2	T3	Total
No of Samples	32	59	99	86	48	83	407

Prior to feature extraction, zero gas concentration values are replaced by a very small constant value. This preprocessing step is required because several ratio features involve division operations, and the presence of zero values in the denominator may lead to undefined or infinite numerical values. Consequently, this operation improves the numerical stability of the feature extraction process.

IV.2.2 Input Feature Extraction

The second stage of the proposed methodology is feature extraction. Instead of using the raw gas concentrations directly, the proposed framework derives more informative diagnostic descriptors through two approaches: ratio-based methods and graphical methods. These two approaches are complementary, as they represent the DGA data from different perspectives.

IV.2.2.1 Ratio-Based Features

To construct the first feature representation, the raw gas concentrations were transformed into diagnostic ratios derived from well-established conventional DGA ratio techniques. These include the Dornenburg ratios method, Rogers four-ratio method, IEC ratio method, ETRA ratio method, Hyosung Corporation ratios, and the Three-Ratios technique. Since several of these approaches share repeated or overlapping ratios, the extracted quantities were consolidated into a compact and non-redundant set of twelve unique ratio features.

In the proposed framework, twelve ratio features are calculated as follows:

$$R_1 = \frac{CH_4}{H_2}, R_2 = \frac{C_2H_2}{C_2H_4}, R_3 = \frac{C_2H_4}{C_2H_6}$$
$$R_4 = \frac{C_2H_2}{CH_4}, R_5 = \frac{C_2H_6}{CH_4}, R_6 = \frac{C_2H_2}{C_2H_6}$$
$$R_7 = \frac{H_2}{CH_4}, R_8 = \frac{C_2H_2}{H_2}, R_9 = \frac{C_2H_6}{C_2H_2}$$
$$R_{10} = \frac{C_2H_4}{CH_4}, R_{11} = \frac{C_2H_6 + C_2H_4}{H_2 + C_2H_2}, R_{12} = \frac{CH_4 + C_2H_2}{C_2H_4}$$

$$X_{ratio} = [R_1, R_2, R_3, R_4, R_5, R_6, R_7, R_8, R_9, R_{10}, R_{11}, R_{12}]$$

These twelve ratios form the first feature subset. They provide a chemically meaningful representation of the transformer condition by emphasizing the relationships between gases generated under different fault types.

IV.2.2.2 Graphical-Method-Based Features

In parallel with the ratio-based representation, a second feature representation was developed using graphical diagnostic methods. These methods are widely used in transformer diagnostics because they transform gas composition information into geometric coordinates or representative points that reflect fault regions in diagnostic diagrams.

In this study, twelve graphical features were extracted from six graphical diagnostic approaches, with each method contributing two features. The resulting graphical feature vector can be written as:

$$X_{\text{graphical}} = [F_1, F_2, F_3, F_4, F_5, F_6, F_7, F_8, F_9, F_{10}, F_{11}, F_{12}]$$

The graphical features were derived as follows.

a) Duval Triangle Method

$$F_1 = x = 100 - \%C_2H_2 - \%CH_4\cos\left(\frac{\pi}{6}\right)\cot\left(\frac{\pi}{3}\right)$$
$$F_2 = y = \%CH_4\cos\left(\frac{\pi}{6}\right)$$

b) Gouda Triangle Method

$$F_3 = x = 100 - \%R_2 - \%R_3\cos\left(\frac{\pi}{6}\right)\cot\left(\frac{\pi}{3}\right)$$
$$F_4 = y = \%R_3\cos\left(\frac{\pi}{6}\right)$$

c) Duval Pentagon Method

$$F_5 = X(1) = \frac{1}{6}\ \frac{\sum_{i=0}^{4}(x_i + x_{i+1})(x_i y_{i+1} - \quad {}_{i+1}y_i)}{\frac{1}{2}\sum_{i=0}^{4}(x_i y_{i+1} - x_{i+1}y_i)}$$

$$F_6 = X(2) = \frac{1}{6}\ \frac{\sum_{i=0}^{4}(y_i + y_{i+1})(x_i y_{i+1} - x_{i+1}y_i)}{\frac{1}{2}\sum_{i=0}^{4}(x_i y_{i+1} - x_{i+1}y_i)}$$

d) Mansour Pentagon Method

$$F_7 = x_m = \frac{\sum_{i=1}^{n} m_i\, x_i}{100}$$

$$F_8 = y_m = \frac{\sum_{i=1}^{n} m_i\, y_i}{100}$$

e) Cartesian Graphical Method

$$F_9 = x_{\text{point}} = (P_2 + P_1 \sin\ 30°) \times L$$

$$F_{10} = y_{\text{point}} = (P_1 \sin\ 60°) \times L$$

f) Circle Method

$$F_{11} = x_i = \%H_2\cos(\theta_1) + \%CH_4\cos(\theta_2) - \%C_2H_6\cos(\theta_3) - \%C_2H_4\cos(\theta_4) + \%C_2H_2\cos(\theta_5)$$

$$F_{12} = y_i = \%H_2\sin(\theta_1) + \%CH_4\sin(\theta_2) + \%C_2H_6\sin(\theta_3) - \%C_2H_4\sin(\theta_4) - \%C_2H_2\sin(\theta_5)$$

IV.2.2.3 Feature Fusion

After extracting the two feature subsets, feature fusion is performed by concatenating the ratio-based features and graphical features into a single input vector. Since each subset contains twelve features, the resulting fused vector contains twenty-four features:

$$X_{final} = [X_{ratio}, X_{graphical}]$$

$$X_{final} \in \mathbb{R}^{24}$$

This fused representation is expected to provide a richer description of the DGA samples by integrating both chemical ratio information and graphical diagnostic information. Therefore, the final 24-dimensional vector is used as the main input representation for the subsequent data processing and classification stages.

IV.2.3 Data Processing

The third stage of the methodology is data processing, which includes normalization and dimensionality reduction. These operations are applied to improve the numerical quality of the input data and to obtain a compact representation that facilitates classification.

IV.2.3.1 Z-score Normalization

Since the extracted features may have different units, ranges, and magnitudes, Z-score normalization is applied before dimensionality reduction and classification. This step prevents features with large numerical values from dominating the learning process.

For each feature, Z-score normalization is defined as:

$$X_{norm} = \frac{X - \mu}{\sigma}$$

where $X$is the original feature value, $\mu$is the mean of the corresponding feature, and $\sigma$is its standard deviation. After normalization, each feature has approximately zero mean and unit variance. This makes the feature space more balanced and improves the stability of the subsequent t-SNE projection and machine learning models.

IV.2.3.2 Dimensionality Reduction Using t-SNE

After normalization, t-distributed Stochastic Neighbor Embedding $(t\text{-}SNE)$is applied to reduce the dimensionality of the feature sets to two dimensions. In the proposed framework, t-SNE is applied separately to the ratio-based features, the graphical features, and the fused 24-dimensional feature vector.

The dimensionality reduction process can be summarized as follows:

$$X_{ratio}^{12D} \rightarrow X_{ratio}^{2D}$$
$$X_{graphical}^{12D} \rightarrow X_{graphical}^{2D}$$
$$X_{final}^{24D} \rightarrow X_{final}^{2D}$$

The purpose of this step is to obtain a compact representation that preserves local similarities between samples. In other words, samples with similar diagnostic characteristics in the original feature space are expected to remain close to each other in the two-dimensional t-SNE space. This representation is useful for both visual inspection and machine learning-based classification.

As illustrated in **Figure IV.2**, the t-SNE projections provide a visual comparison of the class distribution obtained from the three feature configurations. The projection based on conventional ratio features shows considerable overlap between several fault classes, indicating limited separability in the reduced feature space. In contrast, the graphical features produce more compact and distinguishable clusters, which suggests that this representation captures more discriminative fault-related information. The fused 24-dimensional feature vector further improves the spatial organization of the samples by combining ratio-based and graphical information. As a result, the classes become more clearly structured in the two-dimensional t-SNE space, supporting the subsequent classification stage and explaining the improved diagnostic performance obtained with the concatenated features.

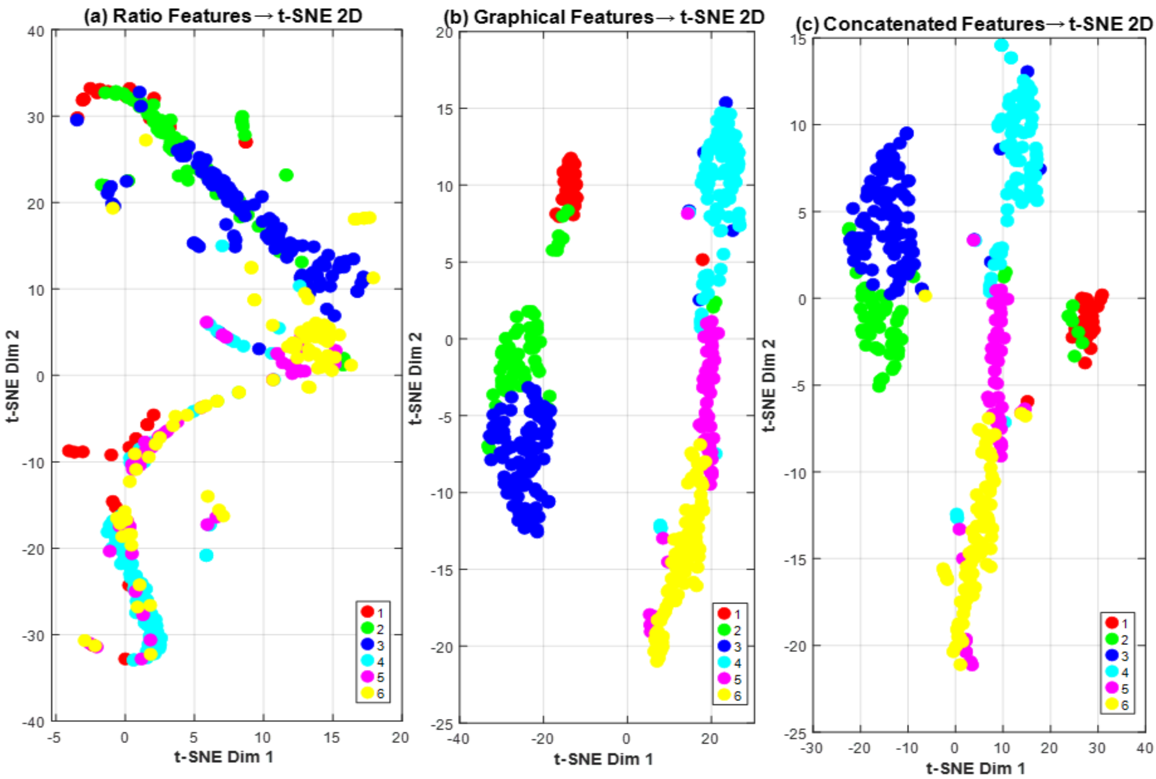

Figure IV.2. t-SNE visualization of the three feature representations: ratio features, graphical features, and concatenated features.

IV.3 Hyperparameters for classification algorithms

The hyperparameter tuning process is a fundamental step for guiding the behavior of machine learning models and enhancing their high-accuracy predictive capabilities. Through the meticulous selection of these parameters, we ensure that the four models KNN, Random Forest, AdaBoost, and SVM—achieve optimal performance while minimizing the likelihood of overfitting. Since the t-SNE technique had previously simplified the feature space and transformed it into more distinct dimensions, the hyperparameter values outlined in Table IV.2 were specifically chosen to align with the nature of the 407 samples utilized in this study.

The final stage of the proposed methodology is fault classification and model evaluation. The processed t-SNE features are used as inputs to machine learning classifiers in order to identify the fault type associated with each DGA sample.

Four classifiers are considered in the experimental evaluation: K-Nearest Neighbors (KNN), Support Vector Machine (SVM), Random Forest (RF), and RUSBoost. These classifiers were selected because they represent different learning strategies. KNN is a distance-based classifier, SVM is a margin-based classifier capable of handling nonlinear decision boundaries, Random Forest is a bagging-based ensemble method, and RUSBoost is a boosting-based ensemble method suitable for imbalanced data.

The dataset is divided using a hold-out validation strategy. Specifically, 70% of the samples are used for training, while the remaining 30% are used for testing. This evaluation is repeated for the three feature configurations: ratio features, graphical features, and fused features. Consequently, the experimental comparison includes twelve classification scenarios.

The output of each classifier is compared with the true fault labels using a confusion matrix. From this matrix, several performance metrics are computed, including accuracy, precision, recall, F1-score, specificity, G-Mean, Matthews correlation coefficient, and Cohen's kappa. These metrics provide a comprehensive evaluation of the diagnostic performance. In particular, F1-score, G-Mean, and MCC are useful for assessing model reliability in the presence of class imbalance.

Table IV.2: Optimized hyperparameters for the four proposed machine learning classifiers.

Model	Hyperparameter	Value
KNN	Number of neighbors (k)	5
	Distance metric	Euclidean
	Weight function	Distance
	Search Algorithm	Linear NN Search
AdaBoost	Number of Estimators	150
	Base Estimator	Decision Stump (depth = 1)
	Learning Rate	1.0
	Algorithm	SAMME.R
Random Forest	Number of Trees	200
	Max Features per Split	sqrt(d)
	Min Samples per Leaf	1
SVM	Kernel	RBF
	Regularization (C)	10
	Kernel Width (γ)	scale
	Multi-class Strategy	One-vs-One

IV.3 Results and Discussion

This section presents the experimental results obtained from the proposed DGA-based transformer fault diagnosis framework. The evaluation was performed using three different feature configurations: conventional ratio features, graphical features, and concatenated features. Four machine learning classifiers were investigated, namely K-Nearest Neighbors (KNN), Support Vector Machine (SVM), Random Forest (RF), and RUSBoost. The performance of each model was assessed using accuracy, AUC, recall, F1-score, and G-Mean.

The results are presented in three main tables according to the adopted feature representation. Then, graphical comparisons are provided through Figures IV.2–IV.5 to support the numerical results and provide further interpretation of the classification behavior.

IV.3.1 Performance of Conventional Ratio Features

Table IV.3 presents the performance obtained using only the conventional ratio features. These features correspond to the twelve gas-ratio descriptors extracted from the dissolved gas concentrations and reduced to a two-dimensional representation using t-SNE.

Table IV.3. Classification results using conventional ratio features

Model	Accuracy (%)	AUC	Recall	F1-Score	G-Mean
KNN	61.48	0.586	0.584	0.585	0.529
SVM	62.30	0.598	0.565	0.581	0.536
RF	56.56	0.527	0.534	0.531	0.468
RUSBoost	58.20	0.577	0.569	0.573	0.501

As shown in Table IV.1, the conventional ratio features achieved relatively limited diagnostic performance. The highest accuracy was obtained by SVM with 62.30%, followed by KNN with 61.48%. RUSBoost achieved 58.20%, while RF obtained the lowest accuracy of 56.56%.

The same trend can be observed for the remaining metrics. The AUC values ranged from 0.527 to 0.598, indicating weak separability between the six fault classes. Similarly, the recall and F1-score values remained close to the range of 0.53–0.58, suggesting that the classifiers were unable to consistently identify all fault categories using ratio features alone. The G-Mean values were also low, particularly for RF, which achieved only 0.468. This confirms that the models did not provide balanced recognition across all classes.

These results indicate that although gas-ratio features contain useful diagnostic information, they are not sufficient by themselves to represent the complex and nonlinear relationships among different DGA fault patterns.

IV.3.2 Performance of Graphical Features

Table IV.4 shows the classification results obtained using the graphical feature representation. These features provide a geometric description of the DGA samples in diagnostic graphical spaces.

Table IV.4. Classification results using graphical features

Model	Accuracy (%)	AUC	Recall	F1-Score	G-Mean
KNN	90.16	0.924	0.901	0.912	0.880
SVM	86.89	0.888	0.862	0.875	0.840
RF	87.70	0.881	0.874	0.877	0.850
RUSBoost	85.25	0.864	0.856	0.860	0.821

Compared with the conventional ratio features, the graphical features produced a substantial improvement in all performance metrics. KNN achieved the best performance in this feature configuration, with an accuracy of 90.16%, AUC of 0.924, recall of 0.901, F1-score of 0.912, and G-Mean of 0.880.

The remaining classifiers also achieved strong results. SVM, RF, and RUSBoost obtained accuracies of 86.89%, 87.70%, and 85.25%, respectively. In addition, all F1-score values were above 0.860, indicating a good balance between recall and precision. The G-Mean values were also significantly higher than those obtained using ratio features, confirming that the graphical representation improved the balanced recognition of the six fault classes.

This improvement can be attributed to the ability of graphical features to encode spatial and geometric relationships among DGA samples. Unlike simple ratio features, graphical descriptors can capture additional diagnostic patterns, which improves class separability and reduces ambiguity among fault categories.

IV.3.3 Performance of Concatenated Features

Table IV.5 presents the results obtained using the concatenated feature vector, which combines the twelve conventional ratio features and the twelve graphical features into a single 24-dimensional representation before t-SNE dimensionality reduction.

Table IV.5. Classification results using concatenated features

Model	Accuracy (%)	AUC	Recall	F1-Score	G-Mean
KNN	91.80	0.909	0.916	0.912	0.900
SVM	91.80	0.910	0.922	0.916	0.900
RF	92.62	0.928	0.935	0.931	0.909
RUSBoost	91.80	0.913	0.925	0.919	0.900

The concatenated feature representation achieved the best overall classification performance. As reported in Table IV.3, RF obtained the highest accuracy of 92.62%, together with the highest AUC of 0.928, recall of 0.935, F1-score of 0.931, and G-Mean of 0.909. This indicates that RF was able to effectively exploit the complementary information provided by the fused feature vector.

KNN, SVM, and RUSBoost also achieved high and similar accuracy values of 91.80%. The recall and F1-score values were also consistently high across all classifiers, confirming that the concatenated representation improved not only the overall accuracy but also the reliability of classification across the different fault classes.

The superior performance of the concatenated features demonstrates the effectiveness of feature fusion. Ratio features provide chemical relationships between dissolved gases, while graphical features provide spatial diagnostic information. Combining both representations produces a richer and more discriminative description of transformer fault behavior.

IV.3.4 Comparative Accuracy Analysis

Figure IV.3 presents the accuracy comparison of the four classifiers using the three feature configurations. As shown in Figure IV.3, the conventional ratio features produced the lowest accuracy for all classifiers. The accuracy values ranged from 56.56% for RF to 62.30% for SVM. This confirms the limited discriminative ability of ratio features when used alone.

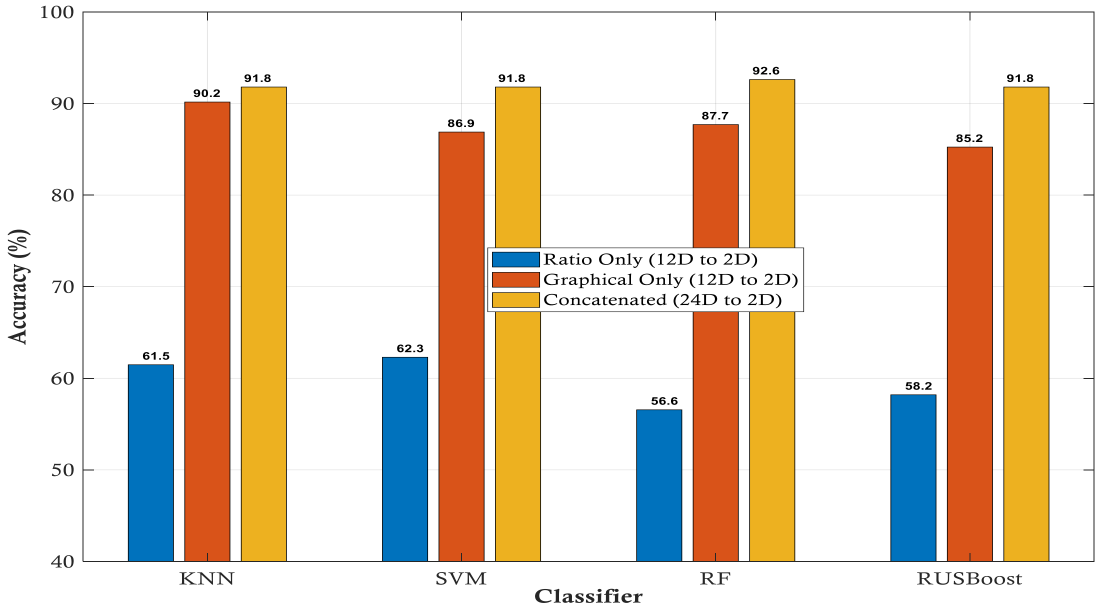

Figure IV.3. Accuracy comparison of the investigated classifiers using ratio, graphical, and concatenated features.

A clear improvement was achieved when graphical features were used. The accuracy increased to 90.16% for KNN, 86.89% for SVM, 87.70% for RF, and 85.25% for RUSBoost. This demonstrates that graphical features provide a more effective representation of DGA fault patterns than conventional ratio features.

The highest accuracies were obtained using the concatenated features. RF achieved the best overall performance with 92.62%, while KNN, SVM, and RUSBoost each achieved 91.80%. These results confirm that the integration of ratio and graphical features improves the classification performance across all classifiers.

In terms of improvement, RF showed the largest gain, increasing from 56.56% with ratio features to 92.62% with concatenated features. This represents an improvement of 36.06 percentage points. Similarly, KNN improved from 61.48% to 91.80%, SVM from 62.30% to 91.80%, and RUSBoost from 58.20% to 91.80%. Therefore, the results clearly indicate that the feature representation has a major influence on the performance of the diagnostic system.

IV.3.5 Multi-Metric Radar Chart Analysis

Figure IV.4 presents radar chart comparisons based on multiple evaluation metrics, including accuracy, precision, recall, F1-score, specificity, G-Mean, and MCC.

The radar charts provide a comprehensive view of the behavior of each classifier. For all classifiers, the ratio-only feature curves occupy the smallest area, indicating weak performance across most metrics. This observation is consistent with the numerical results reported in Table IV.3.

In contrast, the graphical feature curves occupy a much larger area, indicating a significant improvement in diagnostic performance. The improvement is especially visible in recall, F1-score, and G-Mean, which are important metrics for assessing classification reliability in multi-class and imbalanced datasets.

The concatenated feature curves generally show the largest and most balanced profiles, particularly for RF, SVM, and RUSBoost. This indicates that feature fusion improves not only accuracy but also the overall stability of the classification system. The high values of recall, F1-score, G-Mean, and MCC suggest that the fused representation provides better class discrimination and reduces the risk of biased classification.

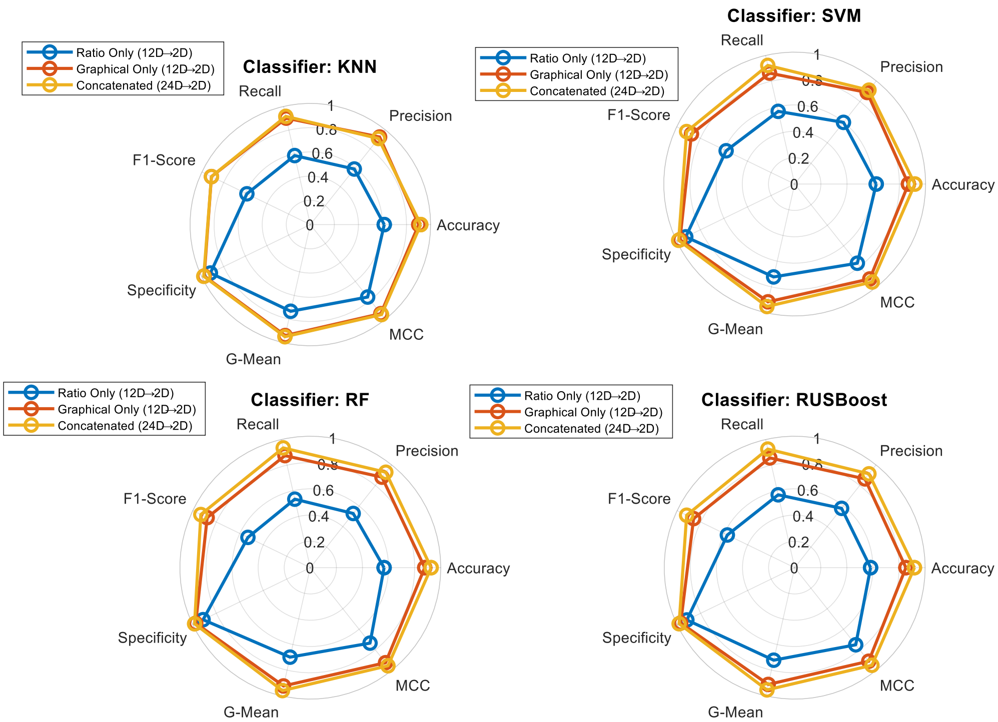

Figure IV.4. Radar chart comparison of the classifiers based on multiple performance metrics.

IV.3.6 Confusion Matrix Analysis

Figure IV.5 shows the complete confusion matrices for the twelve experimental cases, corresponding to three feature configurations and four classifiers.

The confusion matrices obtained using conventional ratio features show considerable dispersion away from the main diagonal. This means that several samples were incorrectly assigned to other fault classes. Such behavior confirms that ratio features alone cannot clearly separate the six transformer fault categories.

For the graphical feature configuration, the confusion matrices show stronger diagonal dominance. This indicates that most samples were correctly classified. In particular, KNN and RF achieved strong classification behavior using graphical features. However, some off-diagonal errors remain, suggesting that certain fault classes still have overlapping DGA patterns.

The confusion matrices obtained using concatenated features show the best classification behavior. The diagonal elements are more dominant, and the number of misclassified samples is reduced. The best matrix corresponds to RF with concatenated features, which achieved an accuracy of 92.62%. This confirms that the fused feature representation improves the separability of the fault classes and enhances the reliability of the final diagnostic decision.

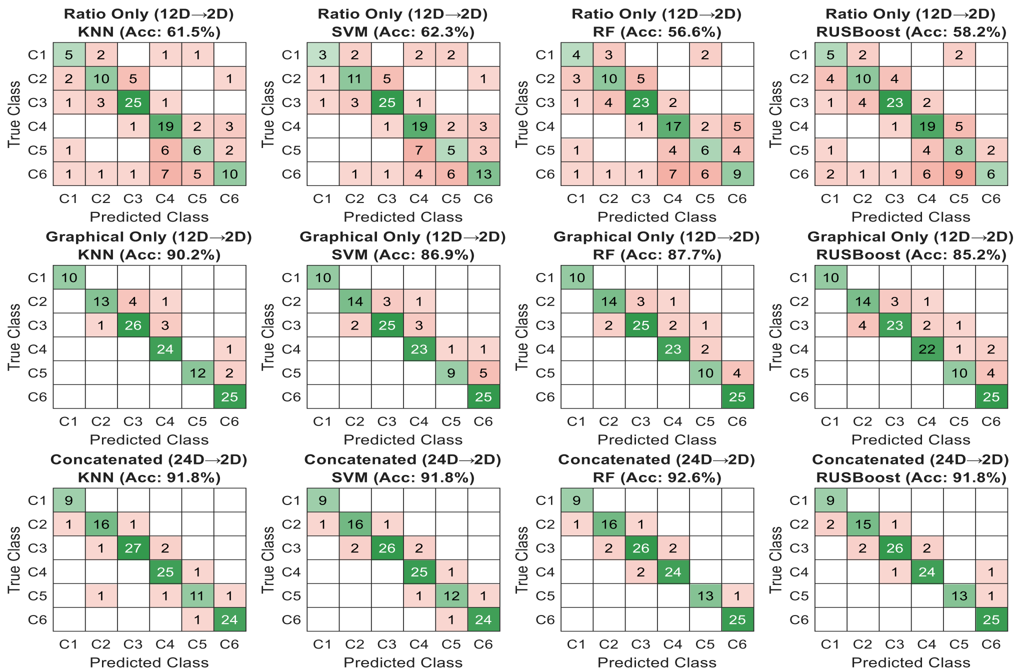

Figure IV.5. Confusion matrices for all classifiers and feature configurations.

IV.3.7 Per-Class Performance of the Best Model

Figure IV.6 presents the detailed per-class performance analysis of the best-performing model, which corresponds to RF using the concatenated feature vector.

The results show that the best model achieved strong classification performance across all six fault classes. Class 1 and Class 6 were perfectly classified, achieving per-class accuracies of 100%. The other classes also obtained high recognition rates, with Class 2 achieving approximately 88.9%, Class 3 approximately 86.7%, Class 4 approximately 92.3%, and Class 5 approximately 92.9%.

The precision, recall, and F1-score analysis further confirms the robustness of the RF model with concatenated features. Most classes achieved values close to or above 0.90, indicating that the model was able to identify the different fault types with high reliability. The few remaining errors mainly occurred between neighboring or similar fault classes, which may be explained by overlapping gas-generation mechanisms.

The confusion matrix of the best model also supports this conclusion. Most samples are concentrated along the main diagonal, while only a small number of samples are misclassified. This demonstrates that the proposed fused-feature framework provides a reliable diagnostic representation for multi-class transformer fault classification.

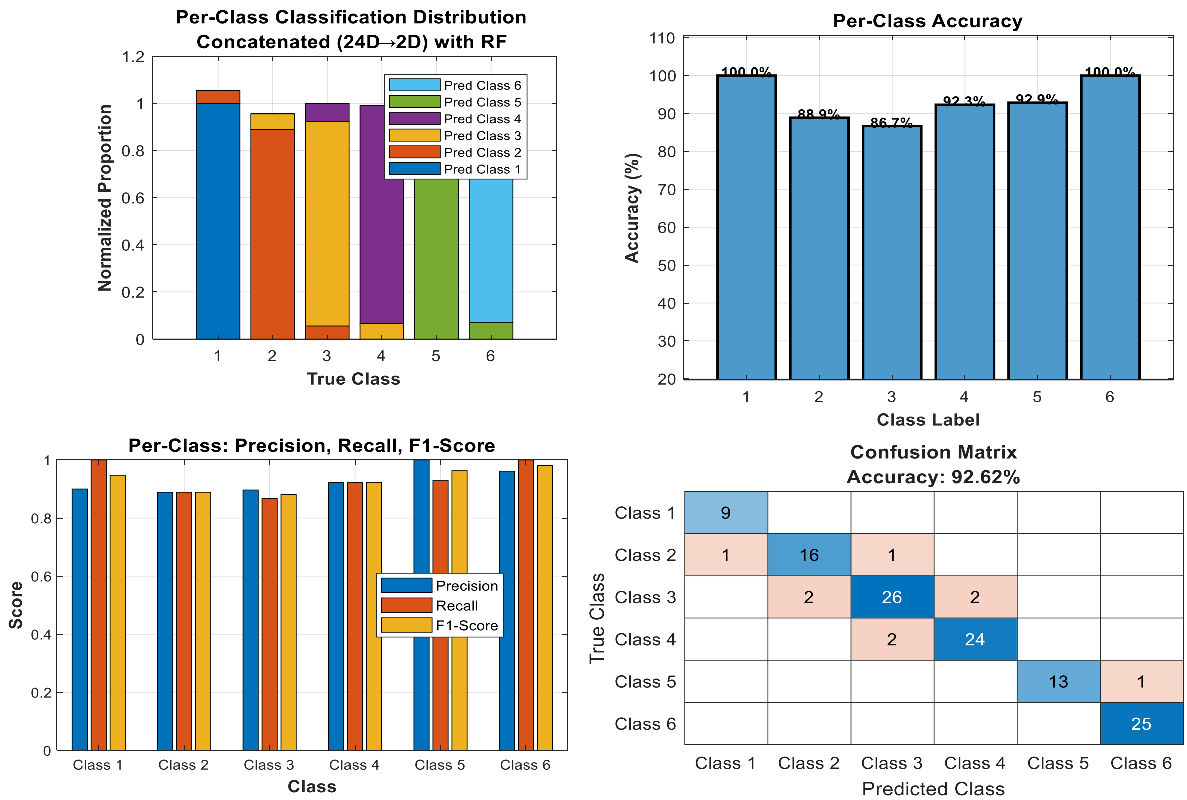

Figure IV.6. Per-class performance analysis of the best model using concatenated features with Random Forest.

IV.3.8 Overall Discussion

The results presented in Tables IV.1–IV.3 and Figures IV.2–IV.5 demonstrate the effectiveness of the proposed feature-fusion-based diagnostic framework. The conventional ratio features produced limited classification performance, with the best accuracy reaching only 62.30%. This indicates that ratio features alone are insufficient to accurately distinguish between the six considered transformer fault classes.

Graphical features significantly improved the classification results, with the best accuracy reaching 90.16% using KNN. This confirms that graphical descriptors provide more informative diagnostic patterns than conventional ratios. However, the best overall performance was obtained when both feature types were concatenated.

The concatenated feature vector achieved the highest performance, particularly with RF, which obtained an accuracy of 92.62%, AUC of 0.928, recall of 0.935, F1-score of 0.931, and G-Mean of 0.909. These results confirm that the fusion of ratio-based and graphical features provides a more discriminative representation of DGA samples.

Overall, the proposed methodology improves transformer fault diagnosis by integrating complementary feature extraction strategies, dimensionality reduction using t-SNE, and machine learning classification. The obtained results demonstrate that the proposed framework is effective, reliable, and suitable for intelligent multi-class fault diagnosis in oil-immersed power transformers.

IV.4 Conclusion

This chapter presented the experimental validation of the proposed intelligent fault diagnosis framework for oil-immersed power transformers using DGA data and machine learning techniques. The study evaluated three feature representations: conventional ratio features, graphical features, and concatenated features combining both approaches. These feature sets were processed using Z-score normalization and projected into a two-dimensional space using t-SNE before being classified using KNN, SVM, RF, and RUSBoost.

The obtained results demonstrated that the conventional ratio features produced limited classification performance, with the best accuracy reaching only 62.30%. This indicates that ratio-based features alone are not sufficiently discriminative for accurately distinguishing between the six considered transformer fault classes. In contrast, graphical features significantly improved the diagnostic performance, achieving up to 90.16% accuracy with KNN. This improvement confirms that graphical descriptors provide a more informative representation of DGA fault patterns.

The best overall performance was achieved using the concatenated feature representation, which combines the diagnostic information provided by both ratio-based and graphical features. Among all tested models, Random Forest with concatenated features achieved the highest performance, with an accuracy of 92.62%, AUC of 0.928, recall of 0.935, F1-score of 0.931, and G-Mean of 0.909. These results confirm that feature fusion enhances the separability of fault classes and improves the reliability of machine learning-based diagnosis.

The confusion matrix and per-class analysis further showed that the proposed framework provides strong classification performance across the six fault categories. Although a small number of misclassifications remained between some closely related fault classes, the overall results demonstrate the robustness of the proposed approach. Therefore, the combination of DGA feature fusion, t-SNE dimensionality reduction, and machine learning classification can be considered an effective solution for intelligent fault diagnosis of oil-immersed power transformers.

Overall, this chapter confirms the potential of the proposed methodology to improve transformer condition monitoring by providing accurate, reliable, and data-driven fault identification. The findings also highlight the importance of selecting appropriate feature representations, as the fusion of complementary features proved to be more effective than using conventional ratio features alone.

General Conclusion

GENERAL CONCLUSION

This dissertation presented a comprehensive study on the intelligent fault diagnosis of oil-immersed power transformers using Dissolved Gas Analysis (DGA) combined with machine learning techniques. Motivated by the critical importance of these devices in modern power systems and the recognized limitations of conventional DGA interpretation methods, the work proposed and evaluated an integrated diagnostic framework based on feature extraction, feature fusion, dimensionality reduction, and supervised classification.

The first chapter established the theoretical foundation by examining the structure, operating principles, and fault typology of oil-immersed transformers. It highlighted the dual role of insulating mineral oil as both an electrical insulator and a cooling medium, and underscored the importance of detecting internal faults at an early stage to prevent catastrophic failures. The second chapter provided an extensive review of conventional DGA interpretation approaches, including key gas methods, ratio-based techniques such as the Rogers, IEC, Dornenburg, CIGRE, and ETRA methods, and graphical tools such as the Duval Triangle, the Duval Pentagon, the Mansour Pentagon, and the Gouda Heptagon. This review revealed that while conventional methods offer practical diagnostic value, they are constrained by rule-based boundaries that fail to fully capture the complexity and overlap of fault signatures in real-world DGA data.

The third chapter introduced the machine learning algorithms employed in this study, namely Support Vector Machine (SVM), k-Nearest Neighbors (k-NN), Random Forest (RF), and adaBoost, alongside the ensemble learning paradigms that underpin their operation. The statistical performance indicators used for model evaluation including accuracy, precision, recall, F1-score, G-Mean, AUC, and confusion matrices were also presented in detail. The fourth chapter described the experimental methodology and reported the classification results obtained across three feature configurations: conventional ratio features, graphical features, and concatenated features combining both representations. Each feature set was processed through Z-score normalization and projected into a two-dimensional space using t-SNE before being passed to the classifiers.

The experimental results demonstrated clearly that the choice of feature representation has a decisive influence on the diagnostic performance of the machine learning system. Conventional ratio features alone proved insufficient, yielding classification accuracies between 56.56% and 62.30% across all tested classifiers. Graphical features substantially improved performance, reaching up to

90.16% accuracy with k-NN, confirming that spatial diagnostic descriptors encode richer fault related information than standard gas ratios. The best overall results were achieved using the concatenated feature representation, which combines the chemical relational information of ratio features with the spatial diagnostic patterns of graphical features. In this configuration, Random Forest achieved the highest performance, with an accuracy of 92.62%, an AUC of 0.928, a recall of 0.935, and an F1-score of 0.931, confirming the effectiveness of feature fusion for multi-class transformer fault classification.

The per-class analysis of the best model further validated the robustness of the proposed framework. Two fault classes were perfectly classified with 100% per-class accuracy, while the remaining four classes achieved recognition rates above 86%, with only minor misclassifications occurring between fault types sharing similar gas-generation mechanisms. The t-SNE visualization confirmed these findings by showing significantly improved class separability for the concatenated features compared to ratio features alone, providing additional visual evidence of the benefits of feature fusion.

Overall, the results of this study confirm that integrating complementary DGA feature extraction strategies within a unified machine learning framework represents an effective and reliable approach to transformer fault diagnosis. The proposed methodology successfully addresses the limitations of conventional DGA interpretation methods by combining the diagnostic strengths of ratio-based and graphical representations, while leveraging the classification power of ensemble learning to handle the complexity of multi-class fault scenarios.

As perspectives for future work, several directions can be considered. The framework could be extended and validated on larger and more diverse DGA datasets collected from different transformer types and operating environments to further assess its generalizability. The integration of online and continuous DGA monitoring data would allow the system to detect fault evolution in real time, supporting proactive maintenance decisions. Deep learning architectures, such as Convolutional Neural Networks (CNNs) or Long Short-Term Memory (LSTM) networks, could be explored to automatically learn feature representations directly from raw gas concentration sequences. Additionally, incorporating multi-source diagnostic data including partial discharge measurements, thermal imaging, and furan analysis into a multi-modal fusion framework could provide a more holistic and comprehensive assessment of transformer condition. Finally, adapting the proposed approach to natural ester insulating oils, which are increasingly adopted as environmentally friendly alternatives to mineral oil, represents an important direction aligned with the current evolution of transformer technology toward greater sustainability.

References

References

[1] S. A. Wani, "Transformer fault diagnosis Based on Dissolved Gas Analysis DGA."

[2] K. F. Thang, *An improved approach to data analysis & interpretation in transformer condition assessment based on unsupervised neutral network*. University of Bath (United Kingdom), 2002.

[3] S. Li, "Study of dissolved gas analysis under electrical and thermal stresses for natural esters used in power transformers," The University of Manchester (United Kingdom), 2012.

[4] Y. Li, "The State of the Art in transformer fault diagnosis with artificial intelligence and Dissolved Gas Analysis: A Review of the Literature," *arXiv preprint arXiv:2304.11880,* 2023.

[5] A. Ahmed, "Power Transformer Condition Monitoring and Diagnosis," *United Kingdom: IET, The Institution of Engineering and Technology,* 2018.

[6] J. Ni, Z. Zhao, S. Tan, Y. Chen, C. Yao, and C. Tang, "The actual measurement and analysis of transformer winding deformation fault degrees by FRA using mathematical indicators," *Electric Power Systems Research,* vol. 184, p. 106324, 2020, doi: 10.1016/j.epsr.2020.106324.

[7] S. X. Qian, Q. Du, X. J. Gu, and J. Y. Song, "Transformer Winding Deformation Fault Diagnose Based on FRA and Energy Feature Extraction by Wavelet Packet," *Advanced Materials Research,* vol. 490, pp. 1486-1490, 2012, doi: 10.4028/www.scientific.net/AMR.490-495.1486.

[8] T.-D. Do, V.-N. Tuyet-Doan, Y.-S. Cho, J.-H. Sun, and Y.-H. Kim, "Convolutional-neural- network-based partial discharge diagnosis for power transformer using UHF sensor," *IEEE access,* vol. 8, pp. 207377-207388, 2020, doi: 10.1109/ACCESS.2020.3038386.

[9] H. Karami, H. Tabarsa, G. B. Gharehpetian, Y. Norouzi, and M. A. Hejazi, "Feasibility study on simultaneous detection of partial discharge and axial displacement of HV transformerwinding using electromagnetic waves," *IEEE Transactions on Industrial Informatics,* vol. 16, no. 1, pp. 67-76, 2019, doi: 10.1109/TII.2019.2915685.

[10] A. Indarto, A. W. Murti, F. Husnayain, I. Garniwa, A. Rahardjo, and C. Hudaya, "Influence of different adhesives on partial discharge in power transformer winding cylinder insulation," *IEEE Transactions on Dielectrics and Electrical Insulation,* vol. 27, no. 3, pp. 964-970, 2020, doi: 10.1109/TDEI.2020.008533.

[11] Y. Shi, S. Ji, F. Zhang, Y. Dang, and L. Zhu, "Application of operating deflection shapes to the vibration-based mechanical condition monitoring of

power transformer windings," *IEEE Transactions on Power Delivery,* vol. 36, no. 4, pp. 2164-2173, 2020, doi: 10.1109/TPWRD.2020.3021909.

[12] H. Zhou, K. Hong, H. Huang, and J. Zhou, "Transformer winding fault detection by vibration analysis methods," *Applied Acoustics,* vol. 114, pp. 136-146, 2016, doi: 10.1016/j.apacoust.2016.07.024.

[13] Y. Zhou *et al.*, "Vibration signal-based fusion residual attention model for power transformer fault diagnosis," *IEEE Sensors Journal,* vol. 24, no. 10, pp. 17231-17242, 2024, doi: 10.1109/JSEN.2024.3382811.

[14] L. Jin, D. Kim, A. Abu-Siada, and S. Kumar, "Oil-immersed power transformer condition monitoring methodologies: A review," *Energies,* vol. 15, no. 9, p. 3379, 2022, doi: 10.3390/en15093379.

[15] N. A. Baka, A. Abu-Siada, S. Islam, and M. El-Naggar, "A new technique to measure interfacial tension of transformer oil using UV-Vis spectroscopy," *IEEE Transactions on Dielectrics and Electrical Insulation,* vol. 22, no. 2, pp. 1275-1282, 2015, doi: 10.1109/TDEI.2015.7076831.

[16] H. Torkaman and F. Karimi, "Measurement variations of insulation resistance/polarization index during utilizing time in HV electrical machines–A survey," *Measurement,* vol. 59, pp. 21- 29, 2015, doi: 10.1016/j.measurement.2014.09.034.

[17] T. Mariprasath and V. Kirubakaran, "A real time study on condition monitoring of distribution transformer using thermal imager," *Infrared Physics & Technology,* vol. 90, pp. 78-86, 2018, doi: 10.1016/j.infrared.2018.02.009.

[18] F. Segovia *et al.*, "Connected system for monitoring electrical power transformers using thermal imaging," *Integrated Computer-Aided Engineering,* vol. 30, no. 4, pp. 353-368, 2023, doi: 10.3233/ICA-230712.

[19] A. Abdali, A. Abedi, H. Masoumkhani, K. Mazlumi, A. Rabiee, and J. M. Guerrero, "Magnetic- thermal analysis of distribution transformer: Validation via optical fiber sensors and thermography," *International Journal of Electrical Power & Energy Systems,* vol. 153, p. 109346, 2023, doi: 10.1016/j.ijepes.2023.109346.

[20] J. Lukic *et al.*, "Changes of new unused insulating kraft paper properties during drying-Impact on degree of polymerization," *Electra (Paris),* no. 312, pp. 76-81, 2020.

[21] S. Gao, L. Yang, and T. Ke, "Failure mechanism of transformer oil-immersed cellulosic insulation induced by sulfur corrosion," *Cellulose,* vol. 27, no. 12, pp. 7157-7174, 2020, doi: 10.1007/s10570-020-03271-x.

[22] A. Kumar, D. Mishra, and A. Baral, "Importance of depolarization current in the diagnosis of oil-paper insulation of power transformer," *IEEE Access,* vol. 11, pp. 56858-56864, 2023, doi: 10.1109/ACCESS.2023.3283914.

[23] D. Mishra, A. Baral, and S. Chakravorti, "Reliable assessment of oil-paper insulation used in power transformer using concise dielectric response measurement," *IEEE Transactions on Dielectrics and Electrical Insulation,* vol. 30, no. 3, pp. 1255-1264, 2023, doi: 10.1109/TDEI.2023.3261824.

[24] B. Standard, "Insulating liquids-determination of breakdown voltage at power frequency-test method," *BSEN60156,* 1996.

[25] M. R. Mahmoudi, M. H. Heydari, and R. Roohi, "A new method to compare the spectral densities of two independent periodically correlated time series," *Mathematics and Computers in Simulation,* vol. 160, pp. 103-110, 2019, doi: 10.1016/j.matcom.2018.12.008.

[26] I. Fofana, A. Bouaicha, and M. Farzaneh, "Characterization of aging transformer oil–pressboard insulation using some modern diagnostic techniques," *European Transactions on Electrical Power,* vol. 21, no. 1, pp. 1110-1127, 2011, doi: 10.1002/etep.499.

[27] J. S. N'cho, I. Fofana, Y. Hadjadj, and A. Beroual, "Review of physicochemical-based diagnostic techniques for assessing insulation condition in aged transformers," *Energies,* vol. 9, no. 5, p. 367, 2016, doi: 10.3390/en9050367.

[28] M. R. Mahmoudi, M. Mahmoudi, and E. Nahavandi, "Testing the difference between two independent regression models," *Communications in Statistics-Theory and Methods,* vol. 45, no. 21, pp. 6284-6289, 2016, doi: 10.1080/03610926.2014.960584.

[29] A. R. Abbasi, "Fault detection and diagnosis in power transformers: a comprehensive review and classification of publications and methods," *Electric Power Systems Research,* vol. 209, p. 107990, 2022, doi: 10.1016/j.epsr.2022.107990.

[30] S. Pramanik, V. C. Duvvury, and S. Sahoo, "Tank current measurement of three-phase transformer: Its resonance behavior and sensitivity to detect mechanical faults," *IEEE Transactions on Power Delivery,* vol. 34, no. 6, pp. 2211-2218, 2019, doi: 10.1109/TPWRD.2019.2914249.

[31] Z. Zhao, C. Yao, C. Li, and S. Islam, "Detection of power transformer winding deformation using improved FRA based on binary morphology and extreme point variation," *IEEE Transactions on Industrial Electronics,* vol. 65, no. 4, pp. 3509-3519, 2017, doi: 10.1109/TIE.2017.2752135.

[32] S. Gajbhiye, "Detection of Incipient Faults in Transformer by Dissolved Gas Analysis Using Artificial Intelligence Techniques," *Available at SSRN 4344852,* 2023, doi: 10.2139/ssrn.4344852.

[33] S. Singh and M. Bandyopadhyay, "Dissolved gas analysis technique for incipient fault diagnosis in power transformers: A bibliographic survey," *IEEE Electrical insulation magazine,* vol. 26, no. 6, pp. 41-46, 2010, doi: 10.1109/MEI.2010.5599978.

[34] J. Faiz and M. Soleimani, "Assessment of computational intelligence and conventional dissolved gas analysis methods for transformer fault diagnosis," *IEEE Transactions on Dielectrics and Electrical Insulation,* vol. 25, no. 5, pp. 1798-1806, 2018, doi: 10.1109/TDEI.2018.007191.

[35] H. G. Zaini, "Diagnosis of the Power Transformer Faults Based on DGA Using Intelligent Classifier," *International Journal of Engineering Research and Technology,* vol. 12, no. 11, pp. 1964-1971, 2019.

[36] J. Rodríguez, J. Contreras, and C. Gaytán, "Evaluation and interpretation of dissolved gas analysis of soybean-based natural ester insulating liquid," *IEEE Transactions on Dielectrics and Electrical Insulation,* vol. 28, no. 4, pp. 1343-1348, 2021, doi: 10.1109/TDEI.2021.009467.

[37] N. S. N. Klairuang, "Condition Assessment of Oil-Impregnated Paper Insulation of Transformers by Using CFA Index and Degree of Polymerization."

[38] M. Buchholz, "The Buchholz protection system and its application in practice," *ETZ,* vol. 49, no. 34, pp. 1257-1262, 1928.

[39] S. D. Myers, J. J. Kelly, and R. H. Parrish, *A guide to transformer maintenance*. Transformer Maintenance Institute, 1981.

[40] J. J. Kelly, "Transformer fault diagnosis by dissolved-gas analysis," *IEEE Transactions on Industry Applications,* no. 6, pp. 777-782, 2008, doi: 10.1109/TIA.1980.4503871.

[41] O.-F. E. Equipment, "Sampling of Gases and Analysis of Free and Dissolved Gases— Guidance," *Standard IEC,* vol. 60567, 2011.

[42] B. Vahidi and A. Teymouri, *Quality confirmation tests for power transformer insulation systems*. Springer, 2019.

[43] C. Riedmann, U. Schichler, W. Häusler, and W. Neuhold, "Online dissolved gas analysis used for transformers–possibilities, experiences, and limitations," *e & i Elektrotechnik und Informationstechnik,* vol. 139, no. 1, pp. 88-97, 2022, doi: 10.1007/s00502-022-00992-8.

[44] D. Pugh, "Advances in fault diagnosis by combustible gas analysis," in *Minutes of Forty-First International Conference of Doble Clients*, 1974.

[45] N. A. Bakar, A. Abu-Siada, and S. Islam, "A review of dissolved gas analysis measurement and interpretation techniques," *IEEE Electrical Insulation Magazine,* vol. 30, no. 3, pp. 39-49, 2014, doi: 10.1109/MEI.2014.6804740.

[46] A. Krontiris, "Fuzzy systems for condition assessment of equipment in electric power systems," 2012.

[47] E. Hubacher, "Analysis of dissolved gas in transformer oil to evaluate equipment condition," in *PCEA Engineering and Operation Section Spring Conference*, 1976.

[48] A. Mollmann and B. Pahlavanpour, "New guidelines for interpretation of dissolved gas analysis in oil-filled transformers," *Electra,* vol. 186, pp. 31-51, 1999.

[49] B. Fallou, "Detection of and research for the characteristics of an incipient fault from analysis of dissolved gases in the oil of an insulation," *Electra,* vol. 42, no. 3, pp. 31-52, 1975.

[50] I. Davidenko and K. Ovchinnikov, "Identification of transformer defects via analyzing gases dissolved in oil," *Russian Electrical Engineering,* vol. 90, no. 4, pp. 338-343, 2019, doi: 10.3103/S1068371219040035.

[51] E. Dornenburg and W. Strittmatter, "Monitoring oil-cooled transformers by gas-analysis,"*Brown Boveri Review,* vol. 61, no. 5, pp. 238-247, 1974.

[52] S. Chakravorti, D. Dey, and B. Chatterjee, "Recent trends in the condition monitoring of transformers," *Power Systems,* 2013.

[53] R. R. Rogers, "IEEE and IEC codes to interpret incipient faults in transformers, using gas in oil analysis," *IEEE transactions on electrical insulation,* no. 5, pp. 349-354, 1978.

[54] S. Babukutty and S. Khule, "Combined Dissolved Gas Analysis: A Prescient Methodology for Recognizing Faults in Transformer by MATLAB GUI," *International Research Journal of Engineering and Technology (IRJET),* 2019.

[55] I. IEC, "599-Interpretation of the Analysis of Gases in Transformer and Other Oil-Filled Electrical Equipment in Service," *International Electro-technical Commission, Geneva, Switzerland,* 1978.

[56] L. Cheng and T. Yu, "Dissolved gas analysis principle-based intelligent approaches to fault diagnosis and decision making for large oil-immersed power transformers: A survey," *Energies,* vol. 11, no. 4, p. 913, 2018, doi: 10.3390/en11040913.

[57] S. EE, "46.501: Diagnosis oil-filled transformer equipment based on the results of chromatographic analysis of free gas with gas relay selected, i gases dissolved in insulating oil," *Kyiv, Ukrainian,* 2007.

[58] O. Shutenko and O. Kulyk, "Comparative analysis of new methods for defect type recognition by dissolved gas analysis," in *2022 IEEE 3rd KhPI Week on Advanced Technology (KhPIWeek)*, 2022: IEEE, pp. 1-6, doi: 10.1109/KhPIWeek57572.2022.9916319.

[59] S.-w. Kim, S.-j. Kim, H.-d. Seo, J.-r. Jung, H.-j. Yang, and M. Duval, "New methods of DGA diagnosis using IEC TC 10 and related databases Part 1: application of gas-ratio combinations," *IEEE Transactions on Dielectrics and Electrical Insulation,* vol. 20, no. 2, pp. 685-690, 2013, doi: 10.1109/TDEI.2013.6508773.

[60] O. E. Gouda, S. H. El-Hoshy, and H. H. EL-Tamaly, "Proposed three ratios technique for the interpretation of mineral oil transformers based dissolved gas analysis," *IET Generation, Transmission & Distribution,* vol. 12, no. 11, pp. 2650-2661, 2018, doi: 10.1049/iet- gtd.2017.1927.

[61] A. Nanfak, C. H. Kom, and S. Eke, "Hybrid Method for Power Transformers Faults Diagnosis Based on Ensemble Bagged Tree Classification and Training Subsets Using Rogers and Gouda Ratios," *International Journal of Intelligent Engineering & Systems,* vol. 15, no. 5, 2022, doi: 10.22266/ijies2022.1031.02.

[62] M. Duval, "Fault gases formed in oil-filled breathing EHV power transformers-Interpretation of gas-analysis data," in *IEEE Transactions on Power Apparatus and Systems*, 1974, no. 6: IEEE- INST ELECTRICAL ELECTRONICS ENGINEERS INC 345 E 47TH ST, NEW YORK, NY …, pp. 1745-1746.

[63] O. C. Кулик, "Analysis of the diagnostic criteria used to defect type recognition based on the results of analysis of gases dissolved in oil," *Вісник Національного технічного університету «ХПІ». Серія: Енергетика: надійність та енергоефективність,* no. 1, pp. 15-25, 2020, doi: 10.20998/2224-0349.2020.01.03.

[64] A. Gupta, K. Jain, Y. R. Sood, and N. K. Sharma, "Comparative study of duval triangle with the new DGA interpretation scheme," in *Advances in System Optimization and Control: Select Proceedings of ICAEDC 2017*: Springer, 2018, pp. 261-268

[65] M. S. Ali, A. Omar, A. S. A. Jaafar, and S. H. Mohamed, "Conventional methods of dissolved gas analysis using oil-immersed power transformer for fault diagnosis: A review," *Electric Power Systems Research,* vol. 216, p. 109064, 2023, doi: 10.1016/j.epsr.2022.109064.

[66] M. Duval and L. Lamarre, "The duval pentagon-a new complementary tool for the interpretation of dissolved gas analysis in transformers," *IEEE Electrical Insulation Magazine,* vol. 30, no. 6,pp. 9-12, 2014, doi: 10.1109/MEI.2014.6943428.

[67] D.-E. A. Mansour, "A new graphical technique for the interpretation of dissolved gas analysis in power transformers," in *2012 annual report conference on electrical insulation and dielectric phenomena*, 2012: IEEE, pp. 195-198, doi: 10.1109/CEIDP.2012.6378754.

[68] D.-E. A. Mansour, "Development of a new graphical technique for dissolved gas analysis in power transformers based on the five combustible gases," *IEEE Transactions on Dielectrics and Electrical Insulation,* vol. 22, no. 5, pp. 2507-2512, 2015, doi: 10.1109/TDEI.2015.004999.

[69] O. E. Gouda, S. H. El-Hoshy, and H. H. EL-Tamaly, "Condition assessment of power transformers based on dissolved gas analysis," *IET Generation, Transmission & Distribution,* vol. 13, no. 12, pp. 2299-2310, 2019.

[70] O. E. Gouda, S. H. El-Hoshy, and H. H. El-Tamaly, "Proposed heptagon graph for DGA interpretation of oil transformers," *IET Generation, Transmission & Distribution,* vol. 12, no. 2, pp. 490-498, 2018, doi: 10.1049/iet-gtd.2017.0826.

[71] F. F. Selim, M. A. Hassan, A. M. Azmy, and E. G. Atiya, "Graphical shape in Cartesian plane based on dissolved gas analysis for power transformer incipient faults discrimination," *IEEE Transactions on Dielectrics and Electrical Insulation,* vol. 32, no. 1, pp. 589-597, 2024, doi: 10.1109/TDEI.2024.3404365.

[72] S. S. Ghoneim and I. B. Taha, "A new approach of DGA interpretation technique for transformer fault diagnosis," *International Journal of Electrical Power & Energy Systems,* vol. 81, pp. 265- 274, 2016, doi: 10.1016/j.ijepes.2016.02.018.

[73] M. M. Emara, G. D. Peppas, and I. F. Gonos, "Two graphical shapes based on DGA for power transformer fault types discrimination," *IEEE Transactions on Dielectrics and Electrical Insulation,* vol. 28, no. 3, pp. 981-987, 2021, doi: 10.1109/TDEI.2021.009415.

[74] A. Nanfak, S. Eke, C. H. Kom, R. Mouangue, and I. Fofana, "Interpreting dissolved gases in transformer oil: A new method based on the analysis of labelled fault data," *IET Generation, Transmission & Distribution,* vol. 15, no. 21, pp. 3032-3047, 2021, doi: 10.1049/gtd2.12239.

[75] S. A. Ward *et al.*, "Towards precise interpretation of oil transformers via novel combined techniques based on DGA and partial discharge sensors," *Sensors,* vol. 21, no. 6, p. 2223, 2021, doi: 10.3390/s21062223.

[76] I. B. Taha, A. Hoballah, and S. S. Ghoneim, "Optimal ratio limits of rogers' four-ratios and IEC 60599 code methods using particle swarm optimization fuzzy-logic approach," *IEEE Transactions on Dielectrics and Electrical Insulation,* vol. 27, no. 1, pp. 222-230, 2020, doi: 10.1109/TDEI.2019.008395.

[77] F. R. Barbosa, O. M. Almeida, A. P. Braga, M. A. Amora, and S. J. Cartaxo, "Application of an artificial neural network in the use of physicochemical properties as a low cost proxy of power transformers DGA data," *IEEE Transactions on Dielectrics and Electrical Insulation,* vol. 19, no. 1, pp. 239-246, 2012, doi: 10.1109/TDEI.2012.6148524.

[78] A. Hechifa, A. Lakehal, A. Nanfak, L. Saidi, and C. Labiod, "Machine learning algorithms fusion based on DGA data for improving fault diagnosis of electrical power transformer," *The Scientific Bulletin of Electrical*

Engineering Faculty, vol. 23, no. 2, pp. 5-11, 2023, doi: 10.2478/sbeef-2023-0014.

[79] C. Wei, W. Tang, and Q. Wu, "Dissolved gas analysis method based on novel feature prioritisation and support vector machine," *IET Electric Power Applications,* vol. 8, no. 8, pp. 320-328, 2014, doi: 10.1049/iet-epa.2014.0085.

[80] D. Tanfilyeva, O. Tanfyev, and Y. Kazantsev, "K-nearest neighbor method for power transformers condition assessment," in *IOP Conference Series: Materials Science and Engineering*, 2019, vol. 643, no. 1: IOP Publishing, p. 012016, doi: 10.1088/1757- 899X/643/1/012016.

[81] S. D. Patil, M. Dharme, A. J. Patil, G. C. AK, R. Jarial, and A. Singh, "DGA based ensemble learning and random forest models for condition assessment of transformers," in *2022International Conference on Smart Generation Computing, Communication and Networking (SMART GENCON)*, 2022: IEEE, pp. 1-6, doi: 10.1109/SMARTGENCON56628.2022.10083672.

[82] I. B. Taha, S. Ibrahim, and D.-E. A. Mansour, "Power transformer fault diagnosis based on DGA using a convolutional neural network with noise in measurements," *Ieee Access,* vol. 9, pp. 111162-111170, 2021, doi: 10.1109/ACCESS.2021.3102415.

[83] B. Qi, Y. Wang, P. Zhang, C. Li, and H. Wang, "A novel deep recurrent belief network model for trend prediction of transformer DGA data," *IEEE access,* vol. 7, pp. 80069-80078, 2019, doi: 10.1109/ACCESS.2019.2923063.

[84] M. S. Katooli and A. Koochaki, "Detection and classification of incipient faults in three-phase power transformer using DGA information and rule-based machine learning method," *Journal of Control, Automation and Electrical Systems,* vol. 31, no. 5, pp. 1251-1266, 2020, doi: 10.1007/s40313-020-00625-5.

[85] S. Gopakumar and T. Sree Renga Raja, "RETRACTED ARTICLE: Determination of Power Transformer Fault's Severity Based on Fuzzy Logic Model with GR, Level and DGA Interpretation," *Journal of Electrical Engineering & Technology,* vol. 19, no. 4, pp. 2527-2548, 2024, doi: 10.1007/s42835-023-01691-w.

[86] X. D. Hoang and X. H. Vu, "An improved model for detecting DGA botnets using random forest algorithm," *Information Security Journal: A Global Perspective,* vol. 31, no. 4, pp. 441-450, 2022, doi: 10.1080/19393555.2021.1934198.

[87] M. Zhang *et al.*, "Fault diagnosis of oil-immersed power transformer based on difference- mutation brain storm optimized catboost model," *Ieee Access,* vol. 9, pp. 168767-168782, 2021, doi: 10.1109/ACCESS.2021.3135283.

[88] L. Breiman, "Random forests," *Machine learning,* vol. 45, no. 1, pp. 5-32, 2001, doi: 10.1023/a:1010933404324.

[89] S. González, S. García, J. Del Ser, L. Rokach, and F. Herrera, "A practical tutorial on bagging and boosting based ensembles for machine learning: Algorithms, software tools, performance study, practical perspectives and opportunities," *Information Fusion,* vol. 64, pp. 205-237, 2020, doi: 10.1016/j.inffus.2020.07.007.

[90] N. Haque, A. Jamshed, K. Chatterjee, and S. Chatterjee, "Accurate sensing of power transformer faults from dissolved gas data using random forest classifier aided by data clustering method," *IEEE Sensors Journal,* vol. 22, no. 6, pp. 5902-5910, 2022, doi: 10.1109/JSEN.2022.3149409.

[91] B. Williams *et al.*, "Data-driven model development for cardiomyocyte production experimental failure prediction," in *Computer aided chemical engineering*, vol. 48: Elsevier, 2020, pp. 1639- 1644.

[92] Z. Wahid, A. Z. Satter, A. Al Imran, and T. Bhuiyan, "Predicting absenteeism at work using tree-based learners," in *Proceedings of the 3rd international conference on machine learning and soft computing*, 2019, pp. 7-11, doi: 10.1145/3310986.331099.

[93] F. Ahmed *et al.*, "SperoPredictor: an integrated machine learning and molecular docking-based drug repurposing framework with use case of COVID-19," *Frontiers in public health,* vol. 10, p. 902123, 2022, doi: 10.3389/fpubh.2022.902123.

[94] M. R. I. Rifat, A. Al Imran, and A. Badrudduza, "Educational performance analytics of undergraduate business students," *International Journal of Modern Education and Computer Science,* vol. 10, no. 7, p. 44, 2019, doi: 10.5815/ijmecs.2019.07.05.

[95] M. Kropf *et al.*, "Cardiac anomaly detection based on time and frequency domain features using tree-based classifiers," *Physiological measurement,* vol. 39, no. 11, p. 114001, 2018, doi: 10.1088/1361-6579/aae13e.

[96] Z. Xiao, Y. Wang, K. Fu, and F. Wu, "Identifying different transportation modes from trajectory data using tree-based ensemble classifiers," *ISPRS International Journal of Geo-Information,* vol. 6, no. 2, p. 57, 2017, doi: 10.3390/ijgi6020057.

[97] L. Zhang and C. Zhan, "Machine learning in rock facies classification: An application of XGBoost," in *International Geophysical Conference, Qingdao, China, 17-20 April 2017*, 2017: Society of Exploration Geophysicists and Chinese Petroleum Society, pp. 1371-1374, doi: 10.1190/IGC2017-351.

[98] X. Zhu, H. Guo, J. J. Huang, S. Tian, W. Xu, and Y. Mai, "An ensemble machine learning model for water quality estimation in coastal area based on

remote sensing imagery," *Journal of Environmental Management,* vol. 323, p. 116187, 2022, doi: 10.1016/j.jenvman.2022.116187.

[99] H. Nasiri and S. A. Alavi, "A Novel Framework Based on Deep Learning and ANOVA Feature Selection Method for Diagnosis of COVID-19 Cases from Chest X-Ray Images," *Computational intelligence and neuroscience,* vol. 2022, no. 1, p. 4694567, 2022, doi: 10.1155/2022/4694567.

[100] ETRA, "Conservation and Control of Oil-insulated Components by Diagnosis of Gas in Oil "*Electr. Coop. Res. Assoc.,* vol. 36, no. 1, 1980.

[101] E. Dornerburg and W. Strittmatter, "Monitoring oil cooled transformers by gas analysis," *Brown Boveri Review,* vol. 61, no. 5, pp. 238-247, 1974.

[102] "Mineral oil impregnated electrical equipment in service. Guide to the interpretation of dissolved free gas analysis," *2nd ed. CEI, IEC 60599,* 2007.

[103] M. Duval, "The duval triangle for load tap changers, non-mineral oils and low temperature faults in transformers," *IEEE Electrical Insulation Magazine,* vol. 24, no. 6, pp. 22-29, 2008, doi: 10.1109/MEI.2008.4665347.

[104] M. Friedman, "The use of ranks to avoid the assumption of normality implicit in the analysis of variance," *Journal of the american statistical association,* vol. 32, no. 200, pp. 675-701, 1937.

[105] F. Wilcoxon, "Individual comparisons by ranking methods," in *Breakthroughs in statistics: Methodology and distribution*: Springer, 1992, pp. 196-202.

[106] S. A. Wani, D. Gupta, M. U. Farooque, and S. A. Khan, "Multiple incipient fault classification approach for enhancing the accuracy of dissolved gas analysis (DGA)," *IET Science, Measurement & Technology,* vol. 13, no. 7, pp. 959-967, 2019, doi: 10.1049/iet-smt.2018.5135.

[107] A. S. Malarvizhi, Q. Liu, D. Sha, H. Lan, and C. Yang, "An open-source workflow for spatiotemporal studies with COVID-19 as an example," *ISPRS International Journal of Geo- Information,* vol. 11, no. 1, p. 13, 2022, doi: 10.3390/ijgi11010013.

[108] "Egyptian Electricity Holding Company (EEHC) Reports, Ministry Electr.," 2016.

[109] M. Duval and A. DePabla, "Interpretation of gas-in-oil analysis using new IEC publication 60599 and IEC TC 10 databases," *IEEE Electrical Insulation Magazine,* vol. 17, no. 2, pp. 31-41, 2001, doi: 10.1109/57.917529.

[110] E. Li, L. Wang, and B. Song, "Fault diagnosis of power transformers with membership degree,"*IEEE Access,* vol. 7, pp. 28791-28798, 2019, doi: 10.1109/ACCESS.2019.2902299.

[111] *Egyptian Electricity Holding Company (EEHC) Reports, Ministry Electr.," 2016.*

[112] J. Li, Q. Zhang, K. Wang, J. Wang, T. Zhou, and Y. Zhang, "Optimal dissolved gas ratios selected by genetic algorithm for power transformer fault diagnosis based on support vector machine," *IEEE Transactions on Dielectrics and Electrical Insulation,* vol. 23, no. 2, pp. 1198- 1206, 2016, doi: 10.1109/TDEI.2015.005277.

[113] S. Seifeddine, B. Khmais, and C. Abdelkader, "Power transformer fault diagnosis based on dissolved gas analysis by artificial neural network," in *2012 first international conference on renewable energies and vehicular technology*, 2012: IEEE, pp. 230-236, doi: 10.1109/REVET.2012.6195276.

[114] O. E. Gouda, S. M. Saleh, and S. H. El-Hoshy, "Power transformer incipient faults diagnosis based on dissolved gas analysis," *TELKOMNIKA Indonesian J. Electr. Eng,* vol. 17, no. 1, pp. 10-16, 2016, doi: 10.11591/telkomnika.v17i1.9405.

[115] G. Zhang, K. Yasuoka, S. Ishii, L. Yang, and Z. Yan, "Application of fuzzy equivalent matrix for fault diagnosis of oil-immersed insulation," in *Proceedings of 1999 IEEE 13th International Conference on Dielectric Liquids (ICDL'99)(Cat. No. 99CH36213)*, 1999: IEEE, pp. 400-403.

[116] J.-t. Hu, L.-x. Zhou, and M.-l. Song, "Transformer fault diagnosis method of gas hromatographic analysis using computer image analysis," in *2012 second international conference on intelligent system design and engineering application*, 2012: IEEE, pp. 1169-1172, doi: 10.1109/ISdea.2012.599.

[117] M. Rajabimendi and E. P. Dadios, "A hybrid algorithm based on neural-fuzzy system for interpretation of dissolved gas analysis in power transformers," in *TENCON 2012 IEEE region 10 conference*, 2012: IEEE, pp. 1-6, doi: 10.1109/TENCON.2012.6412171.

[118] D. S. Sarma and G. Kalyani, "ANN approach for condition monitoring of power transformers using DGA," in *2004 IEEE Region 10 Conference TENCON 2004.*, 2004, vol. 100: IEEE, pp.444-447, doi: 10.1109/TENCON.2004.1414803.

[119] M. Duval, "A review of faults detectable by gas-in-oil analysis in transformers," *IEEE electrical Insulation magazine,* vol. 18, no. 3, pp. 8-17, 2002, doi: 10.1109/MEI.2002.1014963.

[120] R. Soni and K. Chaudhari, "A Novel Proposed Model to Diagnose Incipient Faults of Power Transformer Using Dissolved Gas Analysis by Ratio methods," in *Int. Conf. on Comp. of Power, Energy, Information and Communication*, 2015.

[121] A. Hechifa *et al.*, "Improved intelligent methods for power transformer fault diagnosis based on tree ensemble learning and multiple feature vector

analysis," *Electrical Engineering,* vol. 106, no. 3, pp. 2575-2594, 2024, doi: 10.1007/s00202-023-02084-y.

[122] L. Lessa, C. Grilo, A. Moraes, D. Coury, and R. Fernandes, "A travelling wave-based fault locator for radial distribution systems using decision trees to mitigate multiple estimations," *Electric Power Systems Research,* vol. 223, p. 109646, 2023, doi: 10.1016/j.epsr.2023.109646.

[123] J. Liang, Z. Qin, S. Xiao, L. Ou, and X. Lin, "Efficient and secure decision tree classification for cloud-assisted online diagnosis services," *IEEE Transactions on Dependable and Secure Computing,* vol. 18, no. 4, pp. 1632-1644, 2019, doi: 10.1109/TDSC.2019.2922958.

[124] A. Joshi, R. Khathoon, and A. P. PV, "A very fast and easily implementable support vector machine based relay algorithm to classify the fault and non fault disturbance in VSC HVDC terminals," *Electric Power Systems Research,* vol. 220, p. 109380, 2023, doi: 10.1016/j.epsr.2023.109380.

[125] M. Sheykhmousa, M. Mahdianpari, H. Ghanbari, F. Mohammadimanesh, P. Ghamisi, and S. Homayouni, "Support vector machine versus random forest for remote sensing image classification: A meta-analysis and systematic review," *IEEE Journal of Selected Topics in Applied Earth Observations and Remote Sensing,* vol. 13, pp. 6308-6325, 2020, doi: 10.1109/JSTARS.2020.3026724.

[126] G. Zhang, K. Yasuoka, S. Ishii, L. Yang, and Z. Yan, "Application of fuzzy equivalent matrix for fault diagnosis of oil-immersed insulation," in Proceedings of 1999 IEEE 13th International Conference on Dielectric Liquids (ICDL'99)(Cat. No. 99CH36213), 1999: IEEE, pp. 400-403.

[127] J.-t. Hu, L.-x. Zhou, and M.-l. Song, "Transformer fault diagnosis method of gas hromatographic analysis using computer image analysis," in 2012 second international conference on intelligent system design and engineering application, 2012: IEEE, pp. 1169-1172, doi: 10.1109/ISdea.2012.599.

[128] M. Rajabimendi and E. P. Dadios, "A hybrid algorithm based on neural-fuzzy system for interpretation of dissolved gas analysis in power transformers," in TENCON 2012 IEEE region 10 conference, 2012: IEEE, pp. 1-6, doi: 10.1109/TENCON.2012.6412171.

[129] D. S. Sarma and G. Kalyani, "ANN approach for condition monitoring of power transformers using DGA," in 2004 IEEE Region 10 Conference TENCON 2004., 2004, vol. 100: IEEE, pp.

[130] 444-447 ,doi: 10.1109/TENCON.2004.1414803.

[131] M. Duval, "A review of faults detectable by gas-in-oil analysis in transformers," IEEE electrical Insulation magazine, vol. 18, no. 3, pp. 8-17, 2002, doi: 10.1109/MEI.2002.1014963.

[132] R. Soni and K. Chaudhari, "A Novel Proposed Model to Diagnose Incipient Faults of Power Transformer Using Dissolved Gas Analysis by Ratio methods," in Int. Conf. on Comp. of Power, Energy, Information and Communication, 2015.

[133] A. Hechifa et al., "Improved intelligent methods for power transformer fault diagnosis based on tree ensemble learning and multiple feature vector analysis," Electrical Engineering, vol. 106, no. 3, pp. 2575-2594, 2024, doi: 10.1007/s00202-023-02084-y.

[134] L. Lessa, C. Grilo, A. Moraes, D. Coury, and R. Fernandes, "A travelling wave-based fault locator for radial distribution systems using decision trees to mitigate multiple estimations," Electric Power Systems Research, vol. 223, p. 109646, 2023, doi: 10.1016/j.epsr.2023.109646.

[135] J. Liang, Z. Qin, S. Xiao, L. Ou, and X. Lin, "Efficient and secure decision tree classification for cloud-assisted online diagnosis services," IEEE Transactions on Dependable and Secure Computing, vol. 18, no. 4, pp. 1632-1644, 2019, doi: 10.1109/TDSC.2019.2922958.

[136] A. Joshi, R. Khathoon, and A. P. PV, "A very fast and easily implementable support vector machine based relay algorithm to classify the fault and non fault disturbance in VSC HVDC terminals," Electric Power Systems Research, vol. 220, p. 109380, 2023, doi: 10.1016/j.epsr.2023.109380.

[137] M. Sheykhmousa, M. Mahdianpari, H. Ghanbari, F. Mohammadimanesh, P. Ghamisi, and S. Homayouni, "Support vector machine versus random forest for remote sensing image classification: A meta-analysis and systematic review," IEEE Journal of Selected Topics in Applied Earth Observations and Remote Sensing, vol. 13, pp. 6308-6325, 2020, doi: 10.1109/JSTARS.2020.3026724.

[138] S. Haykin, Neural Networks and Learning Machines, 3rd ed., Pearson, 2009.

[139] L. Breiman, Random Forests, Machine Learning, vol. 45, no. 1, pp. 5–32, 20